WADD TECHNICAL REPORT 60-699
VOLUME V

ENERGY CONVERSION SYSTEMS REFERENCE HANDBOOK

VOLUME V — DIRECT SOLAR CONVERSION

W. Evans
W. R. Menetrey

Electro-Optical Systems, Inc.
Pasadena, California

EOS REPORT 390-FINAL

SEPTEMBER 1960

WRIGHT AIR DEVELOPMENT DIVISION

NOTICES

When Government drawings, specifications, or other data are used for any purpose other than in connection with a definitely related Government procurement operation, the United States Government thereby incurs no responsibility nor any obligation whatsoever; and the fact that the Government may have formulated, furnished, or in any way supplied the said drawings, specifications, or other data, is not to be regarded by implication or otherwise as in any manner licensing the holder or any other person or corporation, or conveying any rights or permission to manufacture, use, or sell any patented invention that may in any way be related thereto.

☆

Qualified requesters may obtain copies of this report from the Armed Services Technical Information Agency, (ASTIA), Arlington Hall Station, Arlington 12, Virginia.

☆

This report has been released to the Office of Technical Services, U. S. Department of Commerce, Washington 25, D. C., for sale to the general public.

☆

Copies of WADD Technical Reports and Technical Notes should not be returned to the Wright Air Development Division unless return is required by security considerations, contractual obligations, or notice on a specific document.

WADD TECHNICAL REPORT 60-699
VOLUME V

ENERGY CONVERSION SYSTEMS REFERENCE HANDBOOK

VOLUME V — DIRECT SOLAR CONVERSION

W. Evans
W. R. Menetrey

Electro-Optical Systems, Inc.

SEPTEMBER 1960

Flight Accessories Laboratory
Contract Nr. AF 33(616)-6791
Project Nr. 4769
Task Nr. 61048

WRIGHT AIR DEVELOPMENT DIVISION
AIR RESEARCH AND DEVELOPMENT COMMAND
UNITED STATES AIR FORCE
WRIGHT-PATTERSON AIR FORCE BASE, OHIO

700 — May 1961 — 30-1129

A B S T R A C T

Volume V describes in detail the performance characteristics of the photovoltaic converter when used to convert solar radiation directly to DC electrical energy. Empirical and analytical relationships are derived which present expected efficiencies of conversion as a function of temperature, solar insolance, and other factors. The effects of environmental degradation due to meteoroids and the Van Allen belts are discussed. The present and anticipated state-of-the-art of fabrication techniques is presented, along with the advantages of using concentrating mechanisms for increasing the solar illumination level. A discussion is also included describing the state of the art and practical and theoretical limitations of the photo-emissive generator. It does not appear at present that the photo-emissive generator offers competition to the photovoltaic cell.

ENERGY CONVERSION SYSTEMS REFERENCE HANDBOOK

LIST OF VOLUME AND SECTION TITLES WITH AUTHORS

LIST OF VOLUME AND SECTION TITLES WITH AUTHORS (CONT'D)

A complete detailed Table of Contents for all volumes of Energy Conversion Systems Reference Handbook is included in Volume I.

ENERGY CONVERSION SYSTEMS REFERENCE HANDBOOK

Volume V - Direct Solar Conversion

Section A

PHOTOVOLTAIC CONVERTERS

W. Evans
Energy Research Division
ELECTRO-OPTICAL SYSTEMS, INC.

Manuscript released by the author
September 1960 for publication in this
WADD Technical Report 60-699 Energy Conversion Systems Reference Handbook

V-A PHOTOVOLTAIC CONVERTERS

CONTENTS

V - A PHOTOVOLTAIC CONVERTERS

ILLUSTRATIONS

Figures

V - A PHOTOVOLTAIC CONVERTERS

T A B L E S

Tables

V DIRECT SOLAR CONVERTERS

A PHOTOVOLTAIC CONVERTERS

The design and utilization of photovoltaic energy conversion systems requires some understanding of the physics of the photovoltaic effect, through knowledge of the characteristics of solar cells under various conditions of operation and acquaintanceship with the current state-of-the-art in solar panel design and operation. In this volume, a substantial amount of solar cell theory and test data, coupled with a discussion of solar cell engineering techniques, is presented with current space vehicles used as examples. Some consideration is also given to developmental work in progress on advanced solar cells and to solar cell application engineering.

In subsection 1.0, the fundamental equations describing solar cell characteristics are given with typical test data of available silicon cells. A simplified work description of the photovoltaic process is also given, designed to give the reader, unfamiliar with semiconductor theory, some feeling for the mechanism of photovoltaic energy conversion.

Subsection 2.0 discusses the engineering approaches used in photovoltaic systems design, such as techniques of temperature control, types of panel geometry, and determination of converter electrical properties. The following subsections discuss environmental problems, advanced cell types in development, current structural design techniques, and the use of solar concentrators. The final subsection, 7.0, presents more detailed theory of the photovoltaic effect in both conventional cells and advanced types under development.

1.0 PERFORMANCE CHARACTERISTICS OF THE PHOTOVOLTAIC CELL

In this subsection, the formulae governing solar cell performance are presented and discussed. Data showing typical characteristics of specific cell types are given.

The basic solar photovoltaic cell current-voltage characteristic is described by the following equation:

$$I = I_L - I_o \left\{ \exp\left[\frac{q\,[V-IR]}{nkT}\right] - 1 \right\} \qquad \text{(A-1)}$$

where

I = the cell current

V = the external cell voltage

R = the internal cell series resistance

I_o = saturation current or dark current

I_L = junction cell current

q = electronic charge

k = Boltzman's constant

T = absolute temperature

n = a dimensionless parameter, usually greater than unity.

Typical silicon cell characteristics are given in Figures V-A-1 and V-A-2. The dark, or saturation current, I_o is given by

$$I_o = a\,T^3 \exp\left(-q\,E_g^1/kT\right) \qquad \text{(A-2)}$$

where E_g^1 is the effective thermal band-gap and "a" is determined by the properties of the semiconducting material and p-n junction comprising the photovoltaic cell. A plot of I_o vs. T at various values of "a" for silicon (E_g^1 approximately 1.2 ev) is given in Figure V-A-3.

The variation of the solar cell characteristics with temperature and incident intensity may be determined if the corresponding variation of the parameters of Equation A-1 is known. These are parametrical relations, shown in Table V-A-1, and are discussed below.

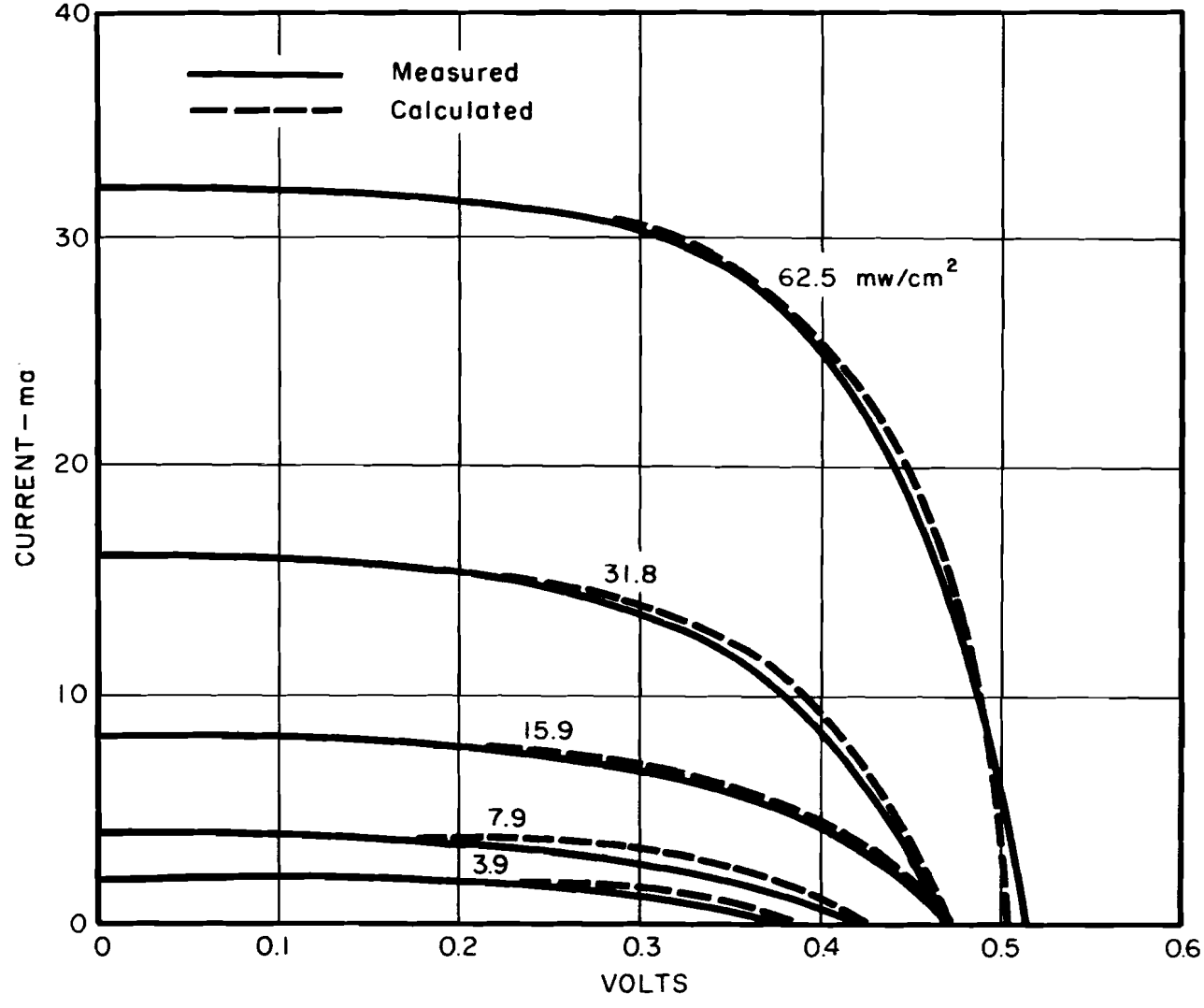

FIGURE V-A-1 CURRENT-VOLTAGE CHARACTERISTICS VS. INTENSITY FOR A TYPICAL SILICON CELL

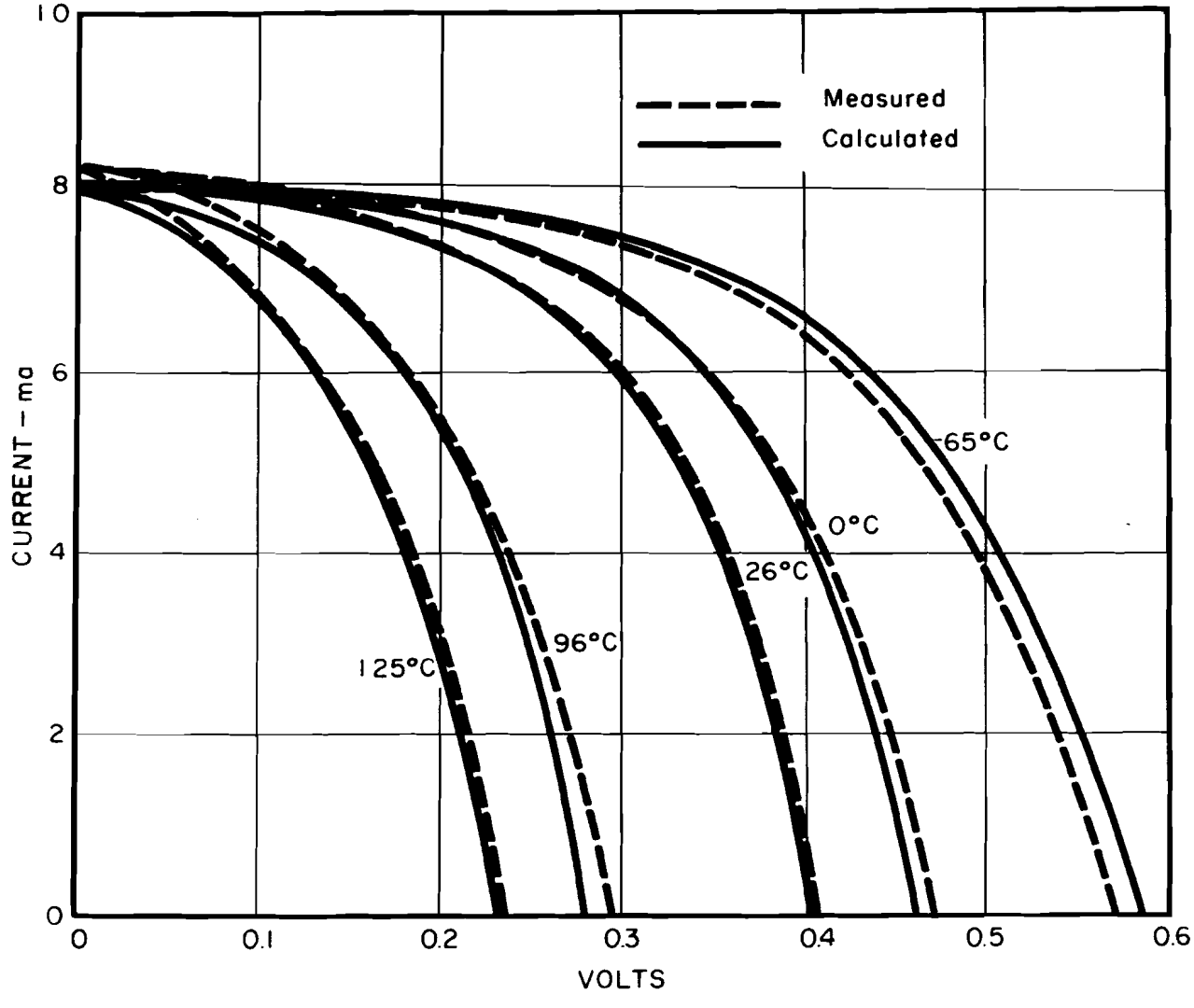

FIGURE V-A-2 SILICON SOLAR CELL CURRENT-VOLTAGE CHARACTERISTICS VS. TEMPERATURE

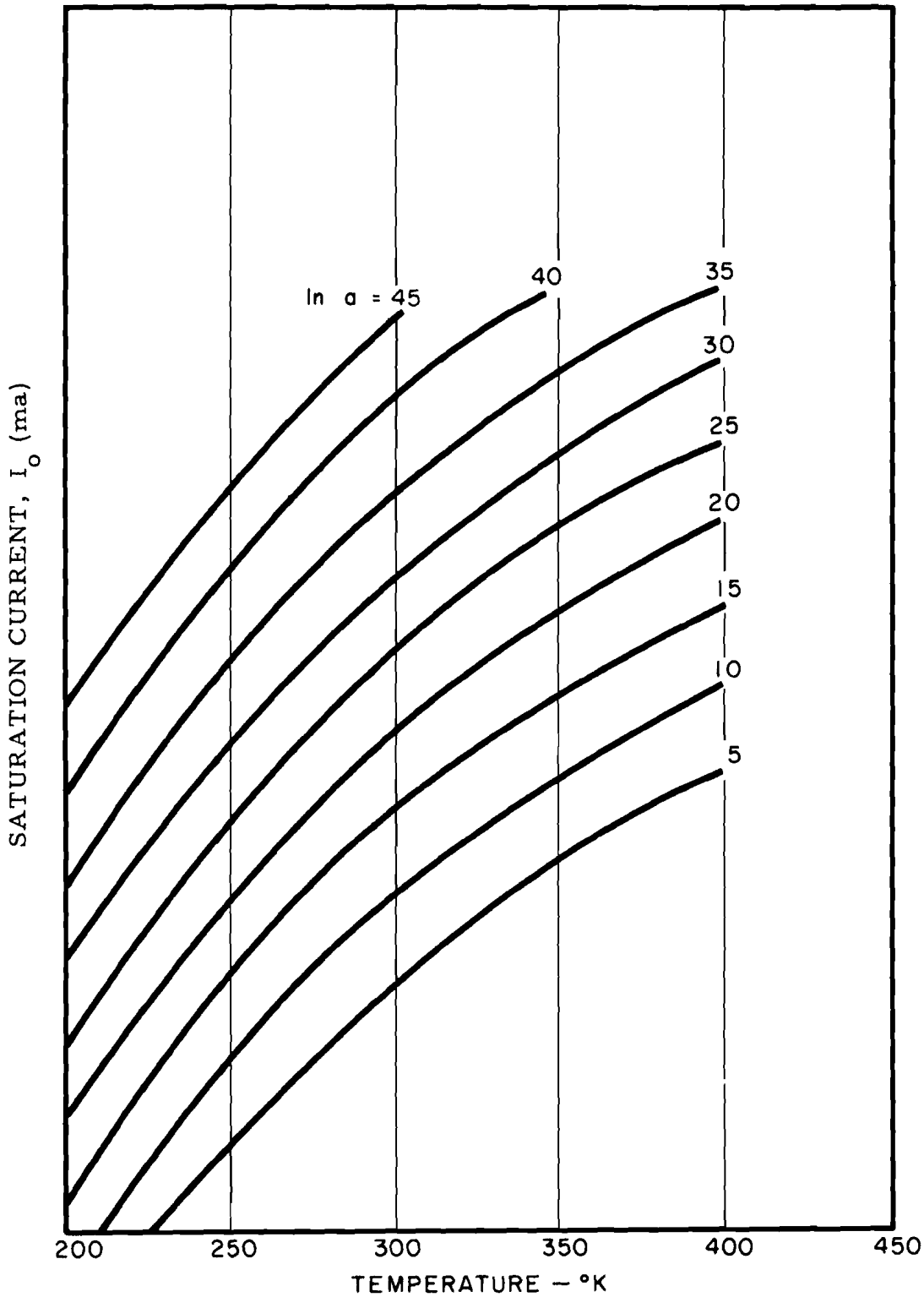

FIGURE V-A-3 I_o VS. TEMPERATURE FOR VARIOUS a WHERE $I_o = aT^3 \exp\left[-q E_g/kT\right]$

TABLE V-A-1

VARIATION OF PARAMETERS

Parameter	Variation with Intensity	Variation with Temperature
I_L	Directly proportional to intensity over a wide range.	Increases very slowly with temperature for most cells.
I_o	Assumed not vary with intensity in this analysis.	Varies with T as shown in Equation A-2 .
n	Decreases with intensity (See Fig. V-A-11).	Decreases with T (See Fig. V-A-10).
R	Does not change with intensity.	Tends to decrease with increasing T.

1.1 Variation of Short-Circuit Current, I_L

Short-circuit current, from Equation A-1 with a V of zero is

$$I_{sc} = I_L - I_o \left[\exp\left(-\frac{q\,IR}{nkT}\right) - 1\right] \qquad \text{(A-3)}$$

If the internal cell series resistance is small enough, I_{sc} is very near I_L, which is the case for high-efficiency silicon cells. The junction current, I_L, increases linearly with intensity for any incidence of constant spectral distribution. The dependence of I_L on spectral distribution may be measured with the aid of a monochrometer by determining short-circuit current vs. wavelength of constant intensity light. The resulting curve, called the spectral response characteristic, is shown in Figure V-A-4 for several typical silicon cells at room temperature. Because the band-gap of semiconductors decreases slightly with

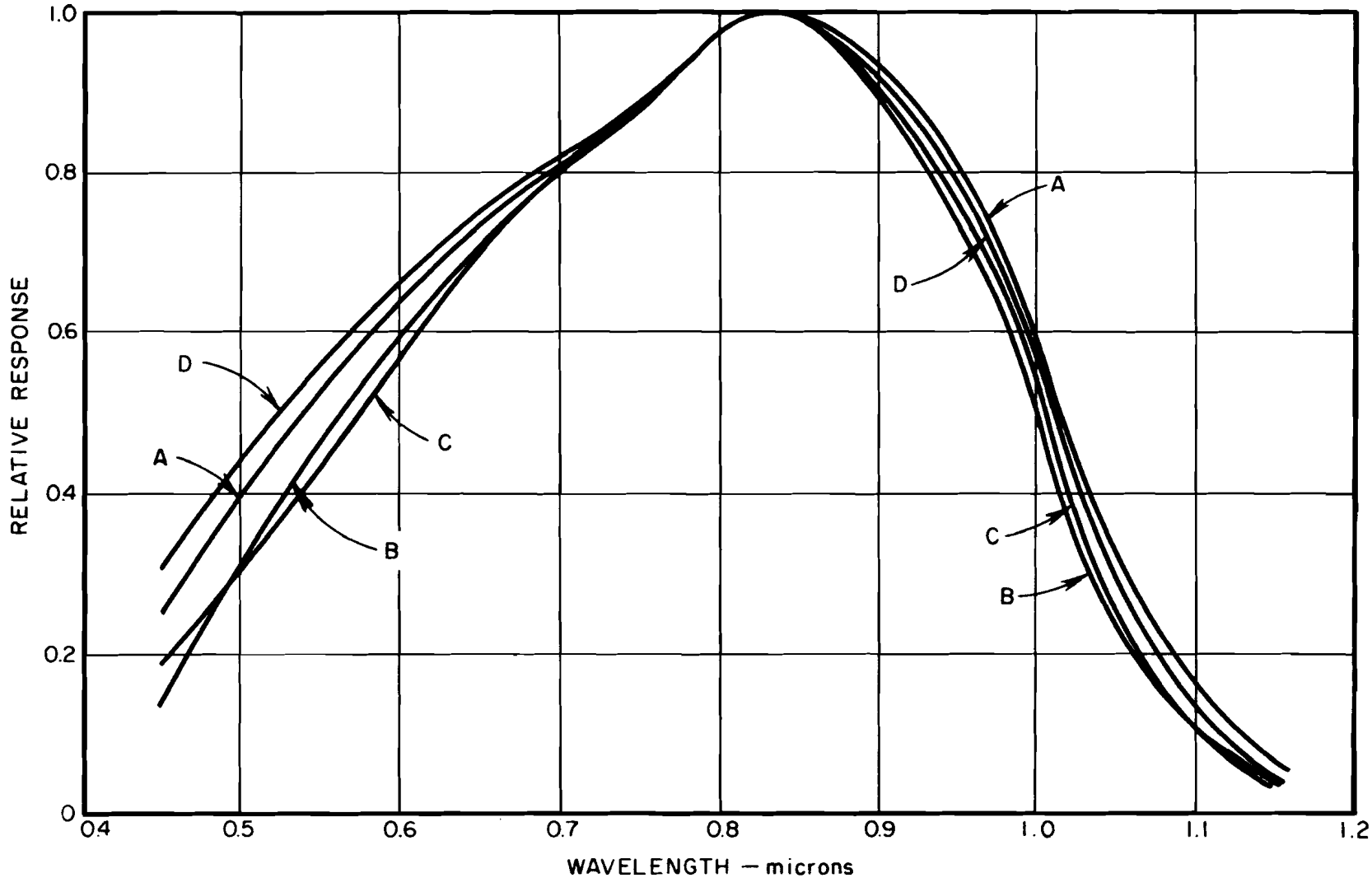

FIGURE V-A-4 SPECTRAL RESPONSE OF FOUR SILICON SOLAR CELLS

increasing temperature as shown in Figure V-A-5, the spectral response characteristic extends further into the infrared as temperature increases. As a result, short-circuit current will increase somewhat with temperature under an incident spectrum rich in the infrared, such as tungsten light. Such a curve is shown in Figure V-A-6. However, under the solar spectrum in outer space (which is not as strong as the infrared), little change of short-circuit current with temperature is expected.

Because short-circuit current is directly proportional to incident intensity at constant temperature, it is often convenient to measure the intensity of incident radiation in terms of the short-circuit current it produces in a given solar cell. A typical calibration curve for silicon cells is shown in Figure V-A-7.

1.2 Variations of Open Circuit Voltage, V_{oc}

The open circuit voltage is found from Equation A-1 by setting I equal to zero and assuming the exponential to be much greater than unity, as follows: (A-4)

$$V_{oc} = \frac{nkT}{q} \ln (I_L/I_o).$$

Substituting Equation A-2 for I_o:

$$V_{oc} = \frac{nkT}{q} \left[\ln (I_L) - \ln (a) - 3 \ln T \right] + n E_g^1 \quad \text{(A-5)}$$

Over the range of practical temperatures, the bracketed term varies slowly with temperature, and Equation A-5 may be assumed to be a linear equation of V_{oc} vs. T. A plot of V_{oc} vs. temperature is shown in Figure V-A-8 for typical silicon cells. Note that the linear relationship does hold over a wide range of temperatures.

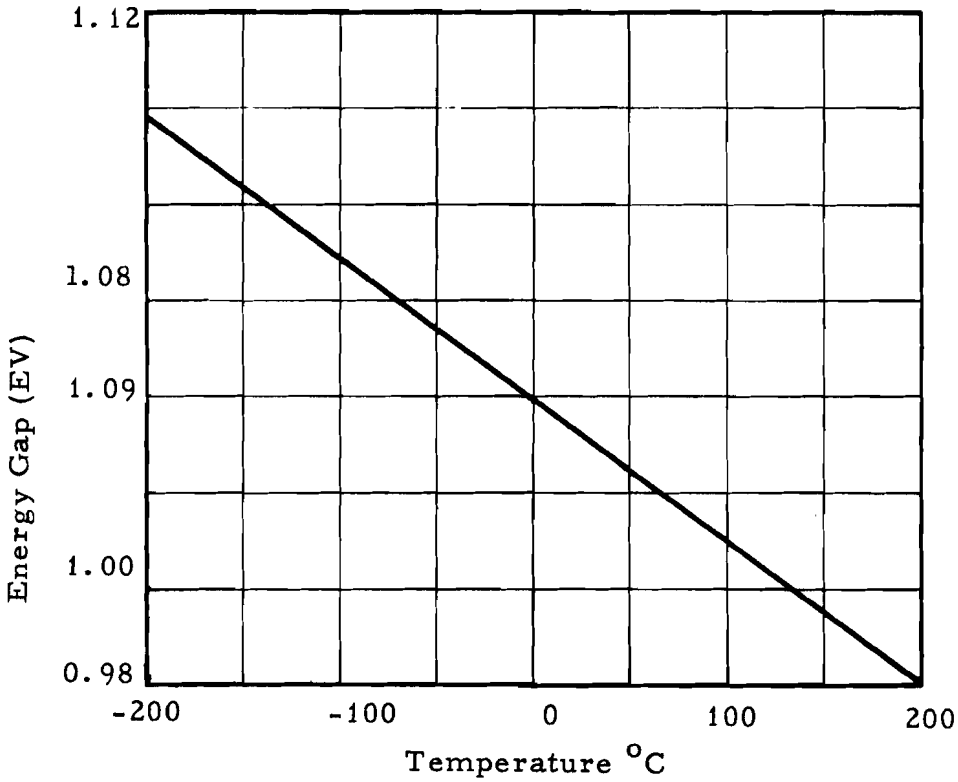

FIGURE V-A-5 ENERGY GAP VERSUS TEMPERATURE FOR SILICON

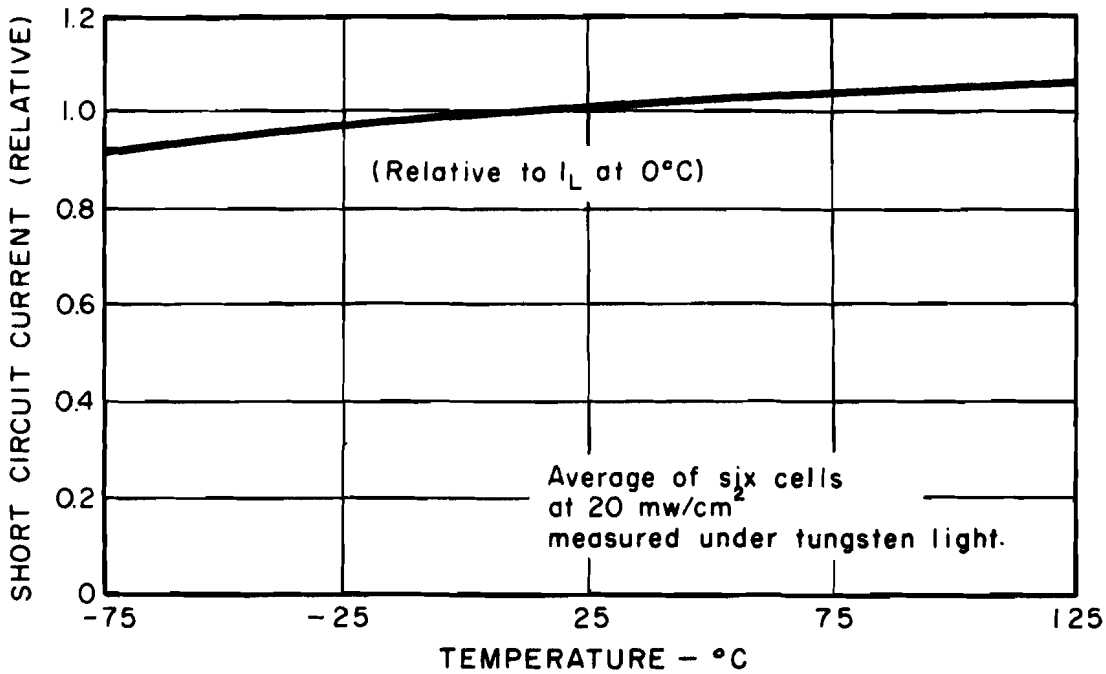

FIGURE V-A-6 SHORT-CIRCUIT CURRENT VS. TEMPERATURE FOR TYPICAL SILICON CELLS

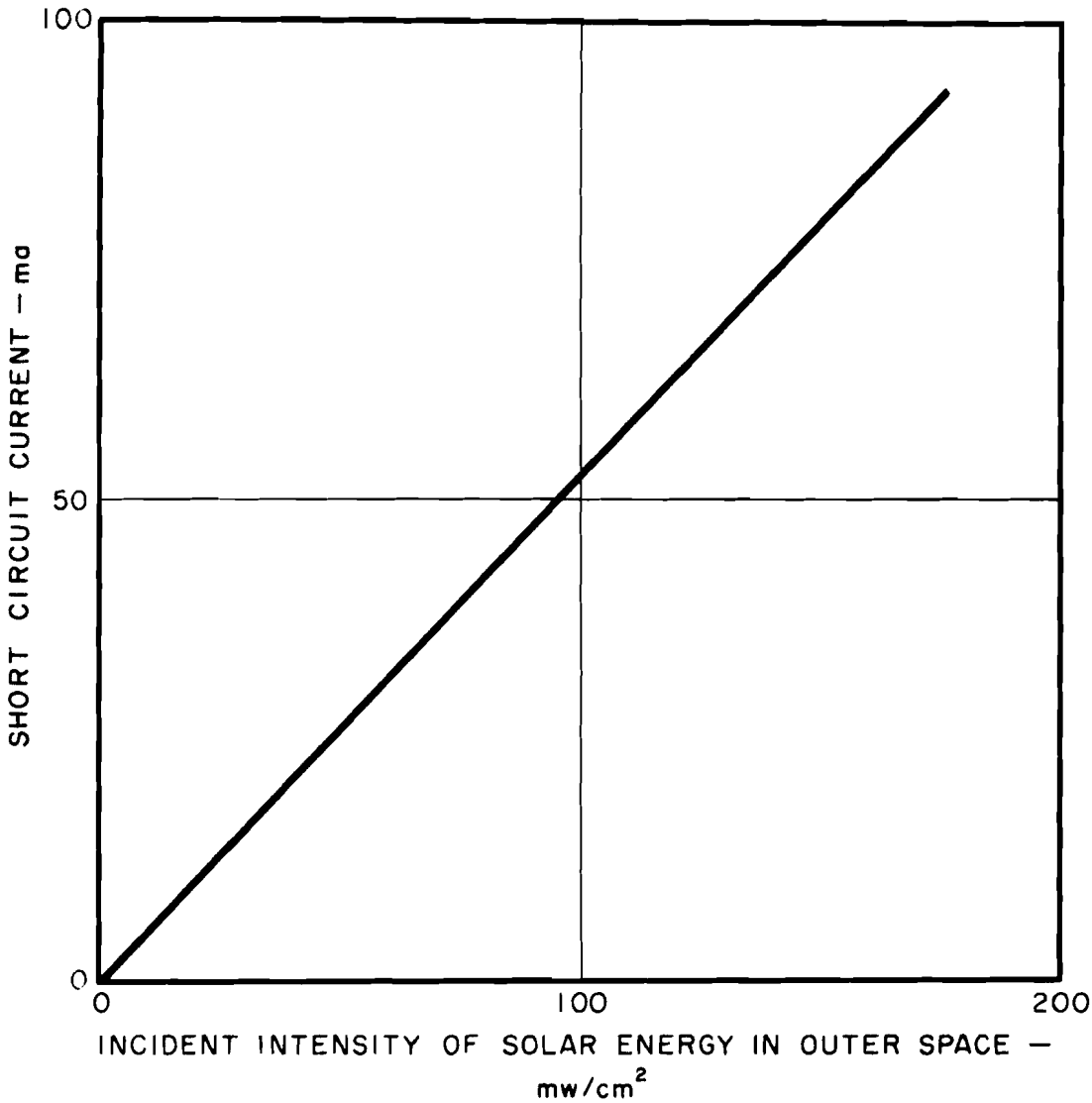

FIGURE V-A-7 SHORT CIRCUIT CURRENT VS. INTENSITY OF INCIDENT SOLAR RADIATION IN OUTER SPACE OF A TYPICAL 1 X 2 SILICON CELL

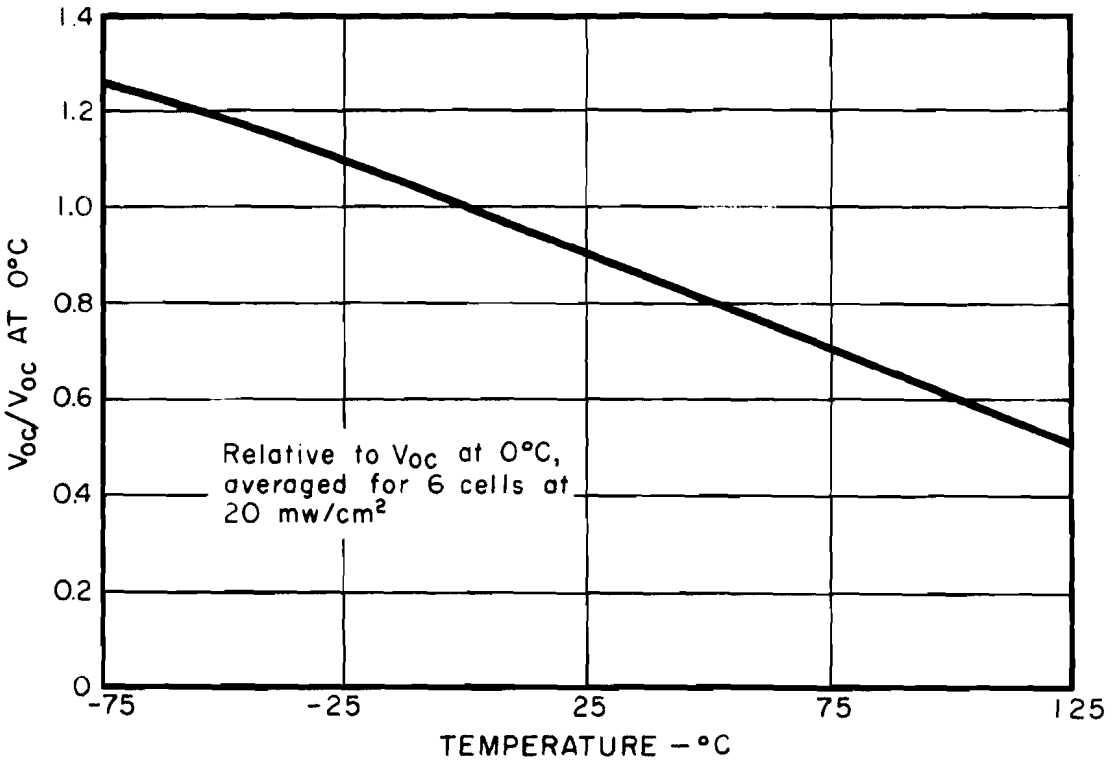

FIGURE V-A-8 OPEN-CIRCUIT VOLTAGE VS. TEMPERATURE FOR TYPICAL SILICON CELLS

To determine the variation of V_{oc} with intensity, Equation (A-4) may be revised to be:

$$V_{oc} = \frac{nk\ T}{q} \ln (I_L) - \frac{nk\ T}{q} \ln (I_o) \qquad (A-6)$$

Thus, using I_L as a measure of incident intensity, V_{oc} varies linearly with the logarithm of I_L. Typical measure curves are shown in Figure V-A-9.

1.3 Variations of n

The parameter n in Equation (A-1) accounts for a large number of effects, the most prominent of which is space charge generation of carriers (Reference V-A-1). According to the theory of Reference V-A-1, n will vary with voltage from one to two in silicon cells; however, the current-voltage characteristics of most silicon solar cells may be closely approximated by assuming n to be constant with voltage and accounting for an empirical variation of n with temperature and insolance. Plots of measured variation of n with temperature and insolence are shown in Figures V-A-10 and V-A-11. It should be noted that the "squareness" of the current-voltage characteristic or the current efficiency as defined in subsection 7, decreases with increasing n and therefore, decreases with decreasing temperature and insolance.

1.4 Variation of Current-Voltage Characteristics

The parameters which are of greatest interest to designers of solar cell systems are the optimum voltage, current, and power output and their variation with temperature and insolance. Typical data are shown in Figures V-A-12 through V-A-20. (Note that optimum power vs. temperature is the same as efficiency vs. temperature.)

Variation of characteristics with angle of incidence has been found to be very nearly that expected by multiplying the

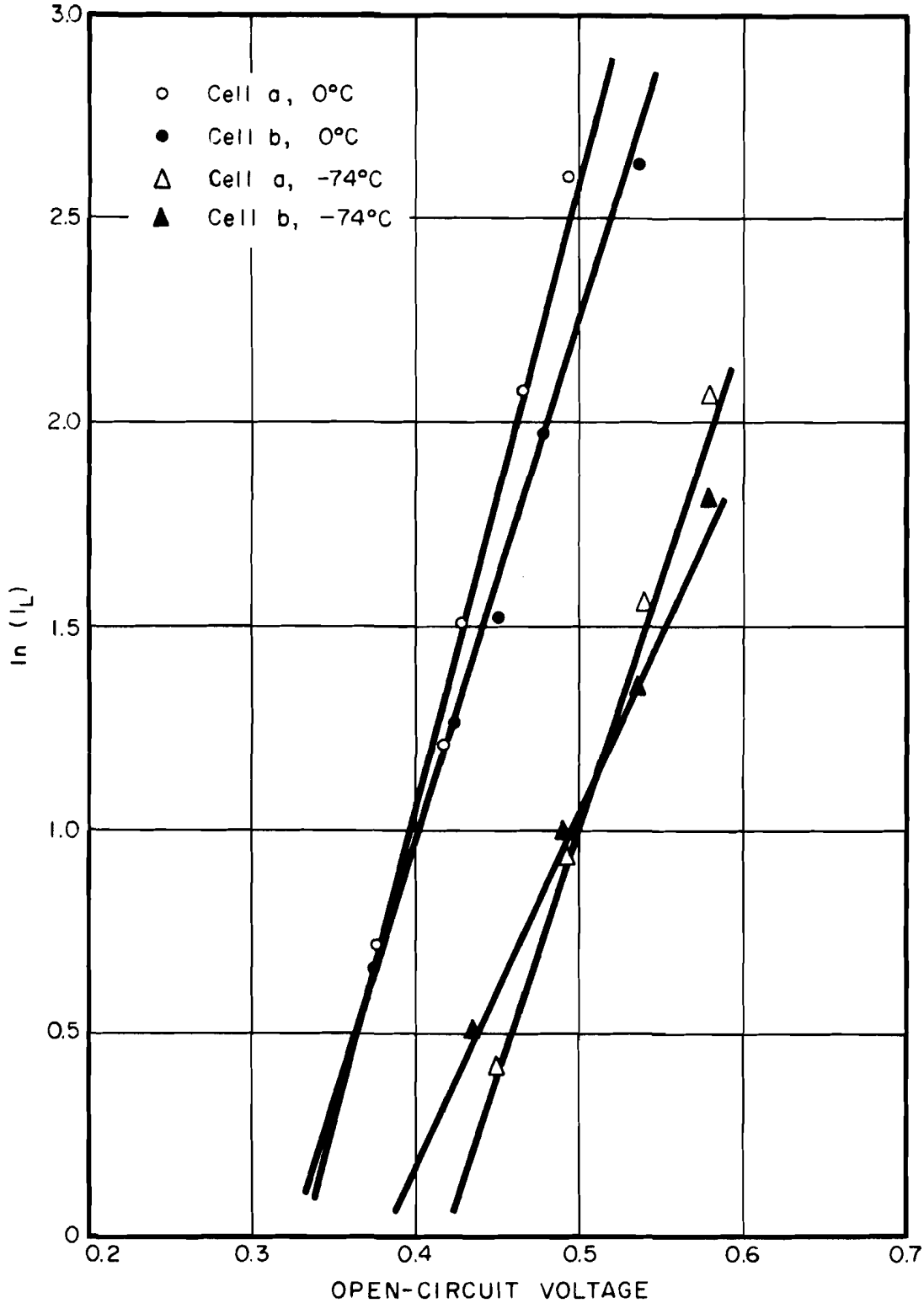

FIGURE V-A-9 OPEN-CIRCUIT VOLTAGE VS. SHORT-CIRCUIT CURRENT FOR TYPICAL SILICON CELLS

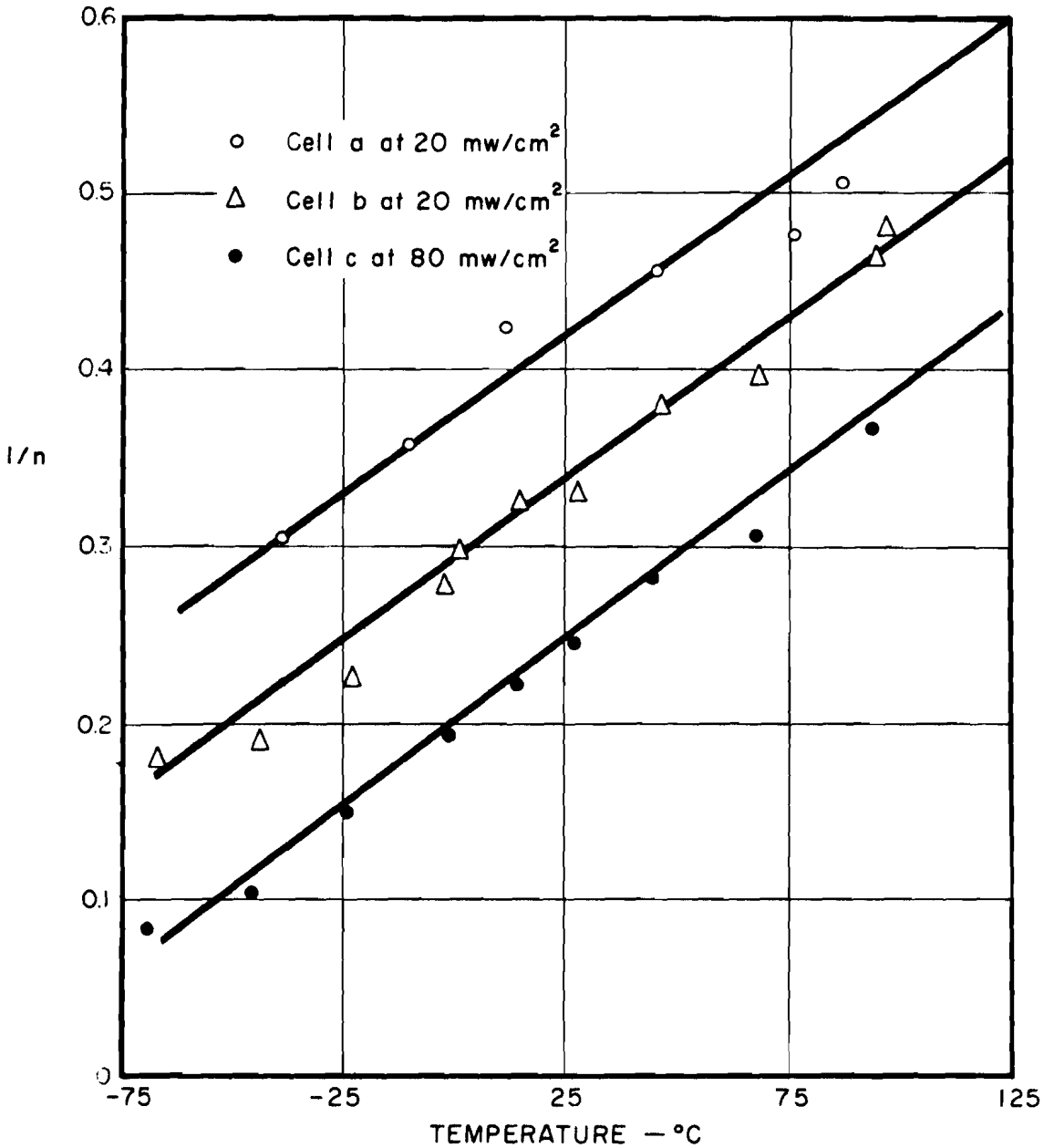

FIGURE V-A-10 VARIATION OF THE PARAMETER "n" WITH TEMPERATURE FOR TYPICAL SILICON CELLS

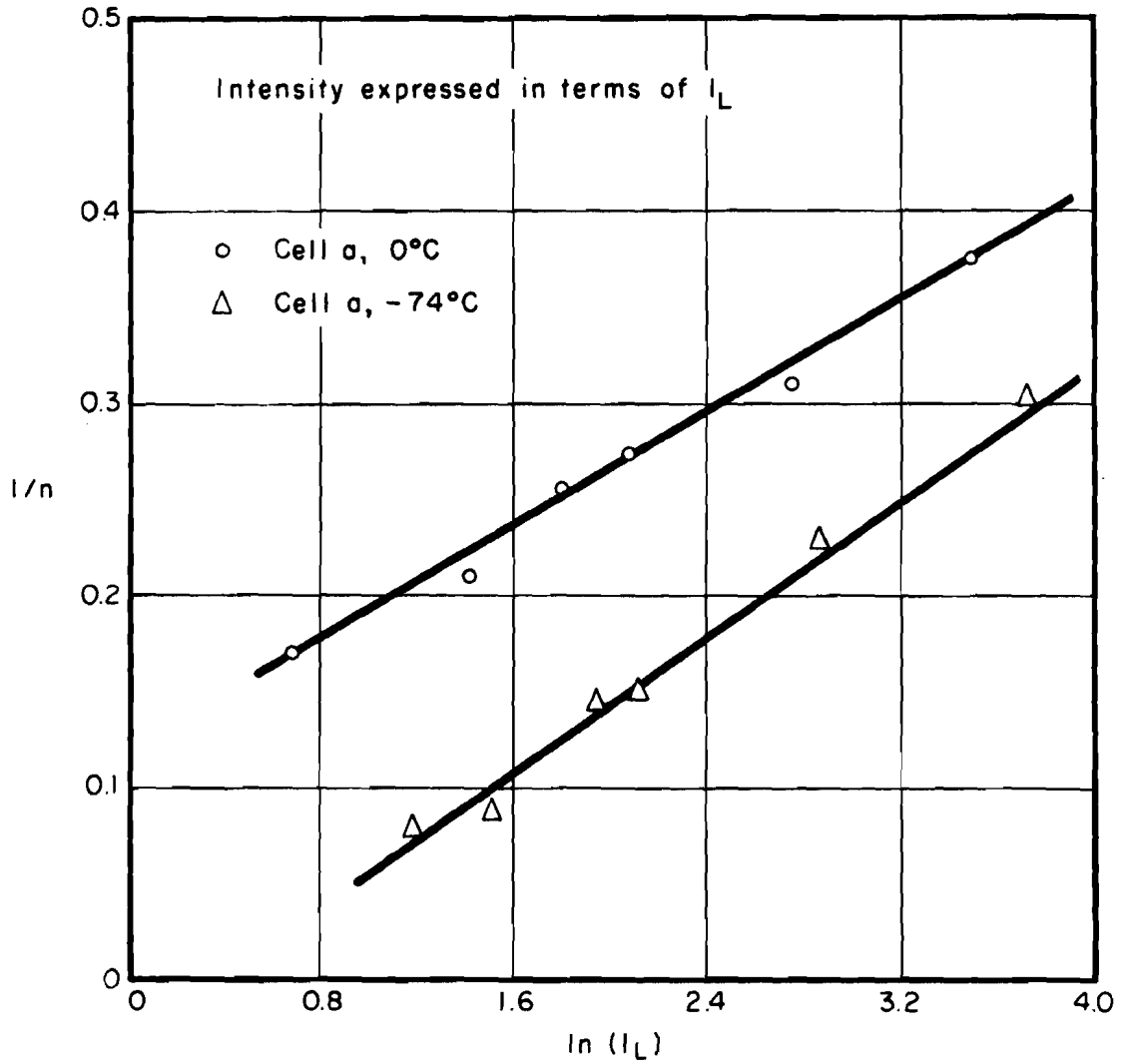

FIGURE V-A-11 VARIATION OF "n" WITH INCIDENT INTENSITY FOR TYPICAL SILICON CELLS

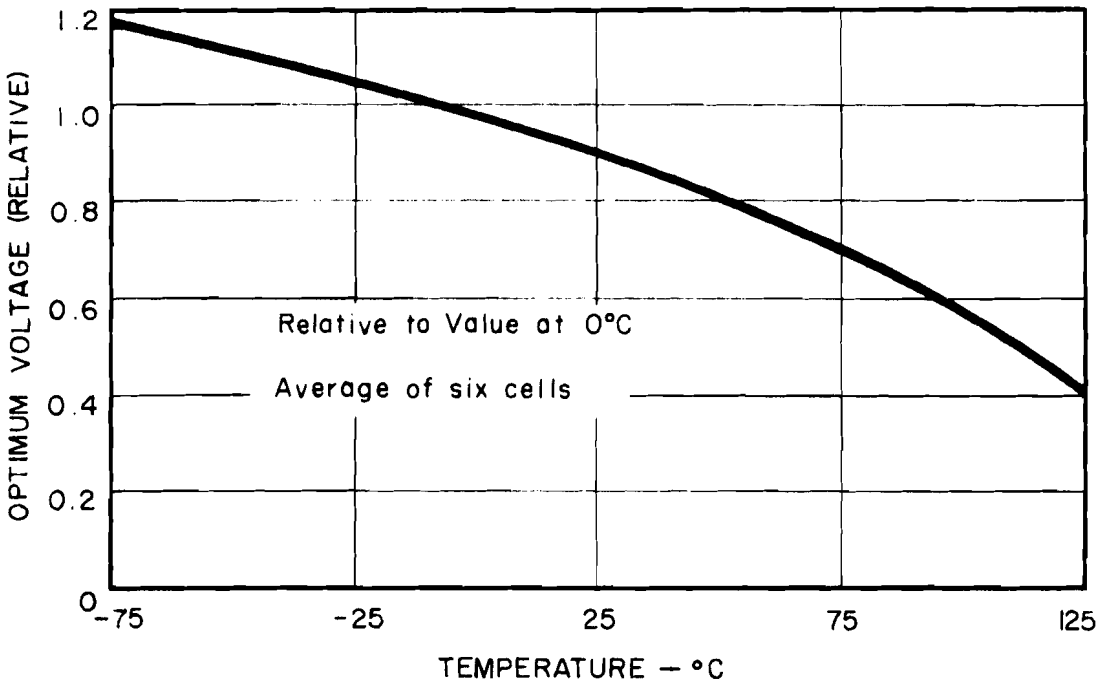

FIGURE V-A-12 OPTIMUM VOLTAGE VS. TEMPERATURE FOR TYPICAL SILICON CELLS

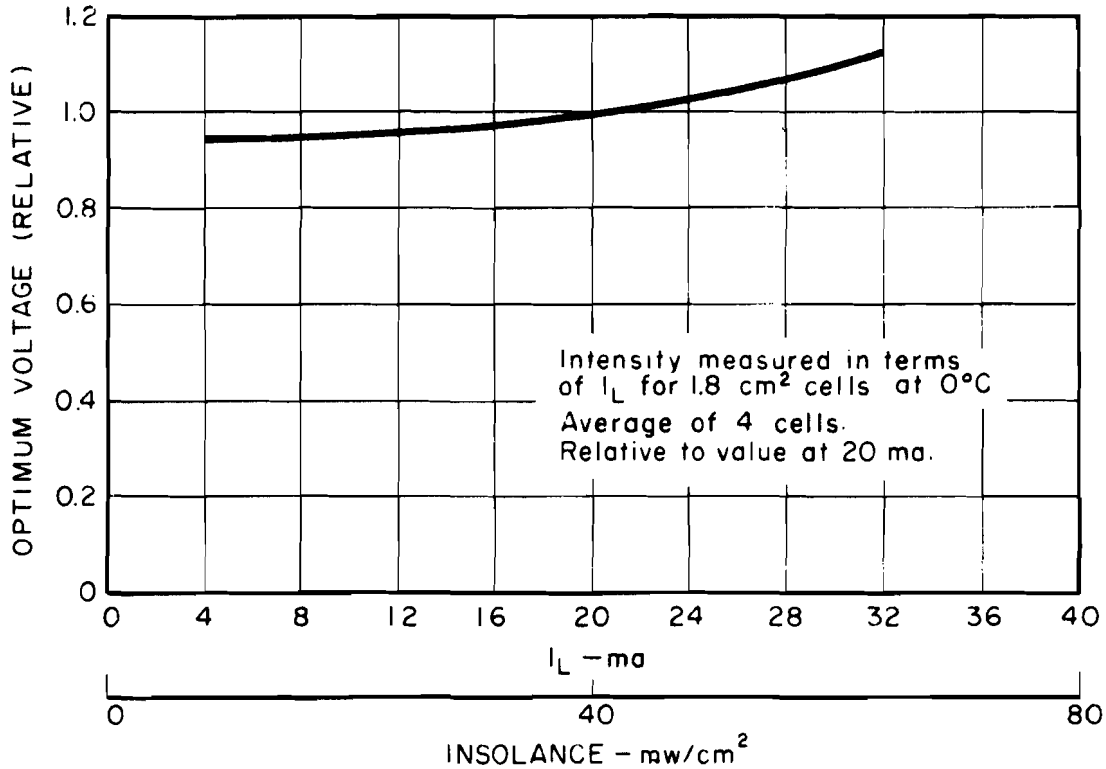

FIGURE V-A-13 OPTIMUM VOLTAGE VS. INTENSITY FOR TYPICAL SILICON CELLS

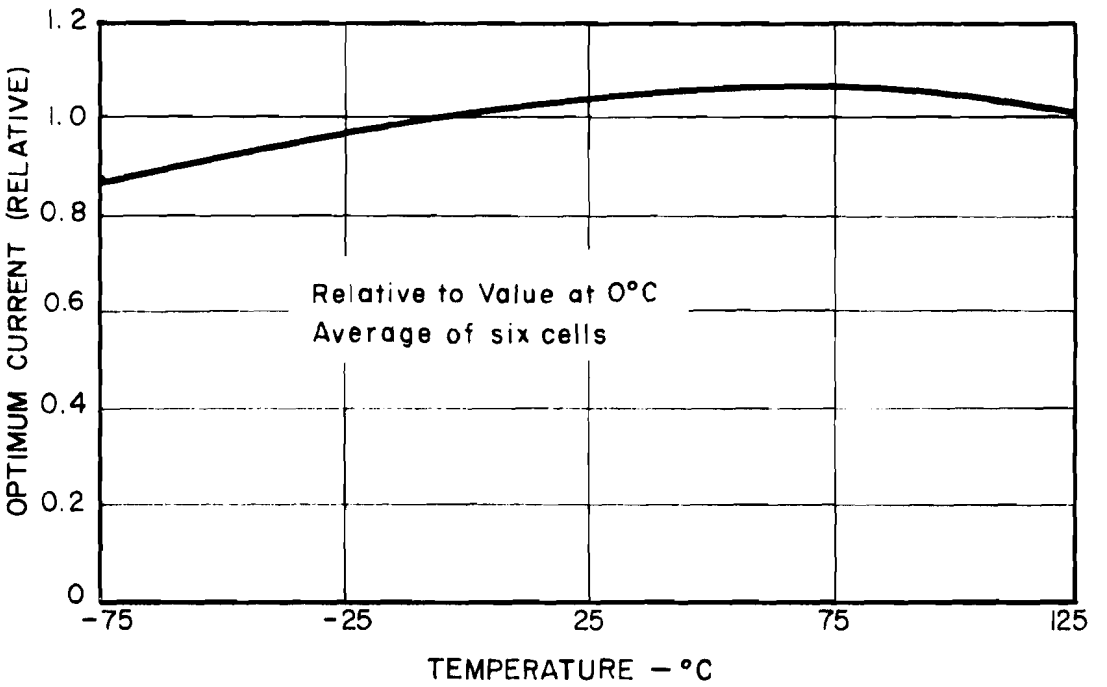

FIGURE V-A-14 OPTIMUM CURRENT VS. TEMPERATURE FOR TYPICAL SILICON CELLS

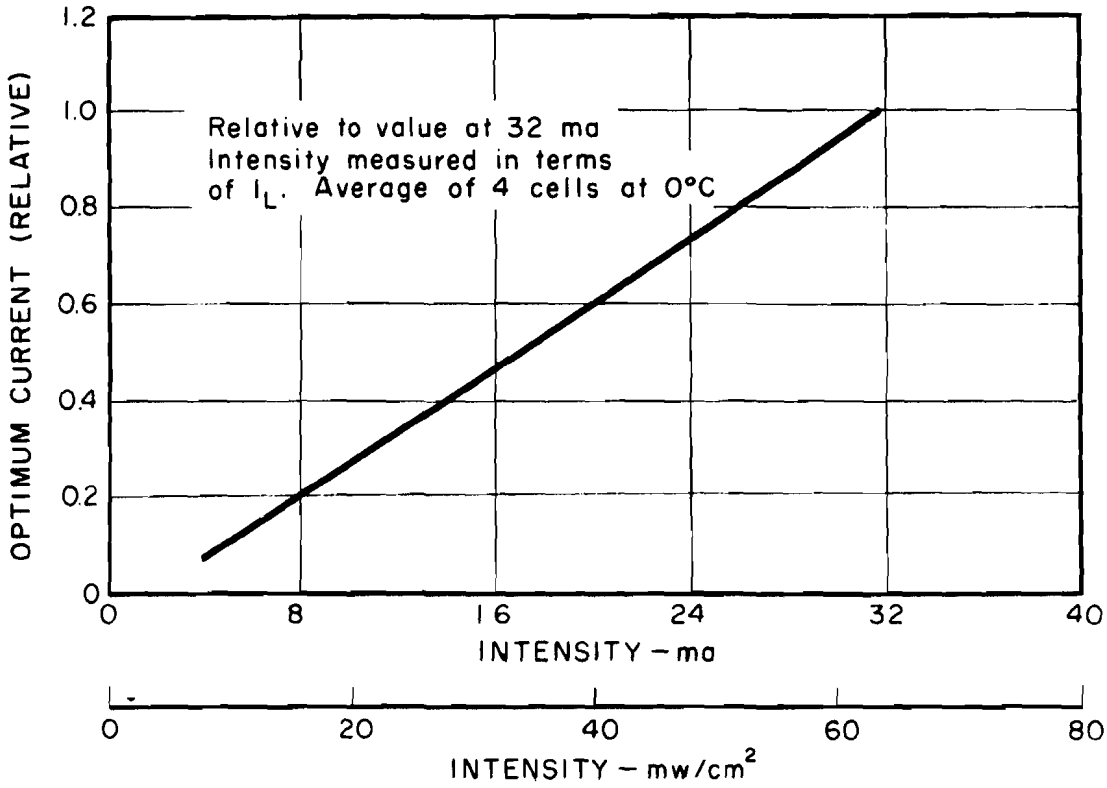

FIGURE V-A-15 OPTIMUM CURRENT VS. INTENSITY FOR TYPICAL SILICON CELLS

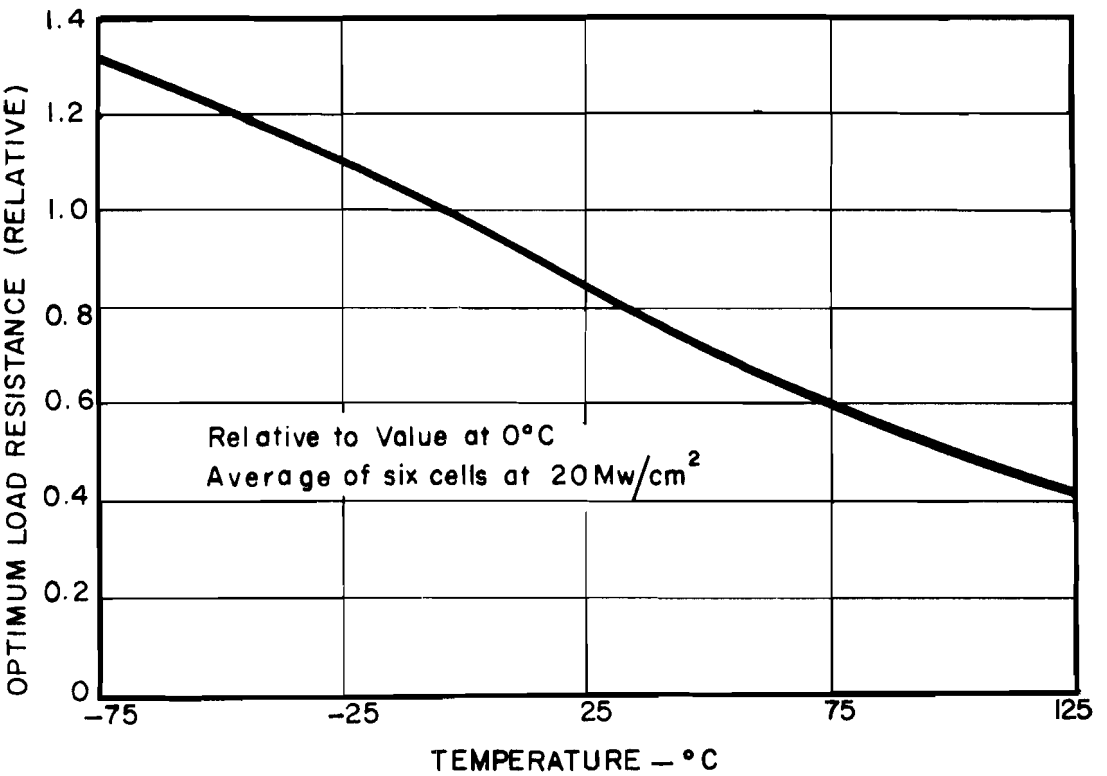

FIGURE V-A-16 OPTIMUM LOAD RESISTANCE VS. TEMPERATURE FOR TYPICAL SILICON CELLS

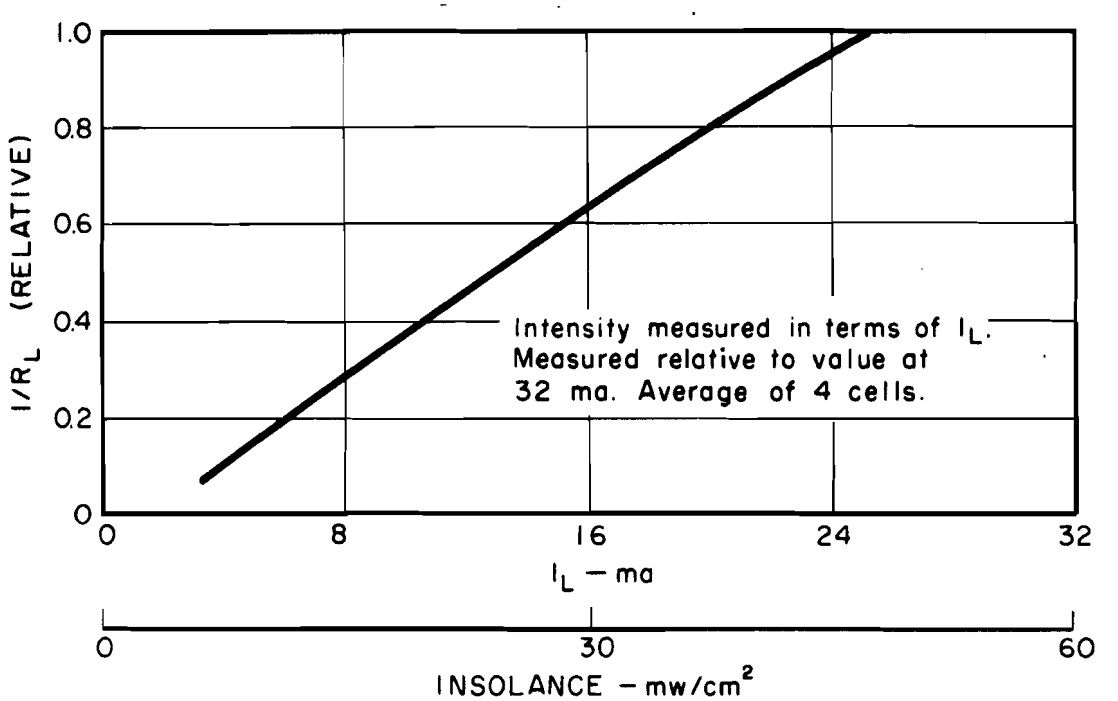

FIGURE V-A-17 OPTIMUM LOAD CONDUCTANCE VS. INCIDENT INTENSITY FOR TYPICAL SILICON CELLS

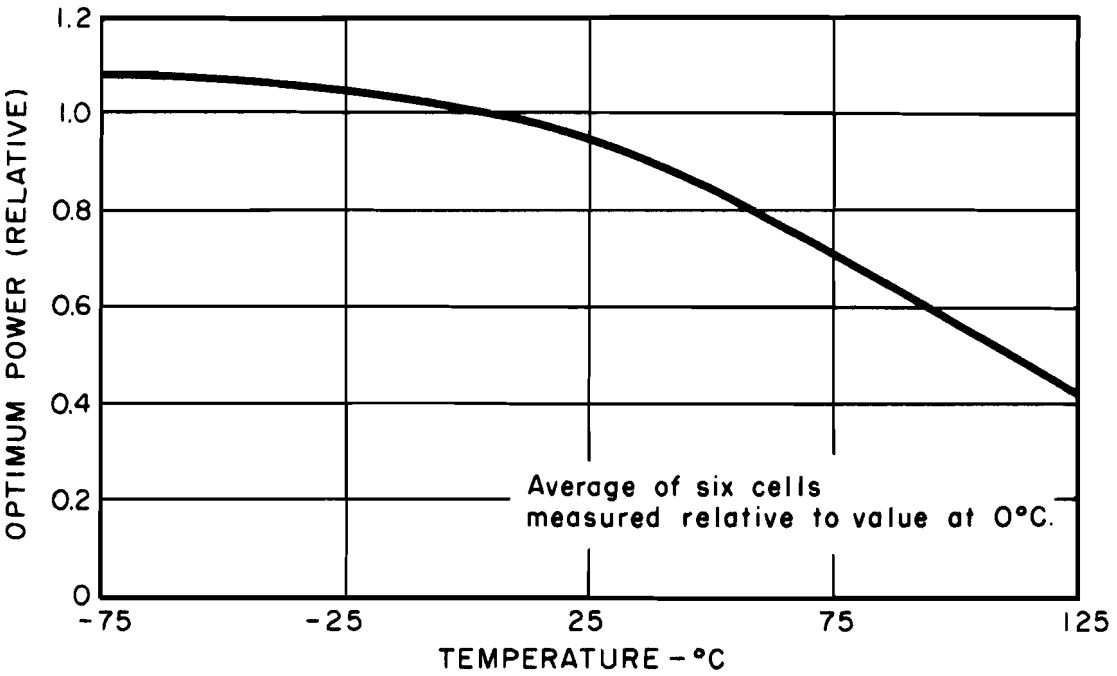

FIGURE V-A-18 OPTIMUM POWER VS. TEMPERATURE FOR TYPICAL SILICON CELLS

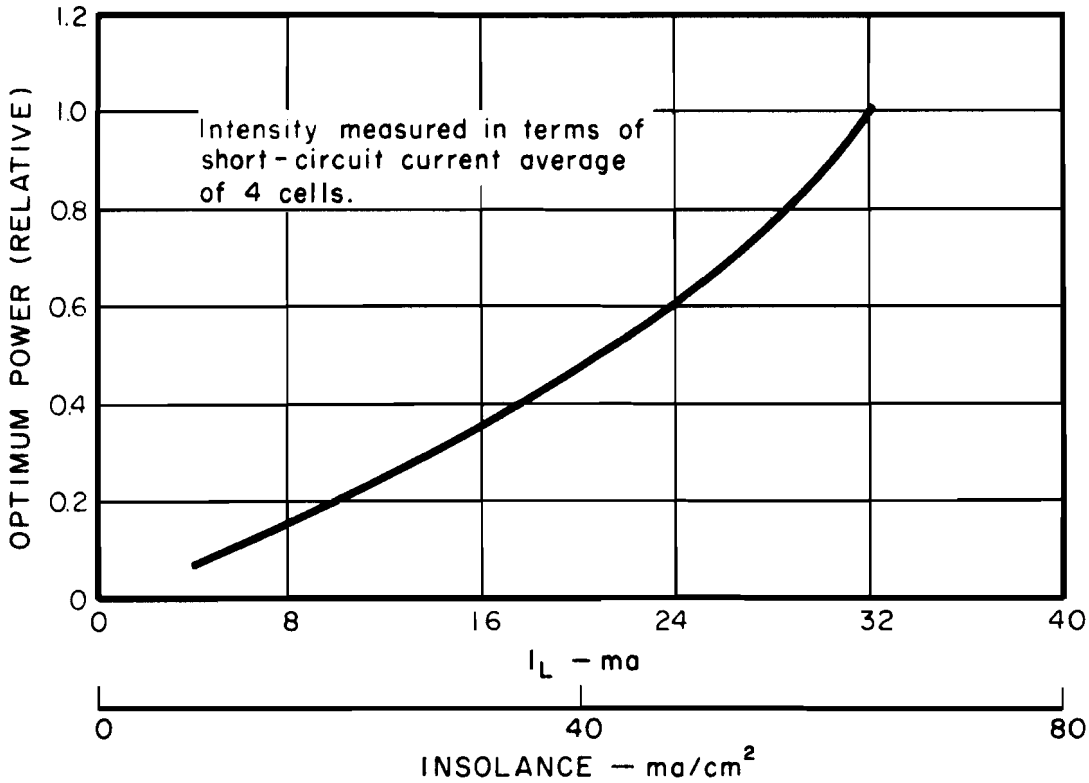

FIGURE V-A-19 OPTIMUM POWER VS. INCIDENT INTENSITY FOR TYPICAL SILICON CELLS

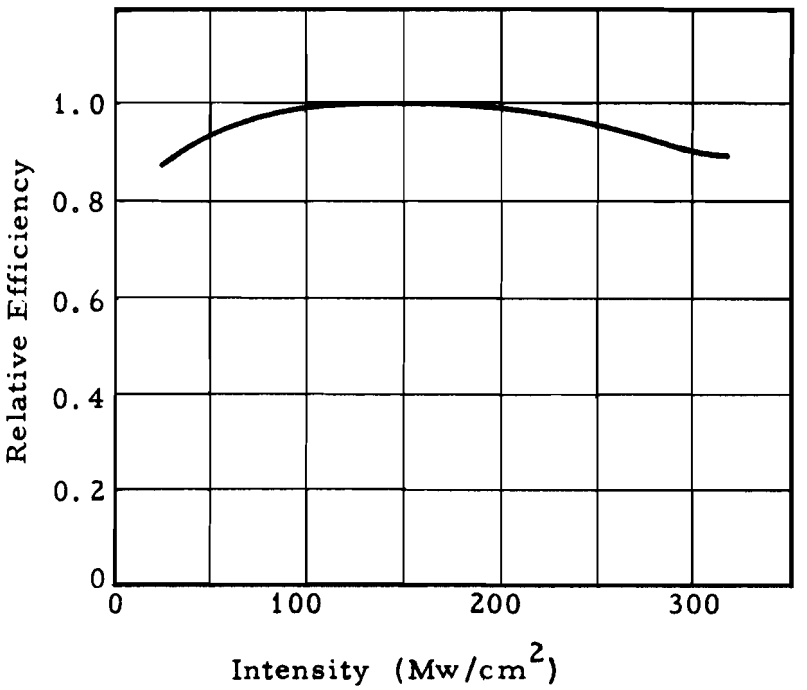

FIGURE V-A-20 EFFICIENCY VERSUS INSOLANCE FOR A TYPICAL NON-GRIDDED SILICON SOLAR CELL

solar intensity by the cosine of the angle of incidence in the case of uncoated or uncovered silicon solar cells such as Hoffman 120C or IRC 1020. In the case of spectrally coated solar cells (See subsection 2), the variation of power output with this angle of incidence has been observed to range between cos θ and $\cos^2\theta$.

The characteristics may be summed up by saying that cell efficiency degrades linearly with increasing temperature above $0^{\circ}C$ and does not change greatly with incident intensity over the range from 10 mw/cm^2 to 150 mw/cm^2. Optimum voltage does not vary greatly with incident intensity over the same range but decreases nearly linearly with increasing temperature. Although optimum current does not change greatly with temperature, it does increase nearly linearly with incident intensity.

The variations of characteristics of cells other than silicon, such as cadmium sulfide and gallium arsenide, follow a similar pattern. However, at present, only silicon solar cells are commercially available in quantity and exhibit the highest available efficiencies by a factor of two.

The characteristics of high-efficiency (12 percent or more) silicon cells do not vary greatly from cell to cell, since in these cells all the parameters affecting cell performance are near optimum. Lower efficiency cells tend to show greater variation in characteristics from cell to cell. However, by combining a number of such cells into a series array, or a parallel configuration, the variation of characteristics is averaged out. By using measured characteristics of such cell groups, rather than of single cells, more reliable designs can be made.

Since the short-circuit current of a cell is directly proportional to both the surface area of the cell and the intensity of the

incident solar radiation, it is convenient to use the short-circuit current density of a cell as a measuring parameter of the incident intensity. Also, frequently the characteristic of the cell is plotted with current expressed as a current density.

Silicon solar cells are available in a variety of sizes, shapes and types. The more widely applied forms are tabulated in Table V-A-2 with a brief discussion of their characteristics.

TABLE V-A-2

SOME SILICON SOLAR CELL TYPES

	Cell Type	Designation	Characteristics
1.	Rectangular 1 x 2 cm	Hoffman 120C IRC S1020	Most popular, easily adapted to arrays.
2.	1 x 2 with alloyed aluminum contact (from IRC)	IRC S-1020	Contact somewhat stronger than usual plated contact, but not as easy to shingle.
3.	1 x 2 cm, gridded	Hoffman 120-CG IRC S-1020	Available in higher efficiencies than Type 1.
4.	Rectangular, 1/2 x 2 cm	Hoffman 52 C IRC S-0520	Higher efficiencies than Type 1.
5.	Circular	Hoffman, 1A, 2A	Lower cost per unit area, not good for use in panels.

Although solar cells have been fabricated from intermetallic compounds such as CaAs, CdS, and CdTe, these materials have not been developed sufficiently to make such solar cells competitive in either cost or performance with silicon cells. These new materials are discussed further in subsection 7.0.

Because of the spectral response characteristics of silicon cells and the difference in the spectral distributions of solar radiation in space as compared with that on earth, efficiencies of cells measured under terrestrial solar radiation will be different from those of the cells in outer space. In general, the atmosphere tends to absorb more of the solar energy in the ultraviolet region than in the visible region. Thus, if on a given day the solar radiation intensity at sea level is one-half that in space, solar cells at sea level will receive only one-half the incident power of cells in space. However, since much of the additional power in space is in the ultraviolet wavelengths which are not efficiently utilized by silicon cells, the cells will not be as efficient in space as they are on earth. Typically silicon cells will have 0.83 of their sea level efficiency in space. However, the efficiencies quoted by manufacturers of cells usually are for performance in the spectrum of outer space.

V-A. 2.0 PHOTOVOLTAIC SYSTEMS APPLICATIONS

In this subsection, current techniques for using solar cells in systems are described,and possible future improvements are discussed.

2.1 Methods of Solar Cell Temperature Control

In the previous subsection, it was shown that the performance of the solar cells degrades significantly as the temperature increases. Therefore, it is imperative that solar cell systems be designed to operate at the lowest possible temperature consistent with mission and vehicle requirements. Temperature control may be accomplished through (1) radiation, (2) conduction, (3) convection, and (4) thermoelectric heat transfer. In general, a temperature control system will utilize more than one process, those used in satellites at present being conduction and radiation.

2.1.1 Radiation Cooling

The primary means of controlling solar cell equilibrium temperature lies in control of the radiative characteristics of the cell and panel surfaces. A development of the basic principles of thermal radiation may be found in Volume VII of this handbook.

The basic parameters of a surface determining its radiative properties are the absorptivity, $\alpha(\lambda)$, and the emissivity, $\epsilon(\lambda)$. At a particular wavelength, $\alpha(\lambda)$ is equal to $\epsilon(\lambda)$. Also the reflectance, $r_{(\lambda)}$ is equal to $1 - \alpha_{(\lambda)}$.

A plot of $r_{(\lambda)}$ versus wavelength for a typical silicon solar cell is shown in Figure V-A-21. This characteristic is readily measured with a spectrophotometer and may be immediately used to determine $\alpha(\lambda)$ and $\epsilon(\lambda)$. A total absorptivity or emissivity may be defined for any given spectral distribution using the relationship

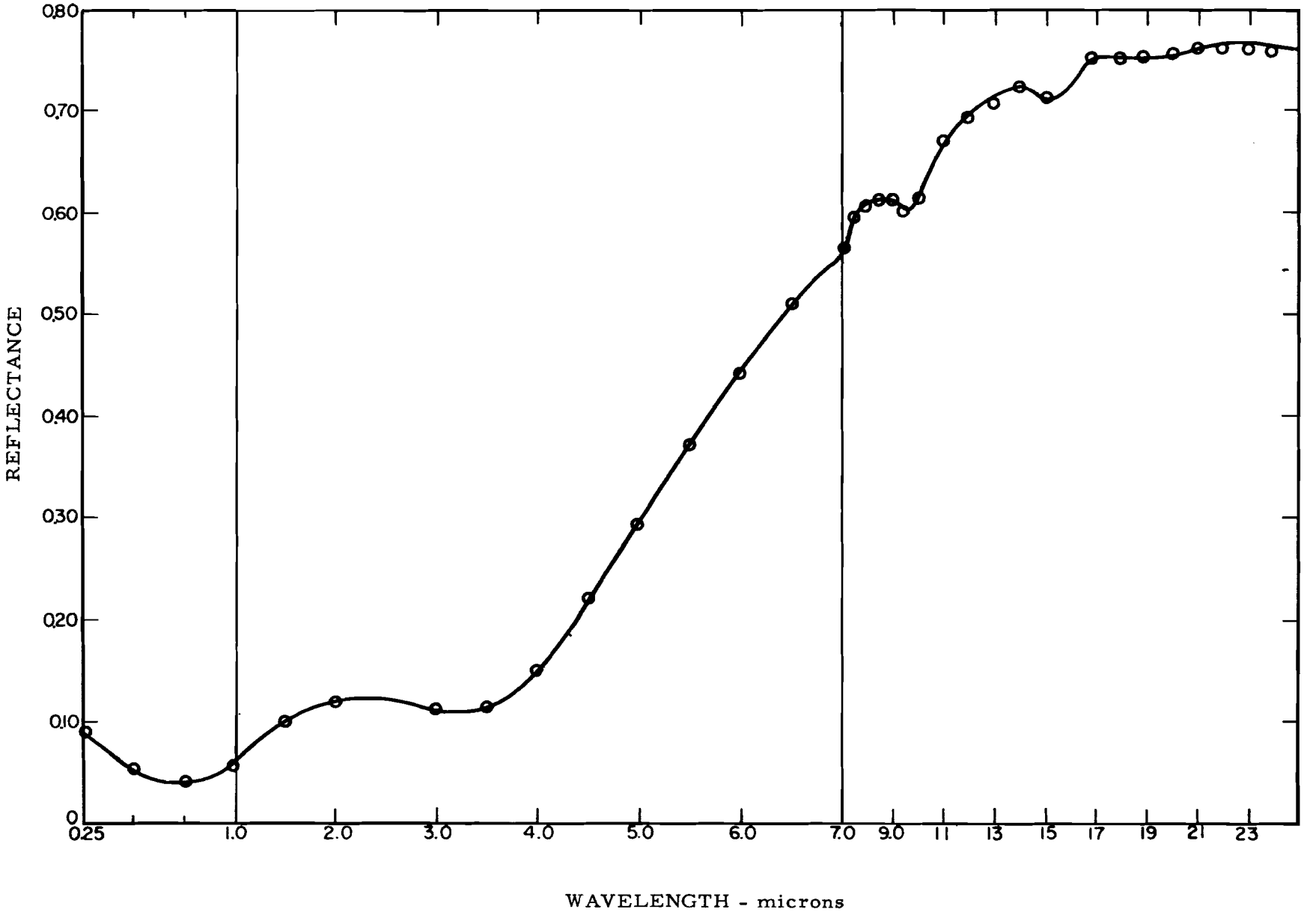

FIG. V-A-21 REFLECTANCE OF AN UNCOATED SILICON SOLAR CELL

$$\begin{matrix} \alpha \\ \text{or} \\ \epsilon \end{matrix} = \frac{\int_0^{\infty} \begin{matrix} \alpha\,(\lambda) \\ \epsilon\,(\lambda) \end{matrix} P_{(\lambda)}\, d\lambda}{\int_0^{\infty} P_{(\lambda)}\, d\lambda} \qquad \text{(A-7)}$$

where $P_{(\lambda)}$ is the total spectral power in the incremental wavelength $d\lambda$ of the incident solar spectrum for calculating α, or of the black-body spectrum for calculating ϵ. Emissivity is defined using the black-body spectrum, which is a function of temperature. Therefore, the total emissivity is itself a function of temperature. ϵ is shown in Figure V-A-22 as a function of temperature for the surface in Figure V-A-21. A plot of the solar spectrum is shown in Figures V-A-23 and V-A-24. By using this spectrum and Equation A-1, the total absorptivity of the surface in Figure V-A-21 is found to be 0.94.

The total power emitted from a surface P, may be found from

$$P = A \epsilon \sigma T^4 \qquad \text{(A-8)}$$

where A is the area of the surface, ϵ is the total emissivity at the absolute temperature, T, and σ is the Stefan-Boltzman constant, 5.67×10^{-12} watts/cm^2-$^oK^4$.

The equilibrium temperature is found by equating the total absorbed radiation with the power emitted and converted to electrical energy.

$$P_{\text{emitted}} = A\epsilon\sigma T^4 = A\,\alpha\,H - P_{\substack{\text{electrical} \\ \text{energy}}} \qquad \text{(A-9)}$$

where H = solar constant

= 1400 W/m^2 outside the earth's atmosphere.

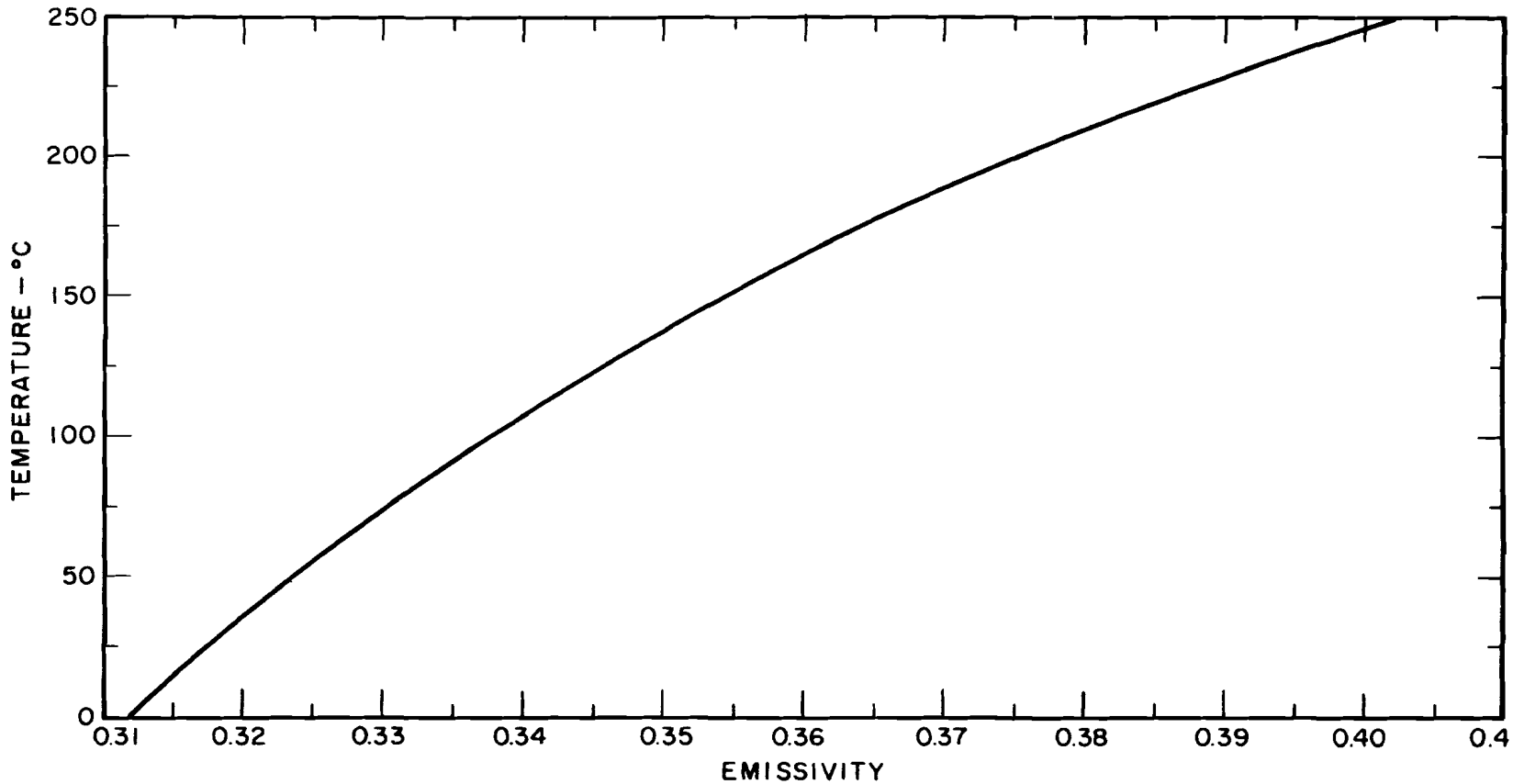

FIGURE V-A-22 SOLAR CELL EMISSIVITY AS A FUNCTION OF TEMPERATURE

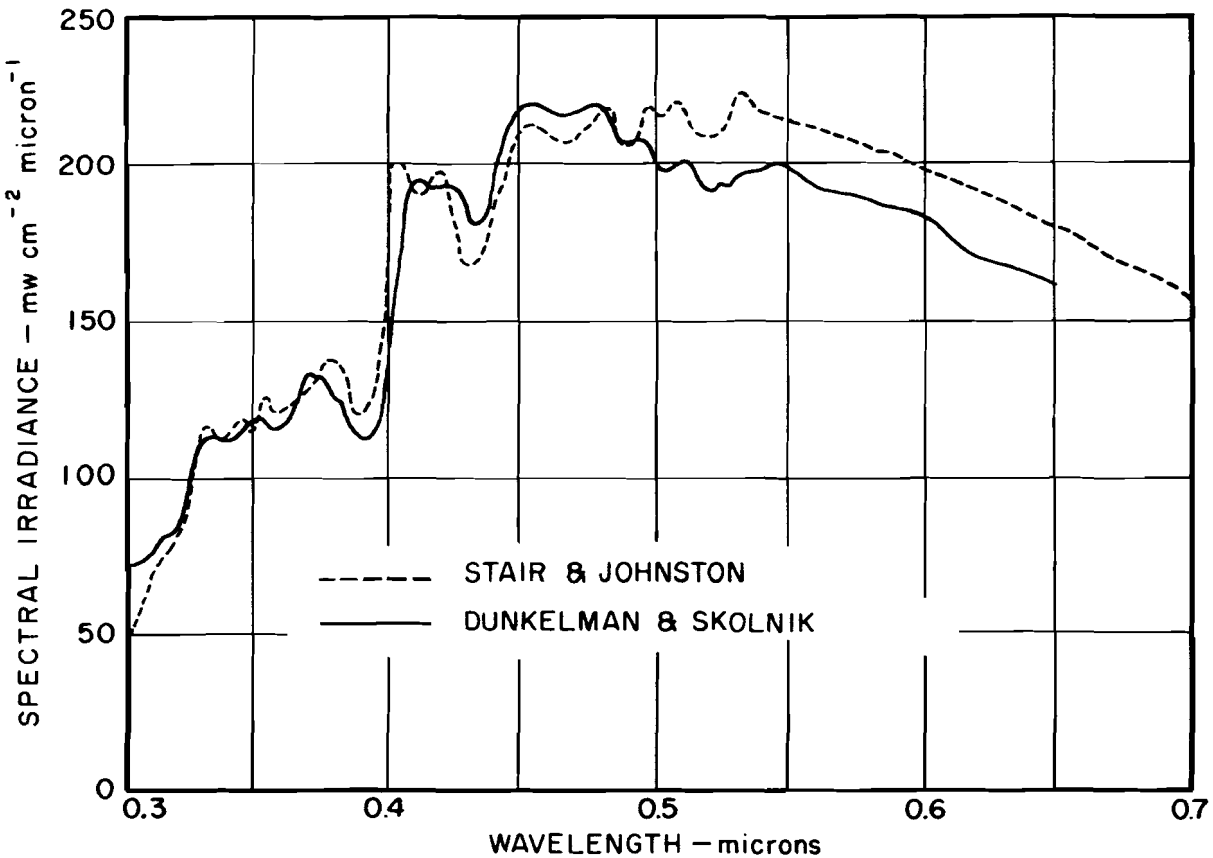

FIGURE V-A-23 SOLAR SPECTRUM BELOW 7 MICRONS OUTSIDE EARTH'S ATMOSPHERE

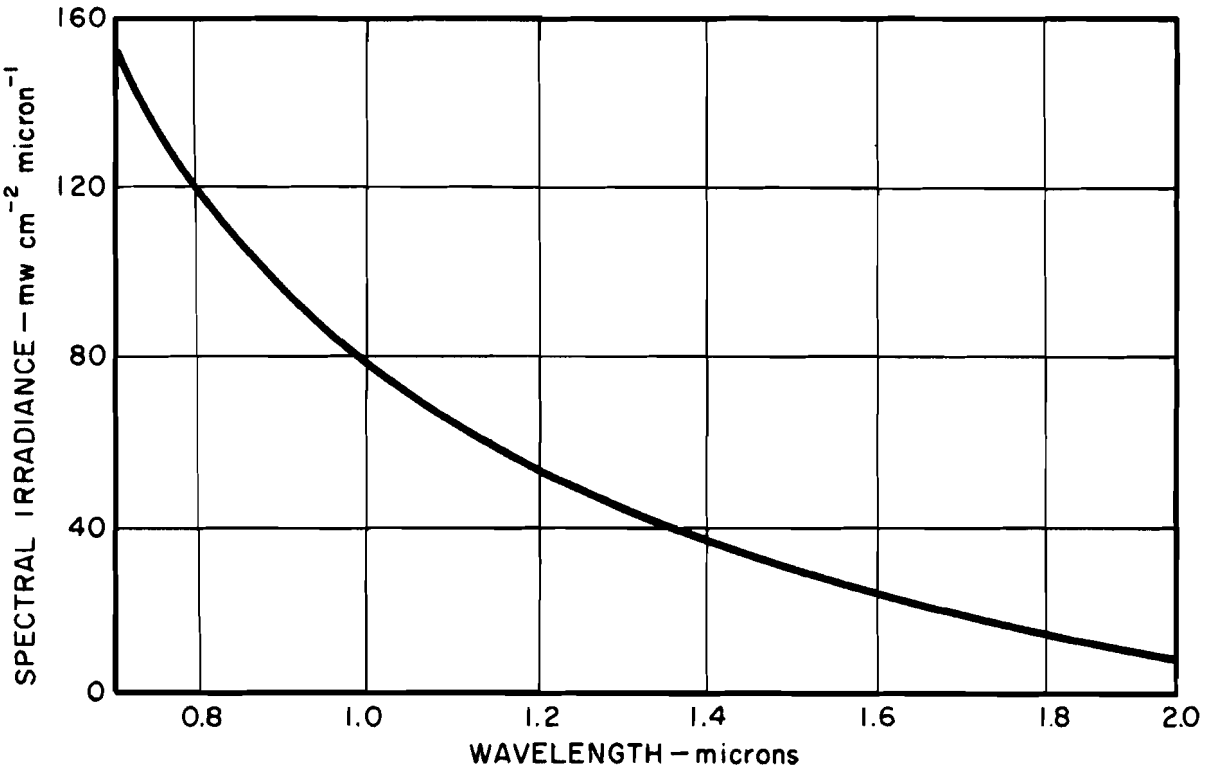

FIGURE V-A-24 SOLAR SPECTRUM BEYOND 7 MICRONS OUTSIDE EARTH'S ATMOSPHERE

In general, a space vehicle will consist of several surfaces, oriented at various angles to the sun, with different values of α and ϵ. A number of general forms of Equation A-9 may be written, neglecting the small amount of useful electrical energy, such as

$$\sum_n A_n \epsilon_n \sigma T^4 = \sum_m A_m \alpha_m H \cos \theta_m \qquad \text{(A-10)}$$

where the r^{th} surface has total absorptivity α_r and emissivity ϵ_r at the absolute temperature T and is oriented at the angle θ_r to the sun.

2.1.2 Conduction Cooling

Thermal conduction enters into photovoltaic temperature control when considering heat flow from the cells to a supplementary reradiating surface. The amount of heat which is conducted is

$$q = \Delta T \frac{A k}{t} \qquad \text{(A-11)}$$

where

ΔT = temperature drop across a body
q = heat flux through the body
t = thickness of the body
A = area
k = thermal conductivity.

2.1.3 Convection and Thermoelectric Heat Transfer

It has been suggested that thermoelectric heat transfer and convective heat transfer to external radiators could be used to cool solar cell panels. At this time, it appears that such techniques show little or no promise of a net weight reduction. It is conceivable that cooling of photovoltaic panels by convection of heat to radiators might be used to reduce the required cell area and over-all vehicle expense. Considerations in the design of liquid cooling systems are discussed in Volume VII of this handbook.

2.1.4 Spectral Temperature Control Techniques

The cell temperature is decreased by minimizing α and maximizing ϵ. Modification of the spectral characteristics of the cell surface may be accomplished by applying multilayered interference coatings on the surface. At the present time, coatings with characteristics similar to that shown in Figure V-A-25a are used. This coating is designed to (1) reflect incident radiation of wavelengths shorter than a cutoff wavelength usually set between 0.4 and 0.5 microns, (2) absorb practically all radiation in the response region of the solar cell, and (3) emit a maximum amount of the black body radiation at the equilibrium temperature of the cell.

These coatings, to date, have been coated on thin (3 to 6 mil) glass slides which were fastened to the cell surface. It is quite feasible to apply such coatings directly to the cell surface. However, it now appears that this technique will not be employed because (1) the cover glasses do not degrade cell performance significantly more than direct coatings, (2) there is a possibility of much higher breakage expense in coating onto cells directly, and (3) the cover glasses offer some significant environmental protection.

Recently, an improved coated cover glass has been developed which reflects much of the incident radiation between the wavelengths 1.0 microns and 2.0 microns. This region contains almost all of solar radiation whose wavelength exceeds that of the solar cell response. The characteristic of such an available spectral surface is shown in Figure V-A-25b. Clearly this is still not an ideal coating and could be improved to approach the optimum shown in Figure V-A-25c. The filter absorptivities to the solar spectrum shown in Figures V-A-25a, V-A-25b, and V-A-25c are 0.8, 0.75, and 0.58, respectively. The emissivity shown in Figures V-A-25a and V-A-25b is approximately 0.9 and in Figure V-A-25c is 1.0 at the temperatures of interest.

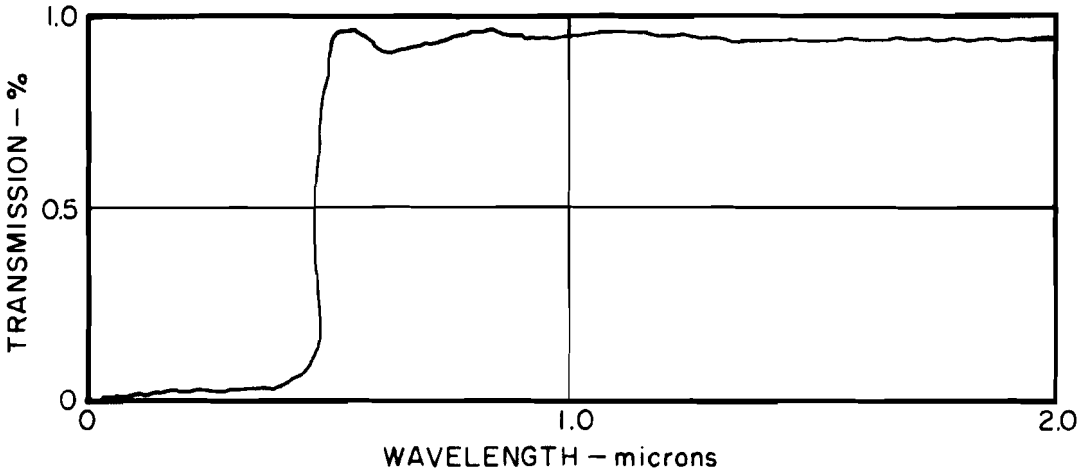

FIGURE V-A-25a TRANSMISSION OF AVAILABLE BLUE FILTER

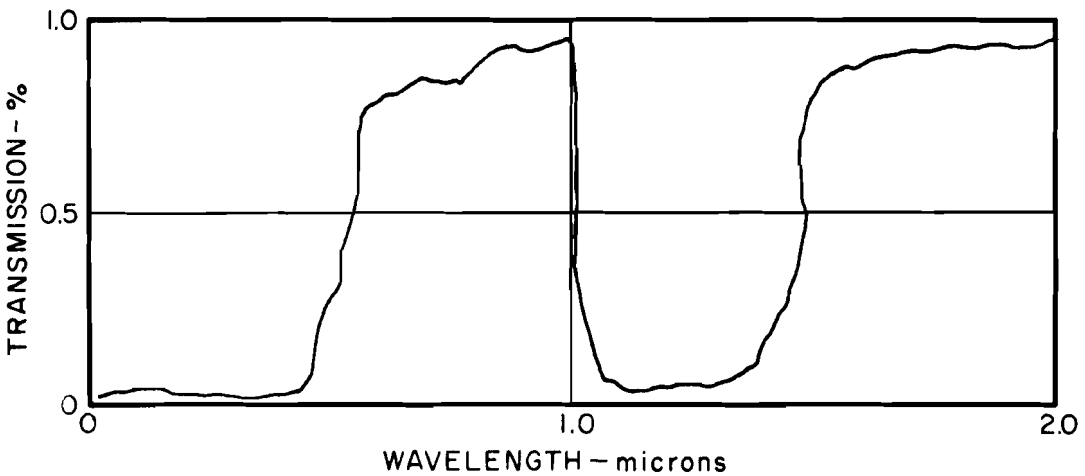

FIGURE V-A-25b TRANSMISSION OF AVAILABLE RED-BLUE FILTER

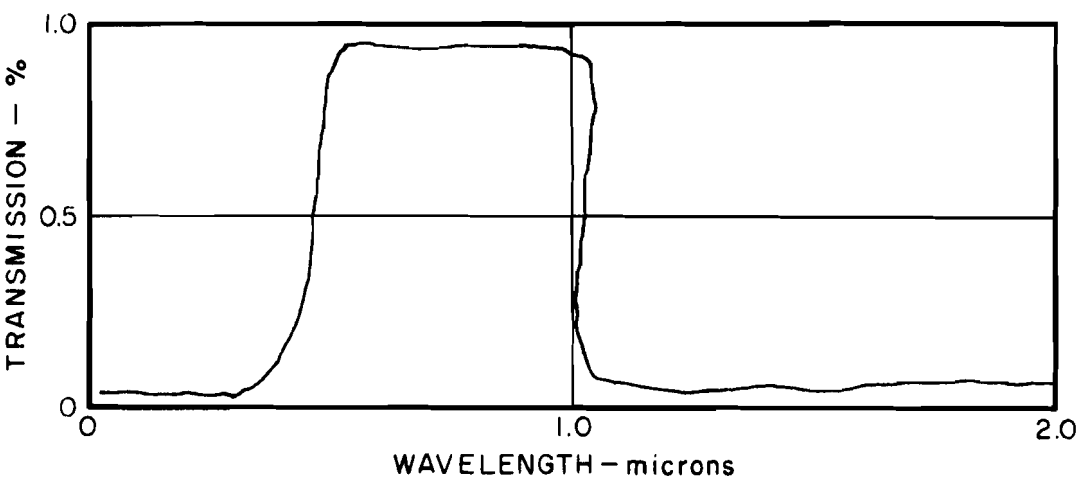

FIGURE V-A-25c TRANSMISSION OF OPTIMUM FILTER

Spectrally coated glass covers of the types described here are currently available from Optical Coating Laboratories in Santa Rosa, California and Spectrolab, Inc., in North Hollywood, California.

The emissivity of SiO coated solar cells is shown in Figure V-A-26. The total emissivity of these cells at temperatures around 300°K is 0.7. However, their absorptivity is similar to that of the noncoated cells. Such cells have been available from Texas Instruments.

If the cells are connected conductively to a good emitting surface, their temperature can be significantly lowered. A variety of materials can be used to provide emissivities of 0.95 or greater at the temperatures of interest. If, at the same time, the surface is exposed to direct solar radiation, it would be profitable to coat the surface with a vacuum deposited interference filter of the type described above, which reflects nearly all radiation up to 2 microns and emits nearly all black body radiation of longer wavelengths.

Spectrally reflective filters will typically increase solar cell efficiency under one sun (140 mw/cm^2) by 30 percent or more. Typically, coated glass covers of the type shown in Figure V-A-25a cost, when purchased in quantity, approximately $1.00 each, or 10 to 20 percent of the cell cost. Thus, they may be justified on the basis of decreased cell cost alone without even considering decreased collector and vehicle weight. Coatings of the red-blue type shown in Figure V-A-25b, cost two to four times as much as those of the blue type but can be justified for many applications where the insolance is great or where a moderate additional collector weight decrease is of great enough value.

2.1.5 Typical Equilibrium Temperature Calculations

In this subsection, several typical solar cell panel configurations will be analyzed in order to determine their equilibrium operating temperatures, and some of the design implications of these analyses will be given.

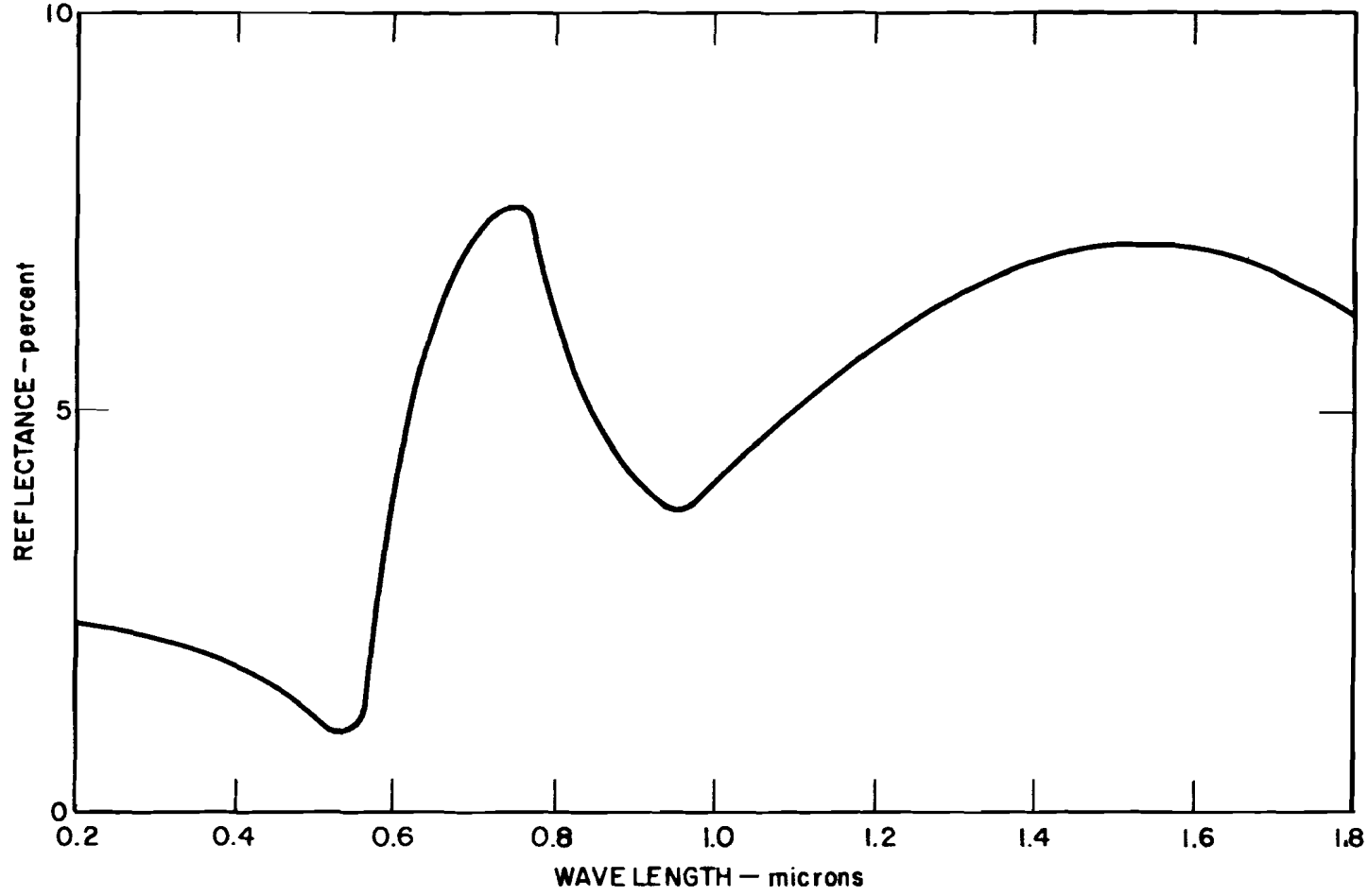

FIGURE V-A-26 REFLECTANCE CHARACTERISTIC OF A TEXAS INSTRUMENT SiO_2 COATED SILICON SOLAR CELL

2.1.5.1 Oriented Solar Panels

Consider a panel oriented normal to the solar flux and covered on the front surface with an area, A, of cells--the remaining area, A_2, being bare. The back surface is of area, A_3, with a uniform emissivity of ϵ_3. The absorptivity and emissivity of the cells (which may be spectrally covered) and of the uncovered area are α, ϵ, and α_2, ϵ_2, respectively. Therefore, if the solar constant is H and the actual incident intensity on the panel is NH, the energy absorbed is

$$E_{in} = NH\left[\alpha_1 A_1 + \alpha_2 A_2\right] = NH\,\alpha' A \tag{A-12}$$

where

$$\alpha' = \frac{\alpha_1 A_1 + \alpha_2 A_2}{A_1 + A_2} \quad \text{and} \quad A = A_1 + A_2 = A_3 \tag{A-13}$$

The energy emitted is:

$$E_{out} = \sigma\left[\epsilon_1 A_1 T_1^4 + \epsilon_2 A_1 T_1^4 + \epsilon_3 A_3 T_2^4\right] \tag{A-14}$$

where

T_1 = temperature of the front surface (assumed uniform)

T_2 = temperature of the back surface.

Now the temperature difference between the back and front surface is determined by Equation A-10. The heat flow through the panel, q, is simply equal to the heat radiated from the back surface, thus

$$T_1 - T_2 = \frac{q\,t}{A\,k} = \frac{\sigma \epsilon_3 T_2^4\, t}{k} \tag{A-15}$$

From Equations A-12 and A-14

$$NH\,\alpha' A = \sigma A\left[\epsilon' T_1^4 + \epsilon_3 T_2^4\right] \tag{A-16}$$

where

$$\epsilon^1 = \frac{\epsilon_1 A_1 + \epsilon_2 A_2}{A_1 + A_2}.$$

The equilibrium temperature of a flat panel may now be found by plotting Equations A-15 and A-16, as is done in Figure V-A-27. The curves are general plots of Equation A-16 using coordinates of $\left(\epsilon^1\right)^{-1/4}(T)$. The lines are plots of Equation A-15 for the case $\epsilon^1 = \epsilon_3 = 1.0$ but hold fairly well for values of greater than 0.8.

Therefore, consider a panel in which the upper surface is covered over 75 percent of its area with spectrally coated cells and the uncovered area is spectrally coated. In this case, let $a_1 = 0.7$, $a_2 = 0.1$ and $\epsilon_1 = \epsilon_2 = \epsilon_3 = 0.9$. Then $a^1 = 0.55$, and $\epsilon^1 = 0.9$. Assume further that the panel is fabricated with a honeycomb substrate having a thermal resistance per unit area of 300 $cm^2\ ^oC\ watts^{-1}$ while the adhesives add another 100 $watts^{-1}\ cm^2\ ^oC$ in series. Then, from Figure V-A-27, if N = 1.0 and $a = 0.55$, $\left(\epsilon^1\right)^{-1/4} T_1 = 288^oK$, and $\left(\epsilon_3\right)^{1/4} T_2 = 280^oK$. Thus, T_1 is 22^oC while T_2 is 14^oC.

From Figure V-A-27, the effects of increasing or decreasing N, a, ϵ^1, ϵ, or R^1 may be readily determined. R^1 is the thermal resistance between the focus of the panel in $cm^2\ ^oC\ watt^{-1}$.

All the photovoltaic power supply systems that have performed successfully to date have been of the nonoriented type. Solution of the equilibrium temperature of such vehicles can be extremely complicated if the transient nature of the incident flux is included in the temperature balance equations. However, the solar cell panel can usually be approximated in one of two ways: (1) it does not rotate, so that the solar flux may be assumed constant at each position of incidence and no transient effects need be considered, and (2) it rotates rapidly, so that transient effects are small and the solar incidence may be integrated over an entire cycle of rotation.

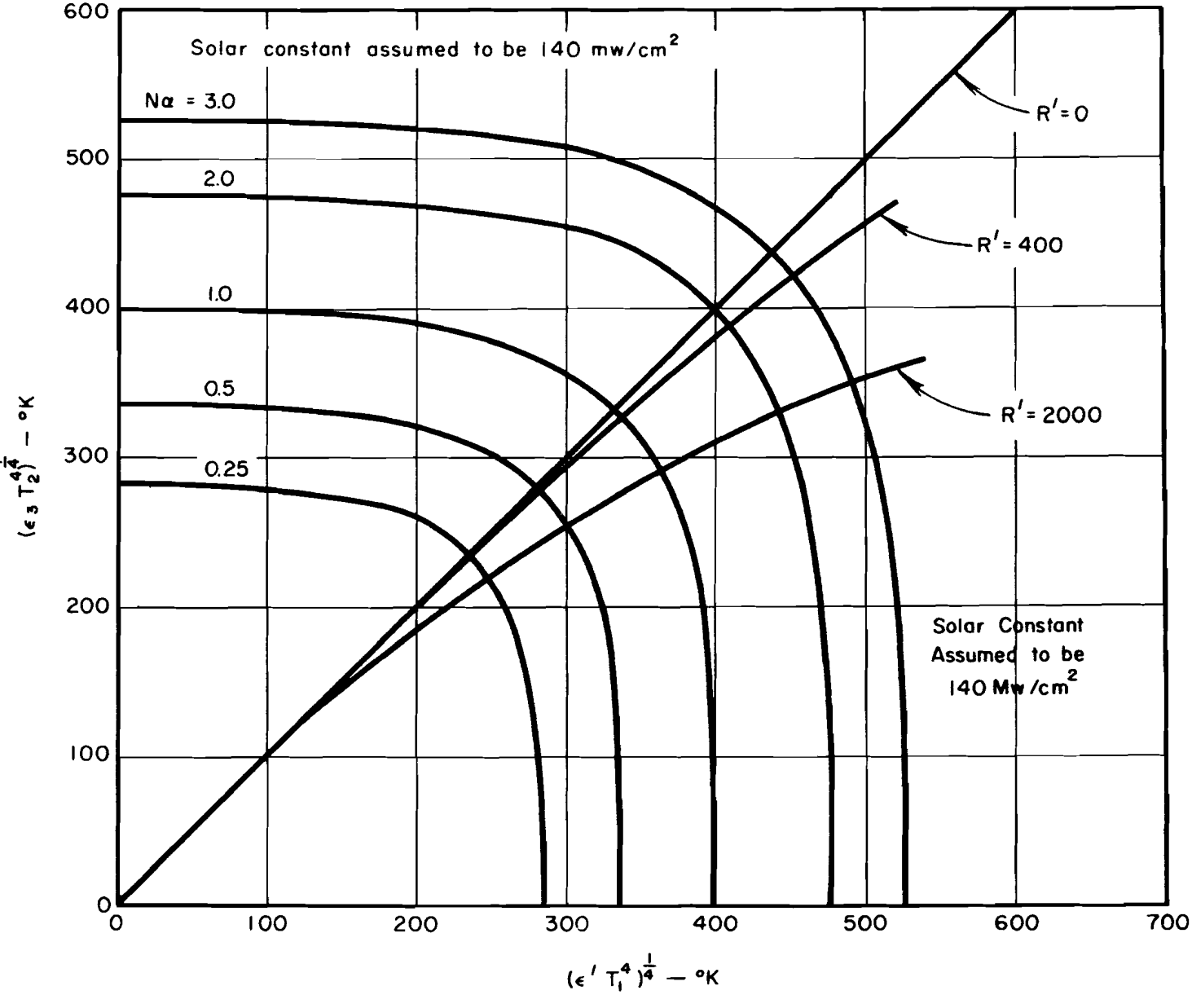

FIGURE V-A-27 TEMPERATURES OF THE SURFACES OF AN ORIENTED PANEL

Solution of the first type of problem is done in a fashion analogous to that of the oriented panel. The total absorbed power on the surface is calculated and balanced with the total emitted power minus the power converted into electrical output.

Thus, consider the vehicle shown in Figure V-A-28, essentially a cylinder covered on the top and side with solar cells. This form of configuration was used in the Tiros payload but was, however, slowly rotating. Since, in Tiros I, the substrate of this vehicle was not an efficient conductor of heat, temperature gradients existed, and the calculations became quite complex. Assume, for this example, that the substrate is a sufficiently good thermal conductor so that a uniform temperature may be assumed over the vehicle. The angle θ_H is the angle of solar incidence. Then the incident power on the top surface is

$$P_{top} = H \pi R^2 \cos \theta_H \qquad \text{(A-17)}$$

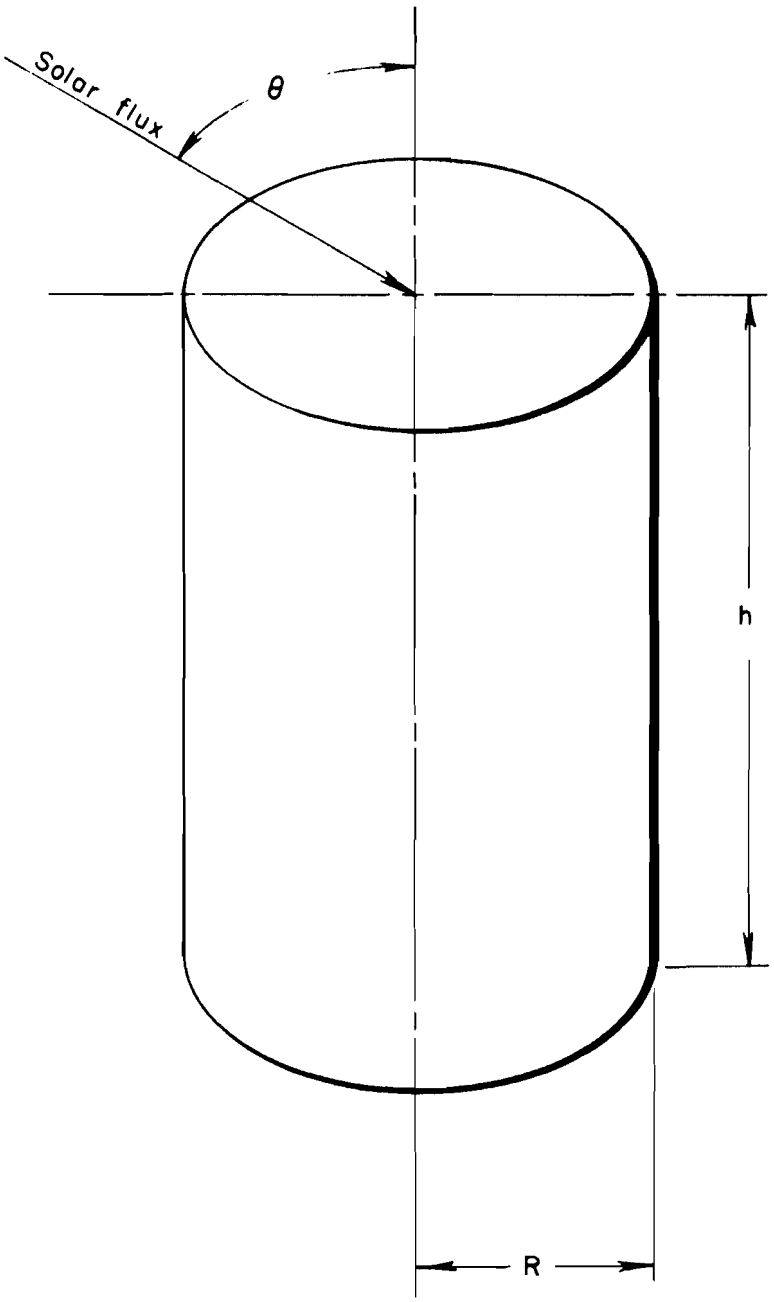

FIGURE V-A-28 A CYLINDRICAL SOLAR COLLECTOR

and on the sides is

$$P_2 = H\ 2hR \sin \theta_H. \qquad \text{(A-18)}$$

Assume that the area is 80 percent covered with coated solar cells of absorptivity (assumed not to vary with θ_H) 0.75 and 20 percent covered with coated metal of absorptivity 0.1. Since the cells convert 10 percent of the incident power into electrical power, it is convenient to account for this by considering α to be 0.65 instead of 0.75. The power absorbed is, then

$$P_{in} = H \left[\pi R^2 \cos \theta_H + 2hR \sin \theta_H\right] \left[0.65\ (0.80) + 0.10\ (0.20)\right]. \qquad \text{(A-19)}$$

The emitting area is assumed to be of uniform emissivity 0.90 including the bottom surface. Thus, the emitted power is

$$P_{out} = \epsilon \sigma T^4 \left[2\pi R^2 + 2\pi Rh\right] \qquad \text{(A-20)}$$

By equating A-19 and A-20, the temperature may be found.

A first improvement on the calculations would be to consider that the dark part of the vehicle is at a lower temperature than the irradiated part. With a vehicle which rotates, such as the Tiros, the temperature distribution will tend to be uniform with respect to the axis of rotation.

Consider, now, a general collector of the second type, rotating such that the elements receive constantly varying intensities of radiation. An example is a vehicle of the "paddlewheel" configuration as shown in Figure V-A-29.

From above, a paddle appears rotated an angle α with respect to the spin axis, while the shaft of the blade makes an angle β

with the horizontal and the solar incidence is normal to a plane which makes an angle γ with the spin axis. The angle describing the spin of the vehicle about the spin axis is θ.

Therefore, to find the total area normal to the solar flux, it is only necessary to project the total panel area onto a plane normal to the flux.

Projecting the area of one blade onto the x, y, and z planes,

$$A_x = A \cos \alpha \cos \beta$$

$$A_y = A (\cos \alpha \sin \beta \sin \theta + \sin \alpha \cos \theta)$$

$$A_z = A (\cos \alpha \sin \beta \cos \theta + A \sin \alpha \sin \theta).$$

Projecting these components onto the plane normal to the solar incidence,

$$A_n = A(\cos \alpha \sin \beta \cos \gamma \cos \theta) + A(\sin \alpha \cos \gamma \sin \theta + \cos \alpha \cos \beta \sin \gamma).$$

The effective area throughout one rotation is

$$A_{eff} = \frac{\int_o^{2\pi} A_n (\theta)\, d\theta}{\int_o^{2\pi} d\theta} = A \left[\frac{\sin \alpha \cos \gamma}{\pi} + \cos \alpha \cos \beta \sin \gamma \right].$$

This function has a minimum or maximum at

$$\text{Tan } 2\gamma = \frac{2 \pi \sin \alpha \cos \alpha \cos \beta}{\sin^2 \alpha - \pi^2 \cos^2 \alpha \cos^2 \beta}.$$

The paddlewheel vehicles, Pioneer V and Explorer VI, used $\alpha = 60^\circ$ and $\beta = 22.5^\circ$ for two of the paddles and $\alpha = 60^\circ$ and $\beta = -22.5^\circ$ for the other two. The resultant effective projected area is calculated

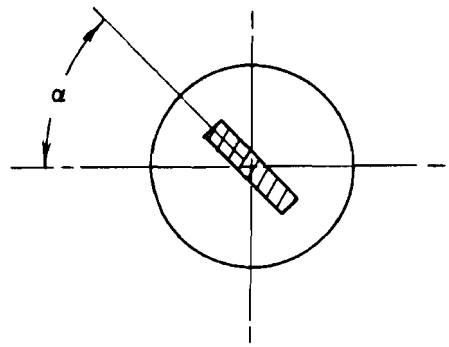

ⓐ LOOKING DOWN ON A BLADE

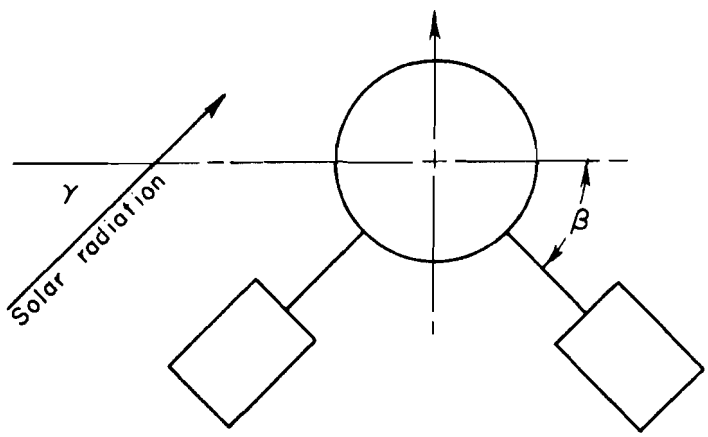

ⓑ LOOKING ONTO A PLANE IN THE AXIS OF SPIN

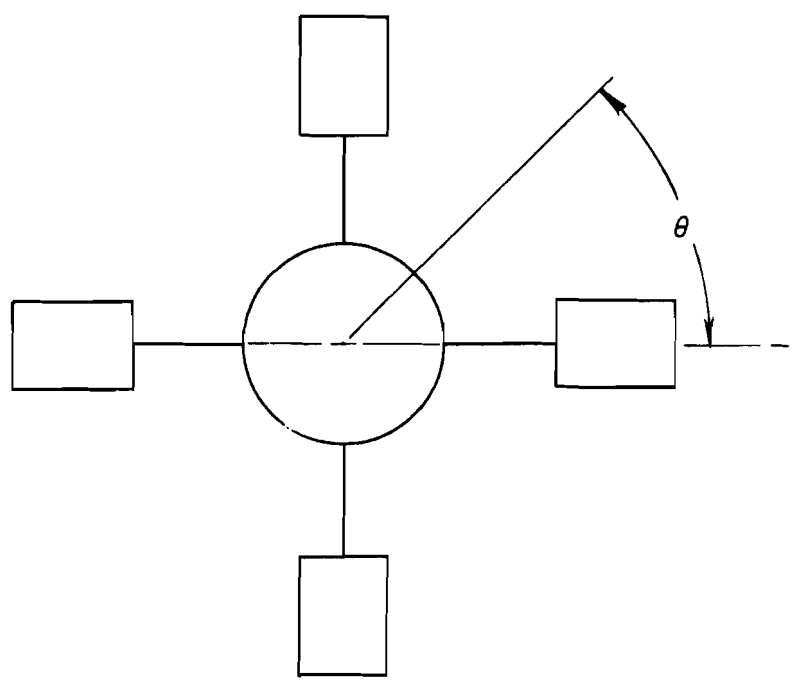

ⓒ LOOKING ONTO A PLANE NORMAL TO THE AXIS OF SPIN

FIGURE V-A-29 THE PADDLEWHEEL GEOMETRY

as above, except that effects of shadowing by the paddles and the vehicle are considered. It can be shown that, for all solar altitudes, the equivalent normally oriented cell area is near 0.25 of the total area.

If the absorptivity of the cells is assumed to be 0.65 (including the effect of electrical output), the absorptivity of the uncovered area (75 percent of the panel area) is assumed to be 0.1, and the emissivity of both regions is assumed to be 0.9, the equilibrium temperature is readily calculated. Thus, using Equations A-10 and A-11 with N equal to 0.50, α^1 equal to 0.51, ϵ^1 equal to 0.9, and R^1 equal to 300 cm^2 $watts^{-1}$ ^oC, it is seen that the temperature is 245^oK or -28^oC. Note that this very low temperature results from the small amount of the total area in direct sunlight and the favorable α/ϵ ratio of the uncovered area.

2.2 Geometry of Solar Cell Array as Related to Orientation and Mission

The geometry of a solar cell array must be selected on the basis of many, often conflicting, requirements. Oriented solar collectors obviously represent the most sophisticated mode of operation while requiring the least number of solar cells to supply a stated power output. On the other hand the engineering problems in making an oriented system reliable over an extended time are highly involved. Nonoriented systems with elaborate, erected solar collectors offer a compromise in collector size for improved reliability. The simplest system of all is that in which cells are simply fastened to the skin of the vehicle, thus requiring no orientation or erection.

2.2.1 Orientation vs. Nonorientation

In a nonoriented geometry at least four times the total cell area of an oriented geometry is required to project a stated cell area normal to the solar incidence. However, nonoriented systems generally have lower equilibrium temperatures than do oriented systems. Therefore, a nonoriented geometry would require closer to three, rather than four, times the number of cells required for an oriented geometry. The following list indicates the geometries of several vehicles, together with commentary on the configuration characteristics.

Vehicle	Geometry	Comments
Vanguard I	Cells mounted on surface of the spherical payload.	First vehicle designed, still operating.
Explorer VI	Nonoriented "paddle-wheel" configuration.	Permits temperature of payload to be independent of panels. Requires erection operation in space.

Vehicle	Geometry	Comments
Tiros I	Nonoriented, cell mounted on cylindrical payload vehicle.	Design for maximum simplicity, no erection, limited temperature control, nonuniform temperature distribution, no erection.
Transit I	Nonoriented, cells mounted on a band around the "equator" of a spherical payload.	Cell location severely constrained by antenna configuration in payload. Limited temperature control, no erection.
Midas	Partially oriented, cells mounted on unfolding panels.	Good temperature control, requires orientation about one axis, and erection in space.
Explorer VII	Nonoriented, cells mounted on vehicle skin (Figure V-A-30).	Limited temperature control, no erection.
Ranger	Oriented, large flat panels, used for space probes.	Sophisticated design, minimizes cell area, requires orientation about two axes and erection, not designed for satellite use, only for space probes. Good temperature control.
Advent and Steer	Oriented flat panels as shown in Figure V-A-31, earth satellite.	Required orientation of both panels and antenna. Good temperature control, erection required, most advanced design.

2.2.2 Determination of Over-all Collector-Converter Characteristics During a Mars Mission

A complete specification of the current-voltage characteristics of the collector-converter system at each point of a mission is desirable for most efficient design of the storage and regulation circuitry. Determination of these

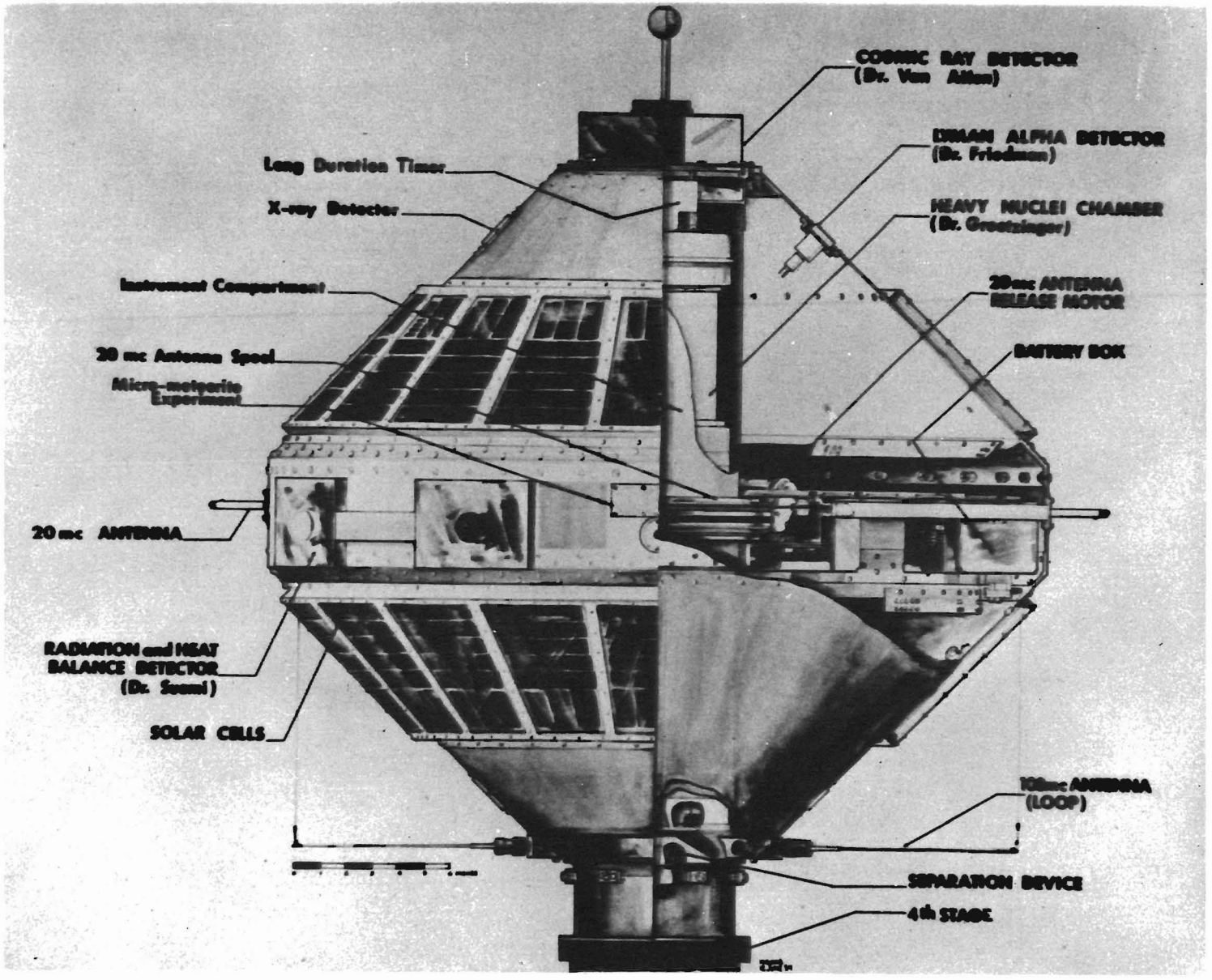

FIGURE V-A-30 RADIATION SATELLITE

A partial cutaway drawing of the composite radiation satellite showing cosmic ray detector, heavy nuclei chamber, X-ray detector, antennas, solar cells, etc.

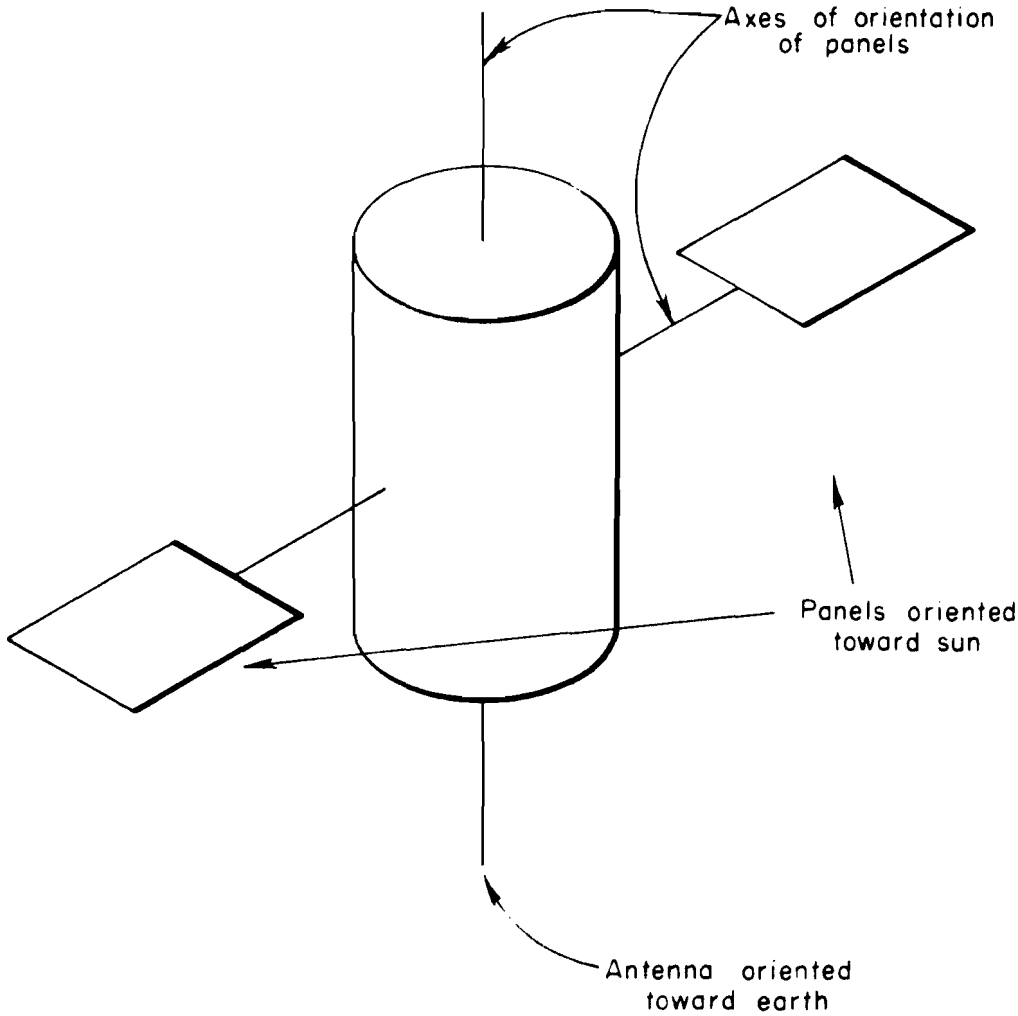

FIGURE V-A-31 THE ADVENT AND STEER CONFIGURATION

characteristics requires prior knowledge of the conditions of insolance, orientation, and cell temperature throughout the mission, together with data on the performance of the cells with respect to temperature and incident intensity. The following procedure is suggested:

a. Specify the insolance as a function of the location during the mission.

b. Determine the cell orientation and specify the total normally projected insolance on the cell surface.

c. Using the thermal characteristics of the payload, determine the equilibrium temperature of the cells throughout the mission.

d. Use the known characteristics of the cells to derive the current-voltage curves of the cells at each point of the mission.

e. Given the circuitry of the cells, determine the total current-voltage characteristic of the collector-converter appearing across the electrical load.

f. From the known characteristics at the load, specify the power output of the collector-converter.

For example, consider a system designed to power the payload of a deep space probe whose mission will carry it to the vicinity of Mars, i.e., into a region where the insolance is much lower than at earth. Orientation equipment on the vehicle keeps the cells facing normal to the solar flux at all times.

The assumed variation of solar flux intensity with respect to position during this mission is shown in Figure V-A-32. The panels are assumed to be flat, totally covered with solar cells coated with a filter of the type shown in Figure V-A-25a. By using the procedures previously discussed,

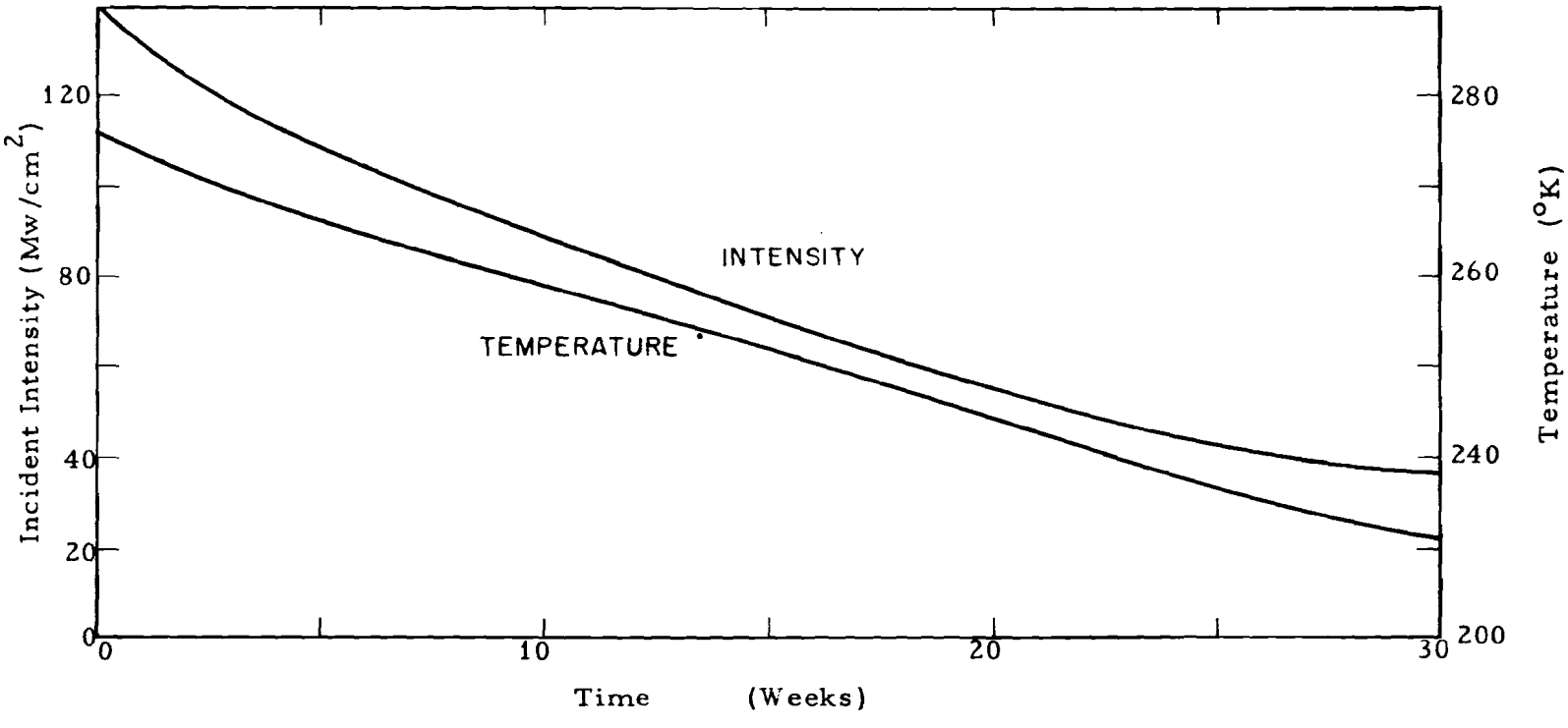

FIGURE V-A-32 INCIDENT SOLAR INTENSITY AND CELL TEMPERATURE VS. TIME DURING A MARS MISSION

the temperature is calculated and is shown at each point of the mission in Figure V-A-32.

Now, having specified the cell equilibrium temperature, incident intensity, and angle of incidence, the current-voltage characteristics of the cells may be drawn, assuming the cell efficiency is 8 percent under 140 mw/cm^2 at 25°C. The resulting characteristics are shown in Figure V-A-33. The maximum power locus is seen to change slowly with voltage but rapidly with current. Assuming a load of an electrochemical storage system presenting a constant voltage of 0.5 volts to the cells at all times, the power from each cell may be plotted as seen in Figure V-A-34.

Such characteristics may be plotted for a solar collector-converter on any type of mission. The resulting information can be used by the circuit designer to predict system characteristics at any time during the mission.

An estimate can be made regarding the range of insolation in which silicon solar cells are effective. Consider the case where the cells are coated so that

$$\alpha = 0.65$$

$$\epsilon = 0.95 \text{ on both sides}$$

and are mounted on a flat, oriented panel. The product of the cell efficiency and the insolation provides an indication of the power that may be realized, as is shown in Figure V-A-35. Note that the silicon cells described appear to be most effective near Venus. However, their power output is sufficiently degraded in the region closer to the sun than Venus and further away than Mars, so that nuclear power sources should be considered for missions in these regions.

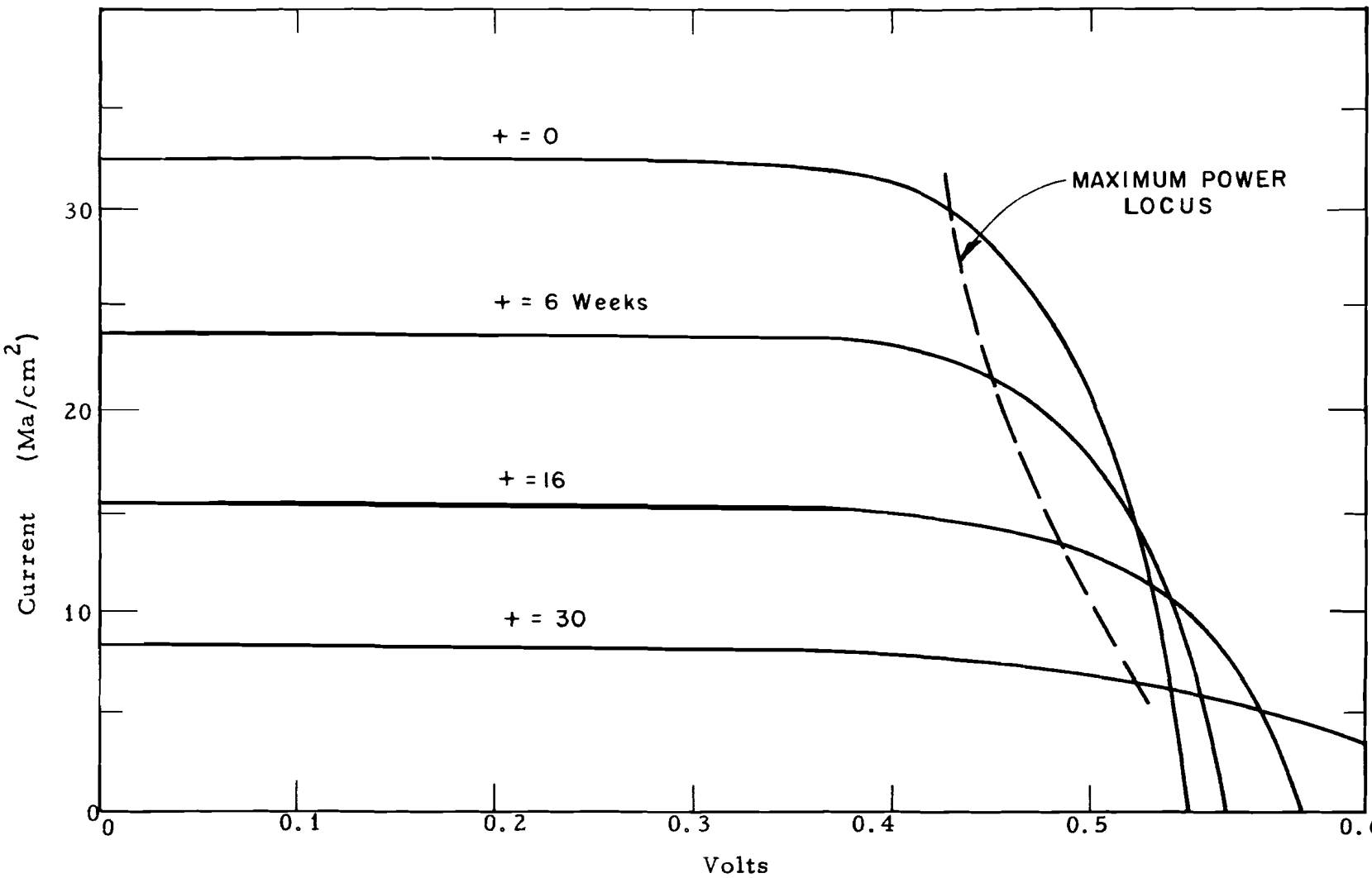

FIGURE V-A-33 CURRENT-VOLTAGE CHARACTERISTICS VS. TIME - MARS MISSION

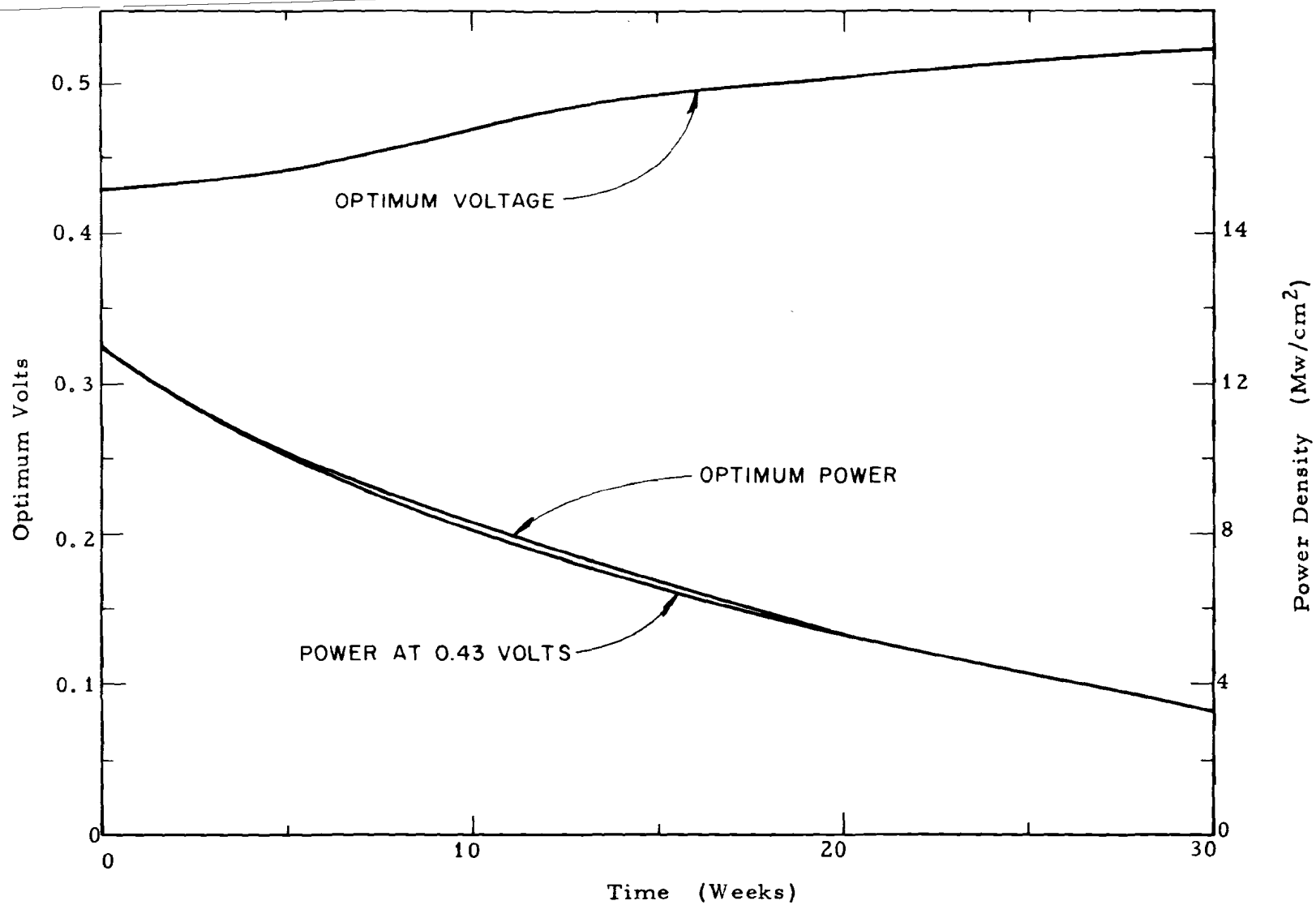

FIGURE V-A-34 OPTIMUM VOLTAGE AND POWER VERSUS TIME - MARS MISSION

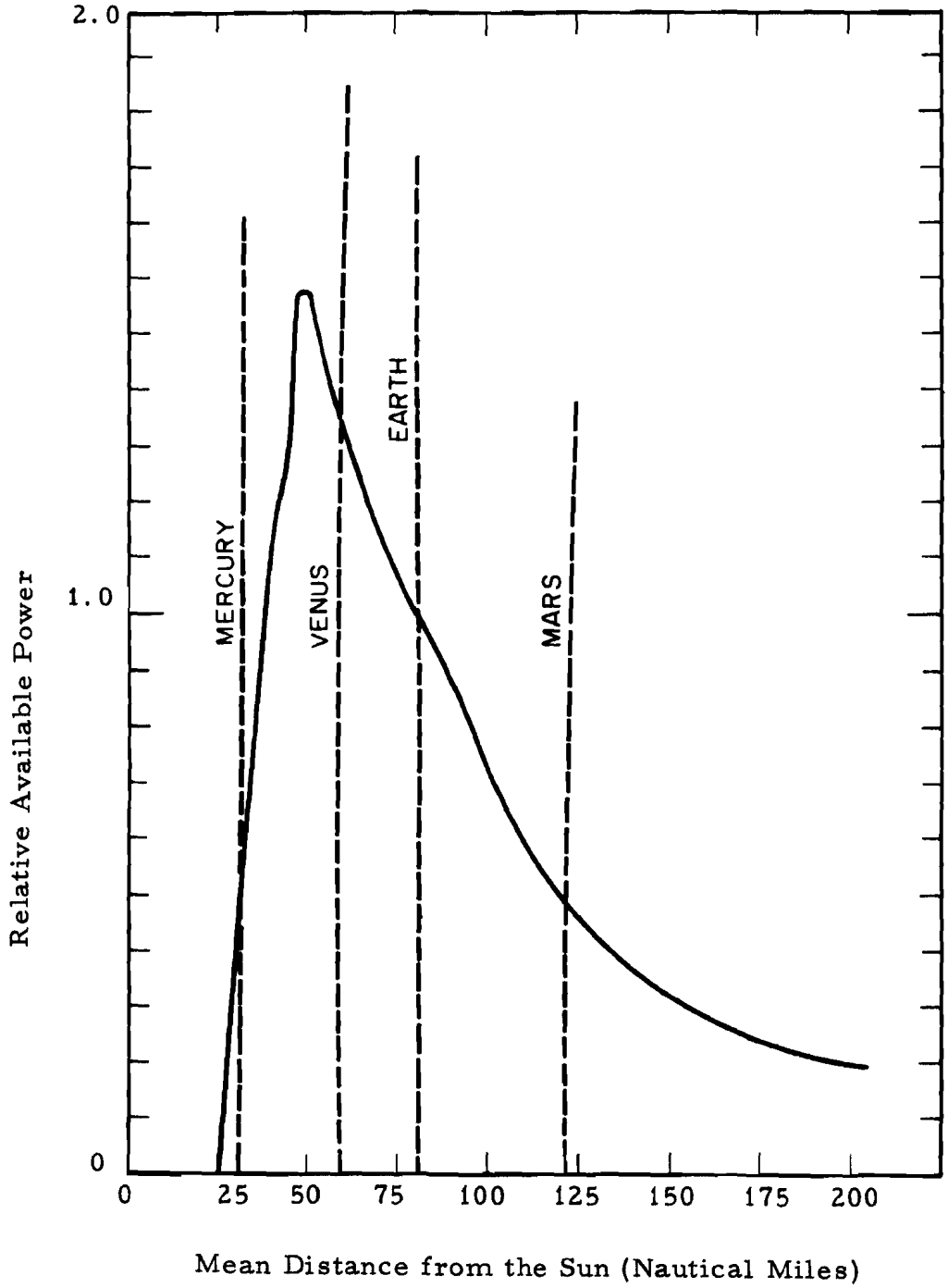

FIGURE V-A-35 POWER AVAILABLE FROM A PHOTOVOLTAIC SYSTEM USING SILICON CELLS VS. MEAN DISTANCE FROM THE SUN

2.2.3 Effect of Radiation From Earth

The distribution of radiation from the earth to an orbiting vehicle varies with satellite altitude and orbital position. To maintain an energy balance, radiation is divided as follows:

	Relative Amount
Incoming solar radiation	100
Radiation scattered upward by the atmosphere	9
Radiation reflected from the earth	27
Radiation emitted by the atmosphere	47
Radiation emitted from the earth	17
Total Outgoing Radiation	100

In general, the spectral distribution of each type of radiation is different. For most applications, the effect of radiation from the earth is small. Assuming that all solar energy incident on the earth is re-emitted or reflected, the relative intensity of radiation from the earth may be plotted as a function of altitude, as shown in Figure V-A-36. Note that, for orbits higher than 400 miles, the radiation from earth is less than 1/5 the direct radiation. The approximation of uniformity of radiation over the entire earth is quite crude, however, and care must be used if Figure V-A-36 is employed in temperature calculations.

2.3 Electrical Aspects of Photovoltaic Systems

2.3.1 Cell Matching

It is obvious that degradation of over-all performance will result if solar cells with a statistical variation in characteristics are used in a power supply system. In this subsection, a quantitative evaluation of these effects will be made, and recommendations for matching criteria will be given.

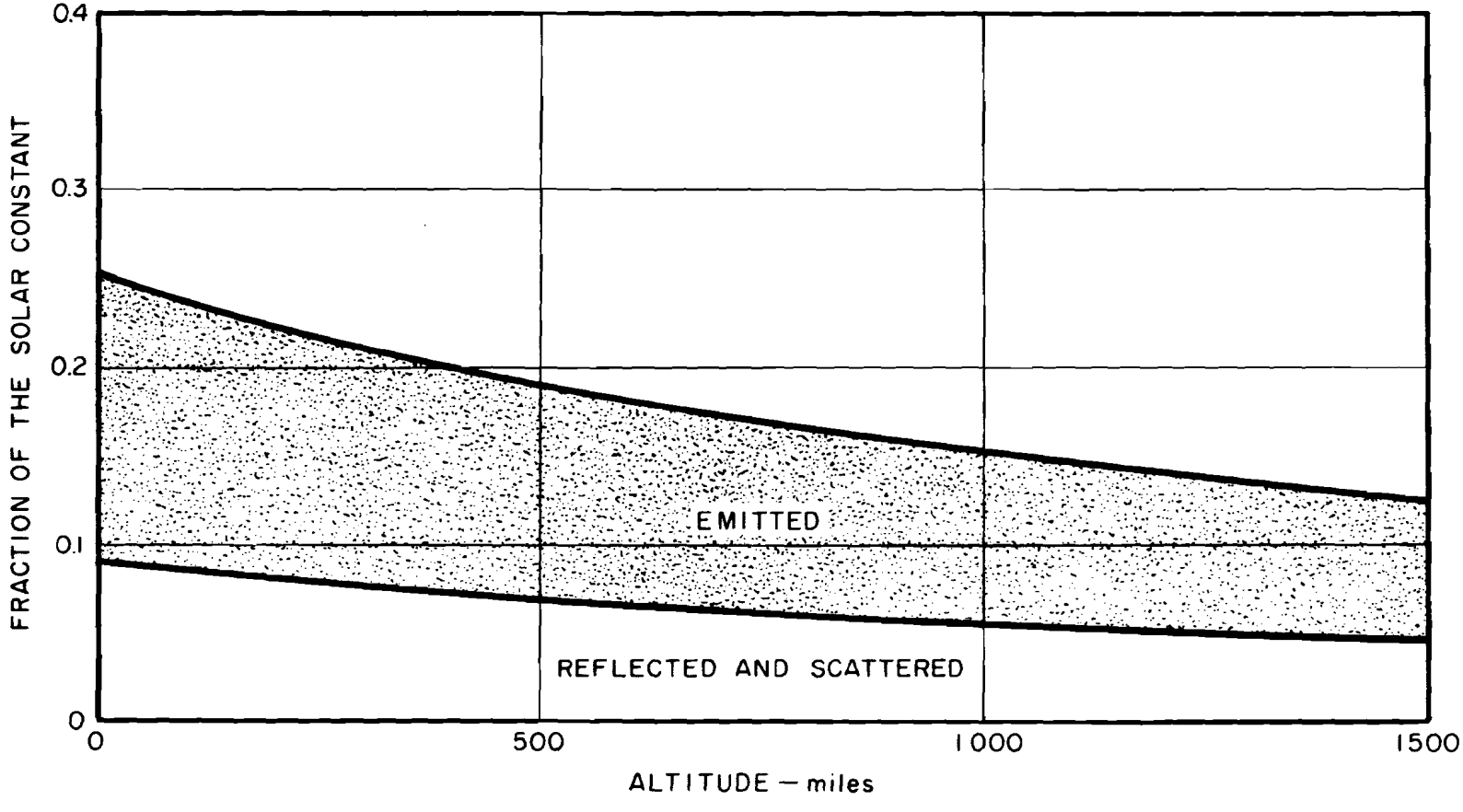

FIGURE V-A-36 RADIATION FROM THE EARTH

The highest efficiency silicon solar cells have almost identical characteristics. The high efficiency of these cells result when all the cell parameters--surface condition, junction depth, crystal perfection, etc.--are very close to optimum. Lower efficiency cells, however, exhibit quite a significant divergence of characteristics. The degradation of efficiency can be due to the following:

a. Loss of junction current from decreased cell area or nonoptimum junction depth.

b. Degraded open-circuit voltage, caused by poor crystal quality.

c. Increased series resistance from too-shallow junction or poor contacts.

The most frequently seen cells of lower efficiency usually exhibit a combination of effects b. and c. Typical current-voltage characteristics of four cells are shown in Figure V-A-37. Curve "a" represents an optimum cell (13 percent efficient); the other curves represent 10-percent cells whose efficiency degradation results from each of the three above-mentioned defects. It should be noted that most cells of lower efficiencies exhibit a combination of more than one degradation effect and that cells of the type shown are not usually encountered.

Since solar cells must be combined either in series or parallel, the effect of mismatch can be determined by investigating lines of constant current and constant voltage. Therefore, note that if cells b, c, and d are connected in parallel and are operated at 0.45 volts, they will all operate at 9.5 to 10-percent efficiency. However, if they are connected in series, the low-current cell will constrain the entire series to a maximum of 24 Ma/cm^2 current.

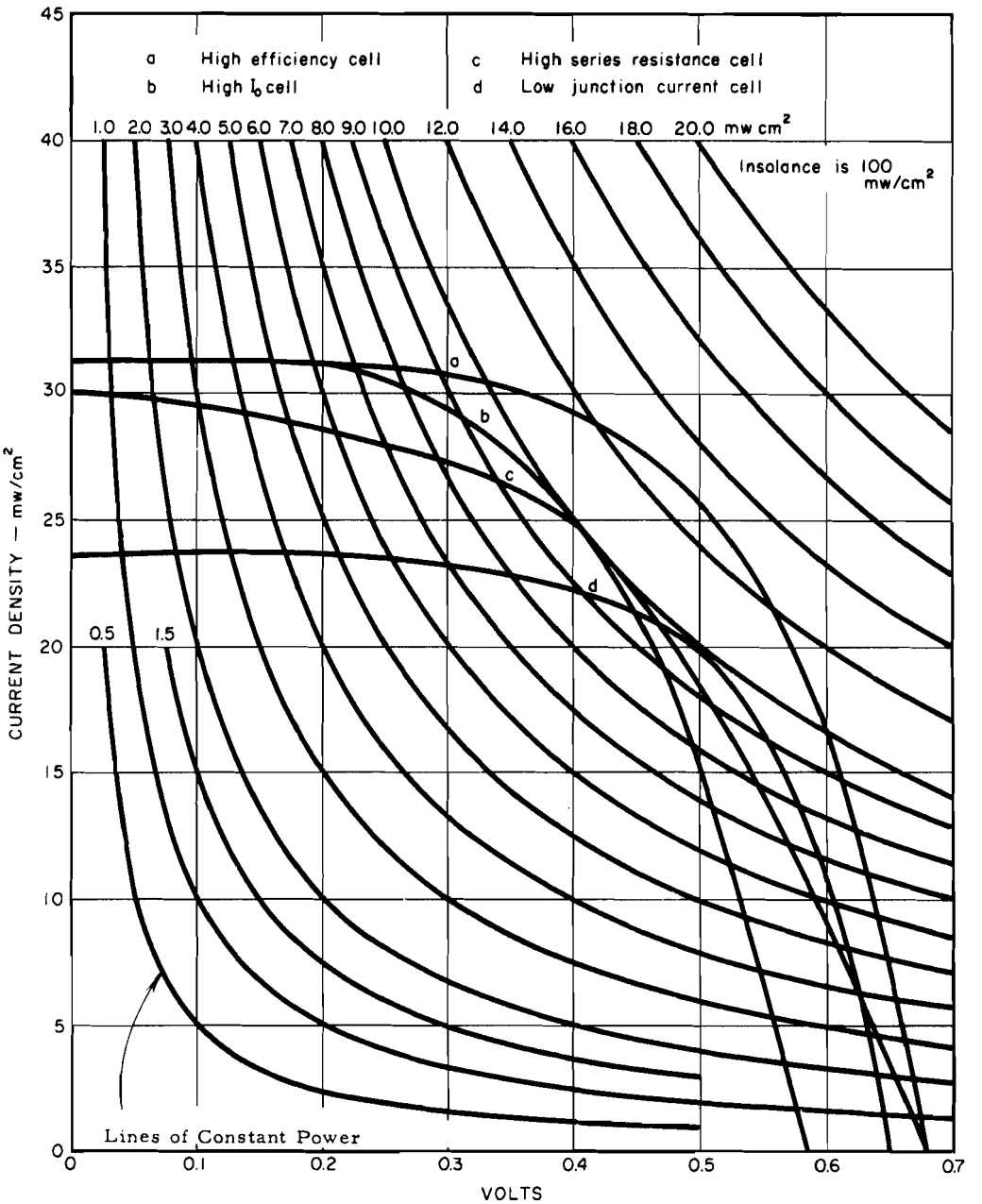

FIGURE V-A-37 TYPICAL SOLAR CELL CURVES SHOWING EFFICIENCY DEGRADATION

If the series string is operated at a current of 20 ma/cm^2, the cells will operate at 9 to 10-percent efficiency. Therefore, it is clear that, under the most severe conditions of mismatch, cells of equal maximum efficiency can be operated within approximately 90 percent of that maximum efficiency, either in series or parallel.

However, many space applications occur in which it is desirable to operate the cells at somewhat varying voltages or currents. It may immediately be seen from Figure V-A-37 that the power output of each cell remains near maximum over a 10 to 20 percent variation of voltage or current. Table V-A-3 shows the range over which cells b, c, and d operate within 9/10 of maximum efficiency.

TABLE V-A-3

RANGE OF CELL EFFICIENCY

Cell	I_{opt}	V_{opt}	I_{min}	V_{min}	I_{max}	V_{max}
b	25	0.41	19	0.31	29	0.47
c	23	0.43	18	0.34	27	0.51
d	20	0.50	16	0.41	22	0.56
b, c, d in Parallel	23	0.43	19	0.36	25	0.48
b, c, d in Series	21	0.45	16	0.40	22	0.50

It may be seen that the composite average characteristic of the three cells in series, shown in Figure V-A-38, has a somewhat narrower range of currents and voltages over which the average efficiency is 90 percent of the average maximum efficiency (10 percent). Note further that, as a direct consequence of the mismatch, the cells in series or parallel can be operated at no greater than 95 percent of the average efficiency per cell. (The dashed curves of

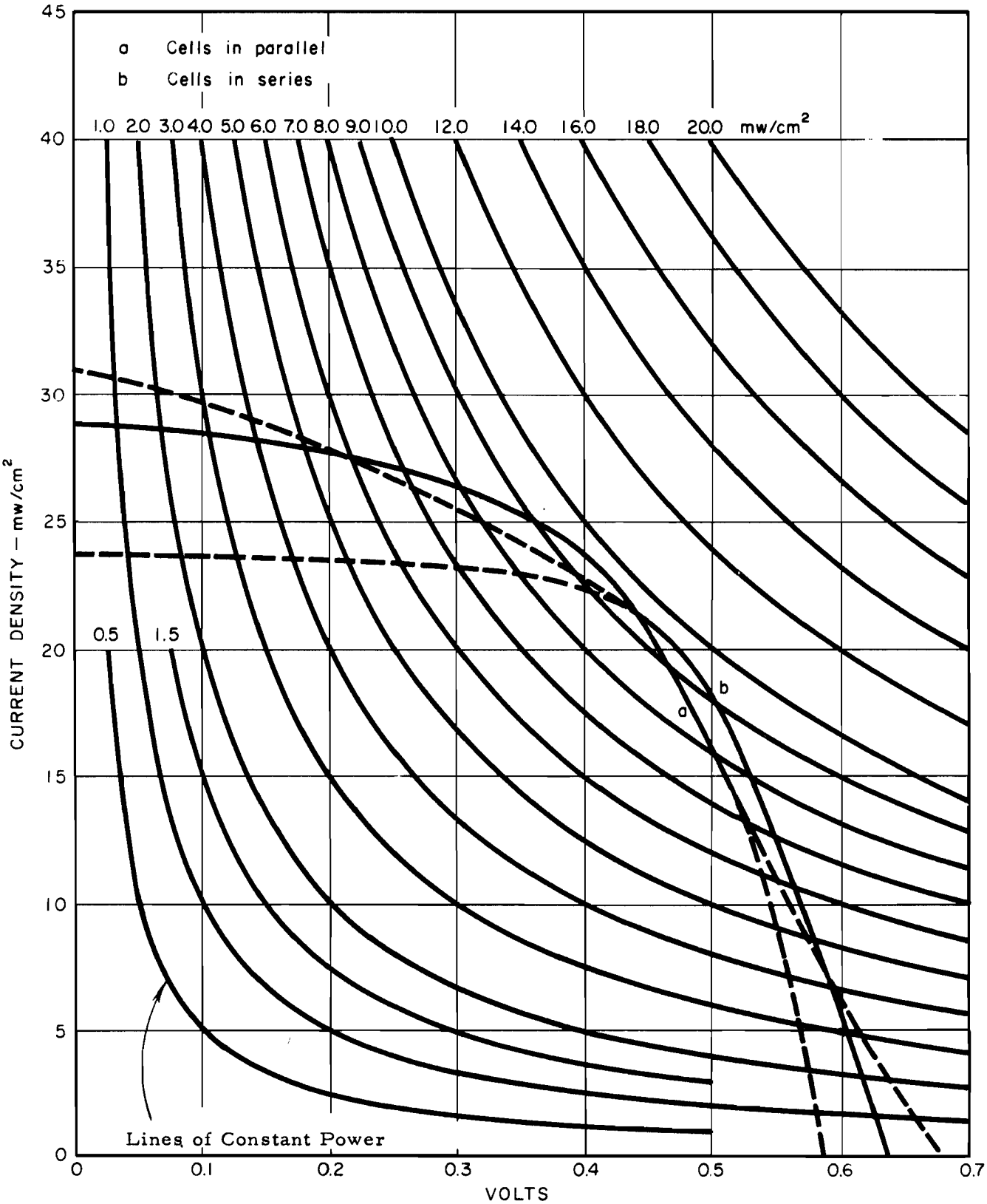

FIGURE V-A-38 COMPOSITE AVERAGE CHARACTERISTIC OF CELLS b, c, AND d

Figure V-A-38 give the region in which at least one of the cells is operating at a negative current or voltage and thus is loading the others.)

Thus, it appears that mismatch of cells can cause undue loss of efficiency if the cell group is operated at a voltage or current greatly different from that at which the cells were tested.

Manufacturers test their production cells by measuring the current at a specified voltage or the voltage at a specified current.

Danger of efficiency loss from mismatch may be minimized by any of the following:

a. Cells of the highest available efficiency are used.

b. Cells are combined into modules of five to ten cells in series or parallel and the circuit design is based on measured characteristics of these modules. It is found that individual cell characteristic variations tend to average out in such groups so that the modules have more uniform characteristics than the single cells from which they are fabricated.

c. Cells are purchased with a rated power at a stated current or voltage and are operated very close to these currents or voltages.

d. Individual cells are measured over the range of currents or voltages over which they are operated.

It should be further noted that nonuniform illumination of series strings of cells, poor contacts, shadowing of one cell by another, nonuniform temperature of cells in parallel, etc., can produce the effects of mismatch by altering the current-voltage characteristics of the cells involved. Degradation of power output from these causes is eliminated through careful design and construction.

2.3.2 Determination of the Optimum Operating Point In a Mission

Determination of the optimum operating point of a photovoltaic power supply requires specification of the cell characteristics throughout the mission, the load characteristics, and the power requirements. The following is a suggested design procedure together with illustrative examples.

a. The over-all collector-converter characteristic should be determined for each point of the mission.

b. The characteristics of the load should be specified.

c. The power output of the entire unit is then calculated at the various points of the mission as a function of operating point.

d. The operating point is selected which provides the maximum power output consistent with the power requirements.

Many sophisticated schemes could be suggested for varying the operating point during the mission. However, in systems which have been orbited to date, such schemes have not been employed because of increased reliability problems.

As an example, consider a mission in which the solar cell characteristics are as given in Figure V-A-39, which describes a mission to regions of low insolance. Consider now that the cells may be loaded by (1) a battery storage system which presents a near-constant voltage to the cells, (2) electronic circuitry which presents nearly a constant resistance, or (3) electronic circuitry which presents a constant current drain.

The constant voltage load will allow for a maximum power output to be obtained throughout the mission. Note that a voltage of 0.41 is very near the optimum at all times. This is typical for situations in which

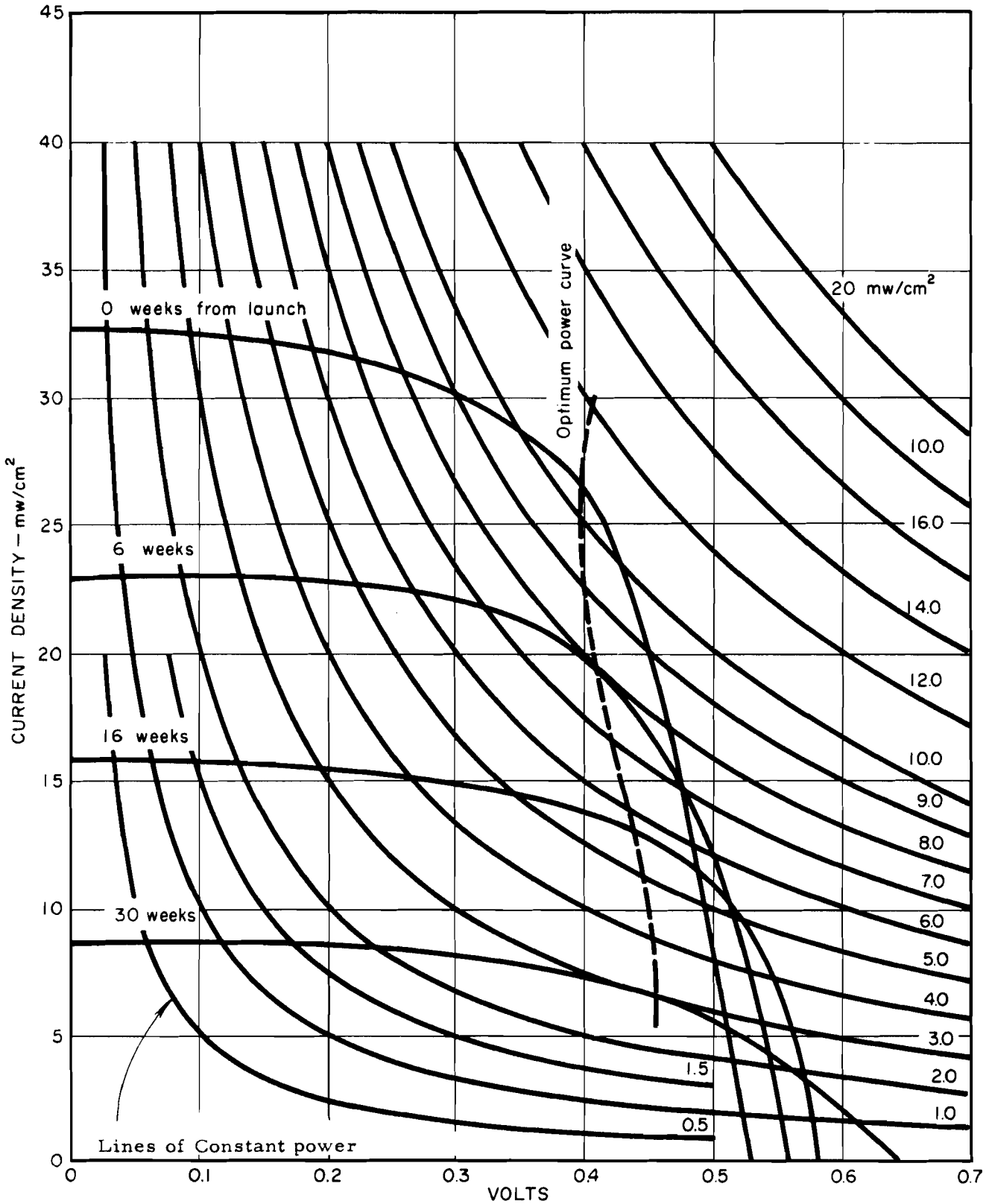

FIGURE V-A-39 CHARACTERISTICS OF A POWER SUPPLY DURING A MARS MISSION

decreasing insolence results in lower equilibrium temperatures and consequent voltage increases. Assume now, that the vehicle is a small transmitter which presents a constant resistance to the solar cell power supply. A plot may be made showing power output versus point of the mission for various resistance loads, as is seen in Figure V-A-40. Note that for a resistance area of 15 ohm/cm^2 (the total resistance to be used is obtained by dividing this value by the area of cell in parallel across the load) the power is a maximum at the start of the mission but low at the end. A resistance area of 60 ohm/cm^2 is much closer to optimum because it provides a more uniform power output and, at the same time, is close to optimum at the end of the mission where most efficient use of the cells must be made.

If a constant-current type of load is used, the output power vs. time relationship is that of Figure V-A-41. Obviously the optimum current is near 6.5 Ma/cm^2. At this current, there is little variation of output during the period of operation, and optimum use is made of the cells at the most distant point from the sun. The procedures illustrated here can be readily used to find an optimum operating point for any variation of cell characteristics into any type of load characteristic.

2.3.3 AC Aspects of Solar Cells

Since solar cells are frequently incorporated into AC electrical circuits, it is occasionally necessary to consider their AC characteristics. The complete equivalent circuit is shown in Figure V-A-42. The junction transition region capacitance, Cj, is in series with a built-in junction potential ϕ. This capacitance is shunted by the R_s, R_{sh}, R_L network. The self-capacitance of a silicon solar cell, as seen looking into the device, is directly proportional to the surface area and is typically 10,000 $\mu\mu$ f per cm^2.

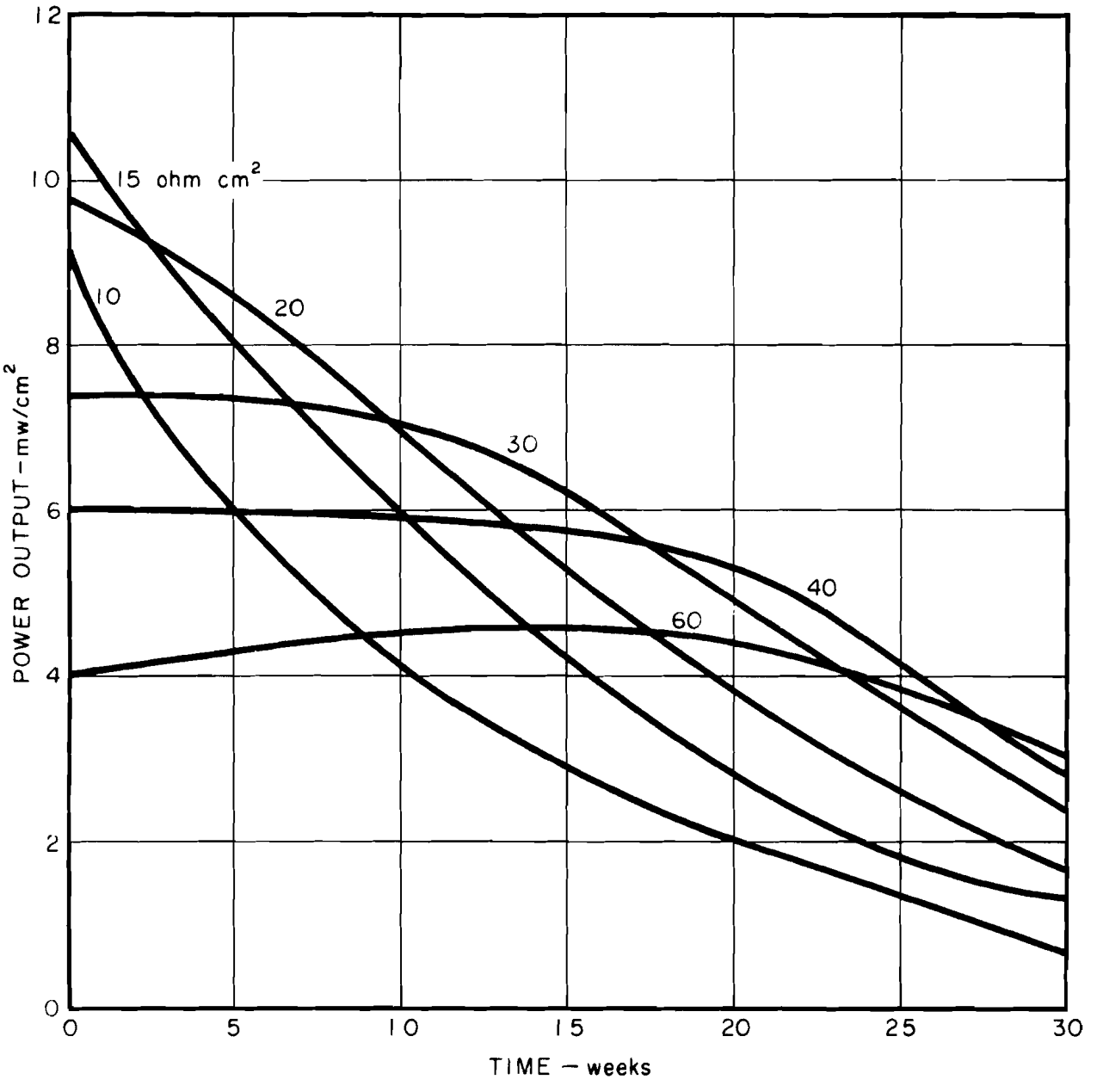

FIGURE V-A-40 POWER OUTPUT VS. TIME DURING MARS MISSION AT VARIOUS VALUES OF CONSTANT RESISTANCE

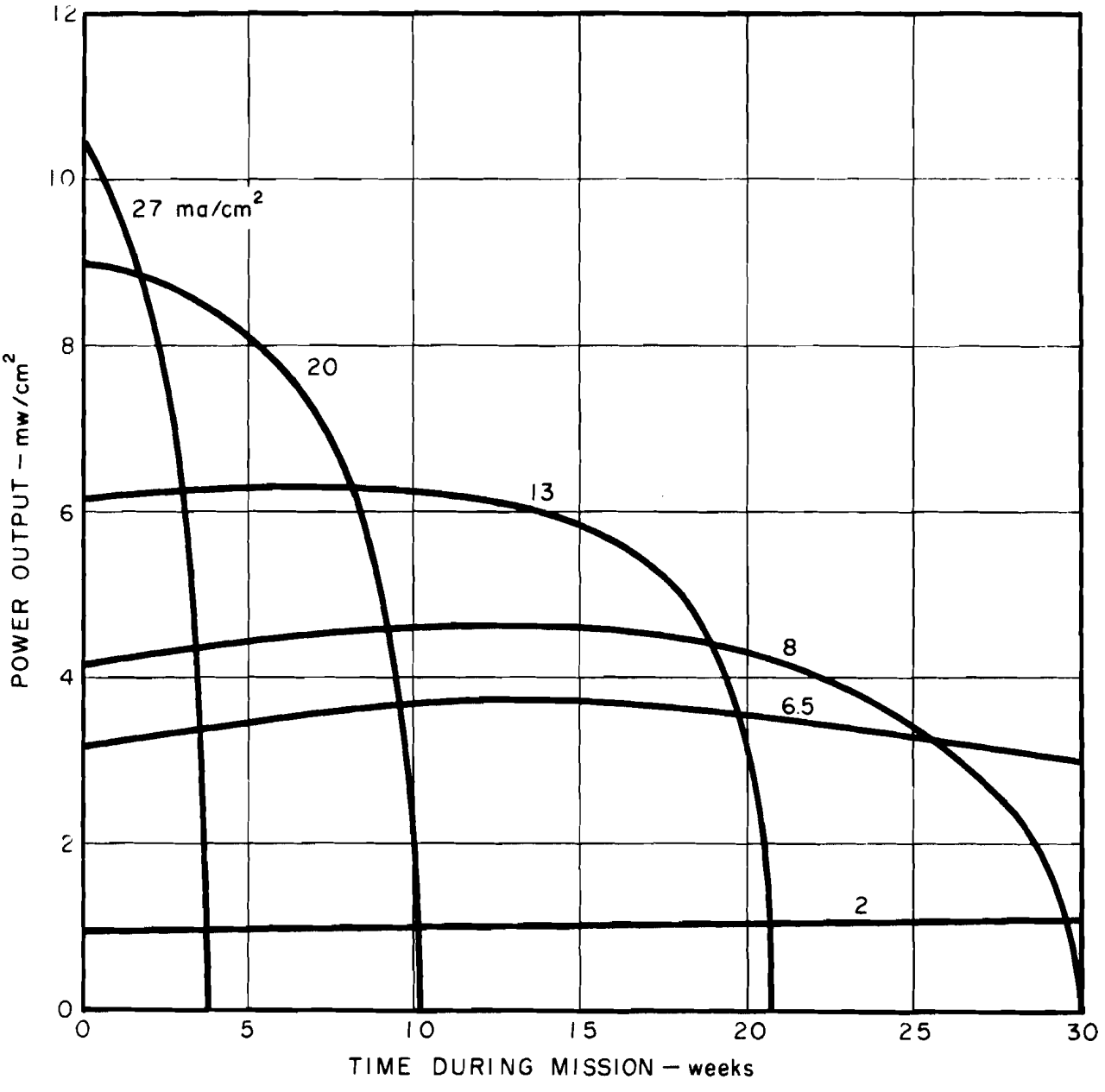

FIGURE V-A-41 POWER OUTPUT VS. TIME DURING MARS MISSION AT VARIOUS VALUES OF CONSTANT RESISTANCE

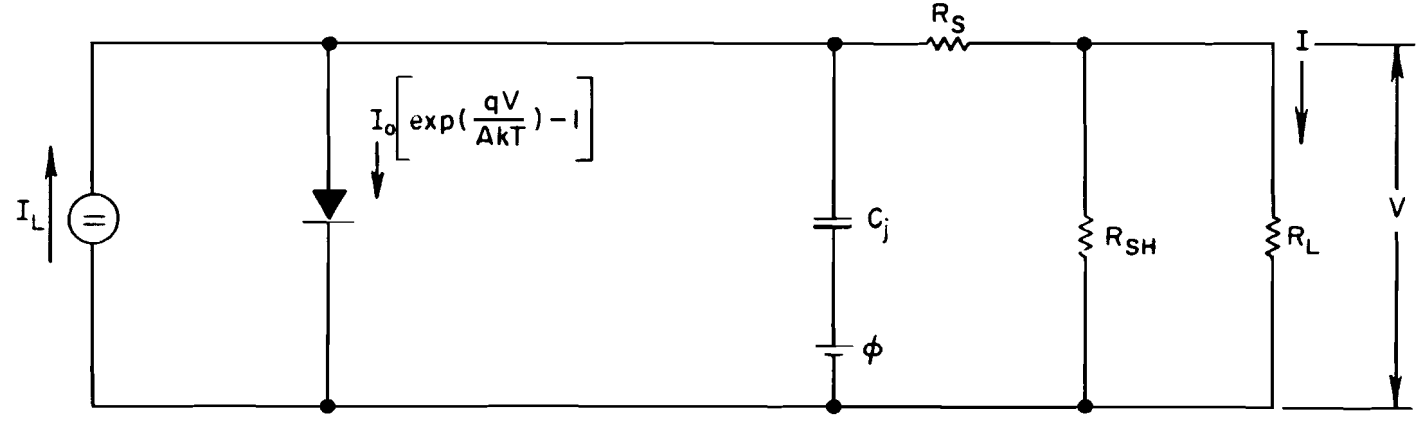

FIGURE V-A-42 AC EQUIVALENT CIRCUIT OF A SOLAR CELL

(From Prince and Wolf, Journal of British IRE, 18 p. 586 - Oct. 1958)

Since the total self-capacitance of a series string of 50 silicon cells is typically 400 to 500 μμf and several hundred of these strings are often connected in parallel, the total cp capacitance of a solar cell power source can easily reach 0.1 μf. Thus, if the solar cell collector-converter is used to power high- frequency electronic circuitry directly, care must be taken to isolate the cells from the AC circuitry.

Prince and Wolf (Reference V-A-2) have reported detailed measurements of transient time response of reverse biased photodiodes. These devices are similar to solar cells in all important respects, except for a somewhat deeper junction depth. The reported data, Figures V-A-43 and V-A-44, should be considered indicative of the transient time response of silicon solar cells.

2.3.4 The Design of Solar Cell Series-Parallel Circuitry

The final decision as to the configuration of the series-parallel arrangement of solar cells in a power supply design is dependent upon such interdependent considerations as the following:

a. Maintaining a uniform illumination over all cells connected in series across the load.

b. Maintaining a uniform temperature over all cells connected in parallel across a load.

c. Utilization of maximum panel area by shingling of cells.

d. Over-all geometry of the collector-converter.

e. Minimizing performance degradation in event of a cell short-circuiting.

f. Minimizing performance degradation in vent of a cell open-circuiting.

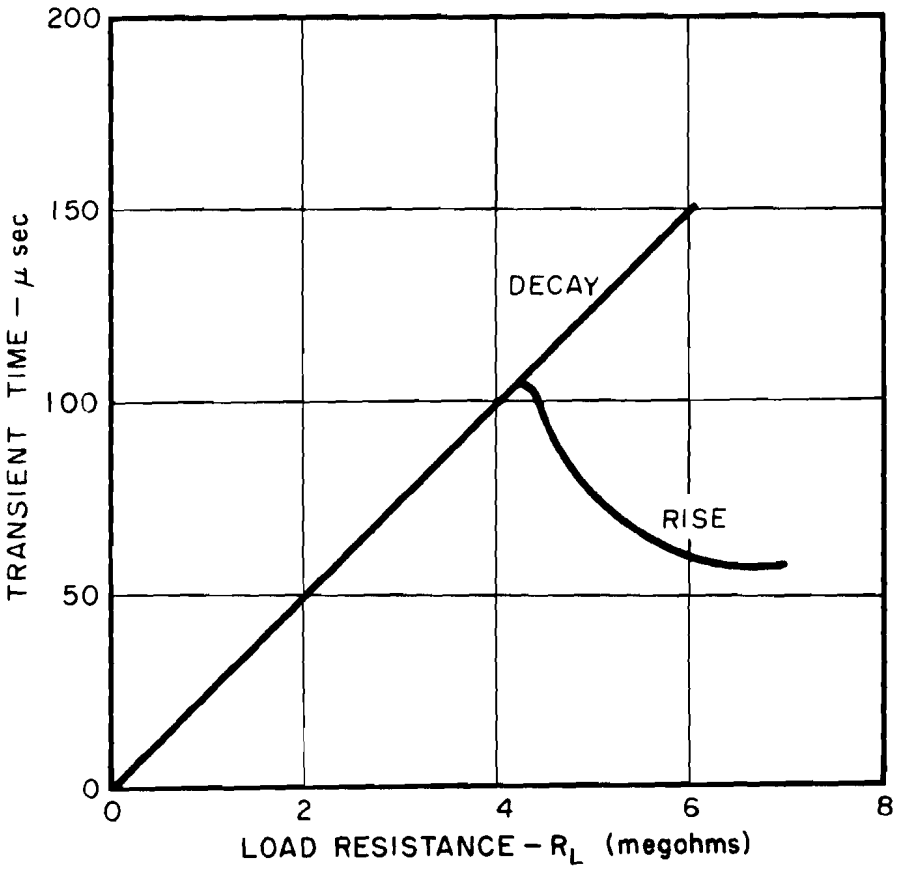

FIGURE V-A-43 TRANSIENT RESPONSE OF A SILICON PHOTOCELL AT 45 FOOT CANDLES AND 100 VOLT BIAS

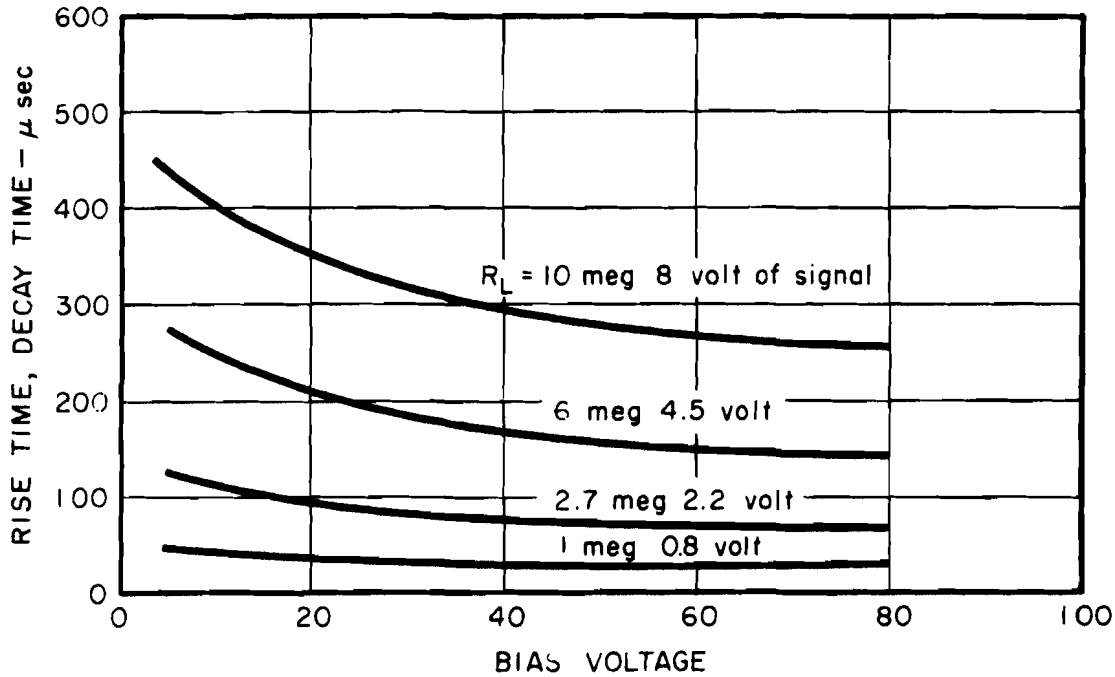

FIGURE V-A-44 RISE TIME AND DECAY TIME VS. BIAS VOLTAGE AT 15 FOOT CANDLES INCIDENT INTENSITY

The first four considerations are discussed elsewhere in this volume. Considerations of the environmental conditions to be met by the vehicle will allow an estimation to be made of the relative probabilities of open-circuiting and short-circuiting of cells, as is discussed later in this report.

Clearly, if a cell open-circuits, it will cause the loss of all cells in series with it. Similarly a cell short-circuiting will cause the loss of all cells in parallel with it. Proper design of a panel series-parallel configuration must consider these extremely important effects.

First, an estimate must be made of the relative liklihood of a cell open-circuiting to that of a cell short-circuiting. The most likely source of cell failure is damage from environmental conditions, such as micrometeorite or radiation bombardment. These effects are considered in more detail in the next subsection.

It is agreed that the probability of failure from open-circuiting is much greater than that from short-circuiting; in fact, dead shorts are highly unlikely. Usually there is sufficient resistance remaining to ground in a "shorted" cell to keep those cells in parallel with it from being completely lost as power sources. It therefore might appear reasonable to expect that the primary cell submodules making up the panel should consist of groups of cells in parallel, so that an open-circuited cell would have a minimum degrading effect. This configuration has actually been used by Lockheed in their Discoverer panels. On these panels, each submodule consists of ten cells connected in parallel. Seventy-four of these submodules are connected in series to form the twenty-eight volt panel.

However, most of the vehicles orbited to date have utilized nonoriented collectors in which problems of uniformity of illumination made it necessary to keep the total area of series strings to a minimum. The Lockheed panels, for example, which are designed for oriented systems, contain 740 cells in each series string. They could, however, be used in a nonoriented geometry, as long as they are uniformly illuminated at all times.

A technique which can be used to keep non-illuminated, or short-circuited, portions of a solar collector from loading the portions which are producing power consists of inserting diodes in series with each series cell string on the panel surface. Since diodes do consume a small amount of power, it is desirable to use the minimum number of diodes to provide the desired protection.

3.0 EFFECTS OF SPACE ENVIRONMENT

The space environment will be detrimental to the solar cells, supporting structure, or any auxiliary mechanisms such as concentrators. It does not appear that vacuum or the relatively low-energy corpuscular radiation encountered at satellite altitudes will seriously effect cell operation. Short wavelength solar radiation and meteoroid damage also appear minor. Severe deterioration may result, however, from the high energy proton and electron bombardment within the Van Allen belt region surrounding the earth. In addition, large numbers of high-energy protons and electrons are contained within the solar plasma, and the damage from primary particles and secondary radiation may constitute a much greater hazard than the Van Allen radiation during an interplanetary journey.

The effects of the space environment on concentrating mechanisms, electrical components, structures, and other appurtenances is considered in Volume I. Experimental data regarding the magnitude of the meteoroid, solar plasma, and/or Van Allen belt hazard are extremely sparse, and a great deal of extrapolation and speculation is used in the design of present solar panels to meet environmental dangers.

The generally accepted solution for preventing damage is to cover the cell surface with glass slides, which may also be coated with spectrally selective surfaces for temperature control. A discussion of the optimum thickness of glass is included in Volume IX.

3.1 Meteoroid Hazard

The anticipated erosive and penetrating effects of meteoroids on exposed surfaces have been discussed in Volume I. It is difficult to extrapolate results from hypervelocity impact experiments to solar cells due to their crystalline, brittle, and inflexible nature. Electro-Optical Systems, Inc., performed the following experiment:

A sharpened rod of about 200 microns diameter on the end was mounted on a weighted arm and allowed to hit a mounted solar cell after falling through different angles. The effects were as follows for different kinetic energies of impact:

At 10^6 ergs - the rod broke completely through the surface.

At 10^5 ergs - the surface was chipped and started to break up after about 10 successive impacts.

At 10^4 ergs - the surface was nicked and started to break up after about 100 successive impacts at the same spot.

The momentum of the rod was over 10^4 that of a meteoroid with corresponding energy. For the cells tested, no electrical shorts or breaks could be detected, and the decrease in short-circuit current was roughly proportional to the damaged area.

These and several other experiments indicate that the following assumptions will provide large safety factors in system design:

a. All incident particles with energy over 10^6 ergs will cause open-circuiting of the solar cell and, consequently, open circuiting of the series circuit in which the cell is placed. The particle energy corresponds to visual magnitudes of between 18 and 19. Referring to Volume I, the average number of hits per year which cause destruction will be less than approximately $10^{-4}/cm^2$ maximum.

b. All incident meteoroids create hemispherical holds of depth/meteoroid diameter ratio of 10. Using Bjork's data for penetration and integrating over the applicable region as shown in Volume I, the fraction of the total

solar cell area destroyed equals about .00435 during one year's operation.

Glass covers used for self-protection will not seriously deteriorate from the "sand blasting" effect of meteoroids. However, low-energy corpuscular radiation is likely to erode the glass cover surface, and slight discoloration may take place due to high-energy electromagnetic radiation. Experiments have shown that sand blasted glass loses approximately 15 percent in transmission efficiency. Consequently, a loss of 15 percent should be assumed for a long-time operation in space.

The probability of an individual cell being destroyed (without glass cover) will be governed by the Poisson distribution.

$$P_{(x)} = \frac{e^{m} m^{x}}{x!} \qquad \text{(A-21)}$$

where

m = mean number of hits

x = number of hits

$P_{(x)}$ = probability of x hits .

The probability of no hits during any time is given by

$$P_{(o)} = \exp\left[\frac{-t}{t_m}\right] \qquad \text{(A-22)}$$

where

t = t_m when m equals 1.

As discussed previously an assumed mean time to failure of about 5000 years for an individual solar cell of 2 cm^2 area provides a large safety factor in design. Substituting into the Poisson equation indicates a probability of no destruction during a year's operation of 99.98 percent for a 2 cm^2 cell.

In the general case, the cells will be grouped in modules consisting of n cells in series, each panel containing a number of modules connected in parallel. If one cell is open-circuited by meteoroid impact, panel performance deteriorates in the resulting mismatch between modules. For a module with n cells in series, the relationship between cell reliability and module reliability, assuming all cells have equal probability of failure is simply

$$R_{module} = R^n \tag{A-23}$$

where

R = individual cell reliability.

This equation is plotted in Figure V-A-45 for different values of n and R.

Assuming a 2 cm^2 cell with a reliability of about 99.98 percent, Figure V-A-45 shows that 99 percent module reliability could be obtained with 50 cells in series and that 100 cells in series would result in about 98 percent module reliability.

The solar cell panel may be designed so that the panel consists of N modules in parallel. Given the probability, p, that one module will fail in one year, the probability that x modules out of a total of N will fail is simply the binomial distribution

$$f(x) = \left(\frac{N}{x}\right) p^x (1 - p)^{N-x} \tag{A-24}$$

The probability that $x \leq a$, is given by

$$P_{(o \leq x \leq a)} = \sum_{x=o}^{x=a} f(x) \tag{A-25}$$

For example, for N = 100 and p = .02, there exists a .99 probability that about five or less modules will fail.

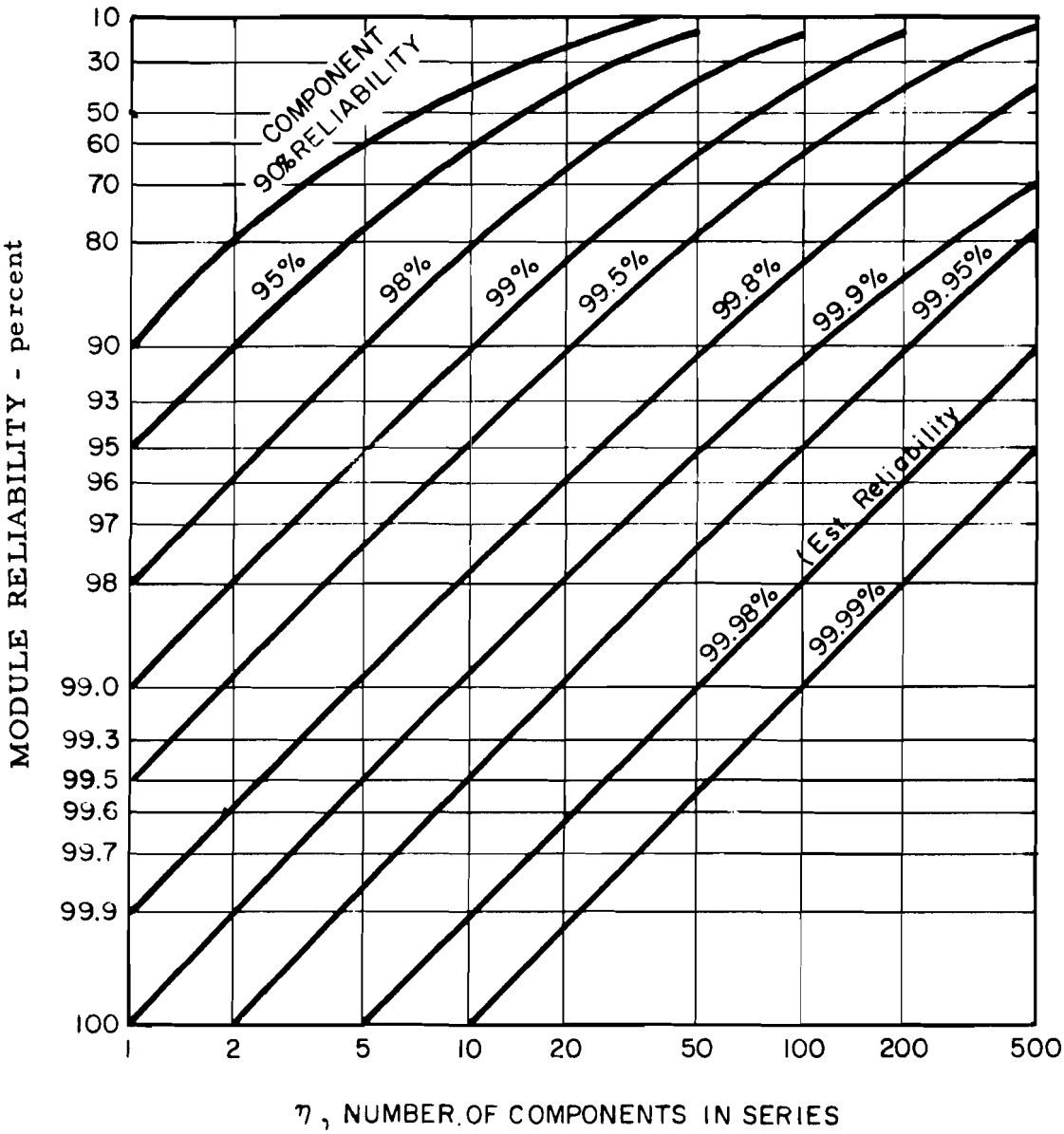

FIGURE V-A-45 MODULE RELIABILITY WITH η COMPONENTS IN SERIES

3.2 Van Allen Radiation

Experimental data accumulated by several organizations have indicated that serious degradation in solar cell performance will result from an extended period of operation in the Van Allen belts. Organizations with active experimental programs include Lockheed Aircraft (LMSD, Ref. V-A-4), General Electric Co., Schenectady (Ref. V-A-5), Space Technology Laboratories (Ref. V-A-6), R.C.A., and others.

Satellite measurements have indicated the density of high energy protons and electrons, as summarized in Table V-A-4 below. No estimates for low-energy particles are available due to inadequate satellite instrumentation. Extrapolating the available data points indicates that the density of relatively low-energy electrons and protons will be higher than the density of high-energy electrons and protons. The threshold energy for damage to the silicon solar cell is about 100 ev for protons and about 145 kev for electrons.

TABLE V-A-4

TYPE, ENERGIES, AND FLUX OF CHARGED PARTICLES

	Location	Energy	Flux
Electrons	Inner belt	> 20 kev	10^{9} cm^{2} sec^{-1} stearadian^{-1}
	Inner belt	> 600 kev	10^{7} cm^{-2} sec^{-1} stearadian^{-1}
	Outer belt	> 20 kev	10^{11} cm^{-2} sec^{-1}
	Outer belt	> 200 kev	10^{8} cm^{-2} sec^{-1}
	Outer belt	> 2.5 mev	10^{6} cm^{-2} sec^{-1}
Protons	Inner belt	> 40 mev	10^{4} cm^{-2} sec^{-1}
	Outer belt	> 60 mev	10^{2} cm^{-2} sec^{-1}

Experimental data are scarce; however, some pertinent results for unprotected cells are listed below in Table V-A-5.

TABLE V-A-5

EXPERIMENTAL DATA

REDUCTION OF SOLAR CELL EFFICIENCY DUE TO PARTICLE BOMBARDMENT

Source	Particle	Energy (mev)	Flux (particles/cm^2)	Percent Power Reduction
Lockheed	Proton	3	5×10^9	25
		12	2×10^{11}	25
		12	10	50
STL	Electron	.5	$2\text{-}8 \times 10^{13}$	25
RCA	Proton	17.6	10^{15}	50
	Electron	1.7	5×10^{14}	50

Several tests have been conducted using electrons and glass covers. STL measurements for example, have indicated that about 22 mils of glass would increase life (25 percent reduction in power), by a factor of 2-1/2 (530 kev electrons) using glass densities of 2.2 gr/cm^3.

Table V-A-5 indicates the possibility that particles of low energy are more likely to damage the solar cell, as indicated by the greater number of high energy protons necessary to reduce cell efficiency by a given amount. This is due primarily to the decreasing cross section presented by silicon to the lower energy particles. Therefore, any assumptions regarding proton damage, based on the measurements of high-energy protons in the Van Allen belt, are likely to seriously **under estimate** damage.

The decrease in solar cell power output vs. radiation has experimentally been shown to be approximately proportional to the log of the integrated flux, as shown in Figure V-A-46. A sharp drop occurs in short circuit current, while open circuit voltage also exhibits a less severe decrease. A typical change

in I-V characteristics is shown in Figure V-A-46. If a power decrease is anticipated in system design, the voltage drop which occurs during system lifetime must also be compensated by increasing the number of cells in series and/or providing flexible voltage conversion and regulation circuits.

The reduction of particle energies incident on the solar cell surface without attenuation of the solar energy may be accomplished by bonding thin glass covers on the solar cell surfaces. The incident particles dissipate a considerable portion of their kinetic energy through ionization in traversing the glass cover before reaching the solar cell surface. The glass thickness required to reduce incident particle energies to threshold levels is a function of the initial particle energy. A graph of this function is shown in Figure V-A-47 for glass of density 2.2. grams/cm^3 stopping electrons. The required glass thickness is approximately linearly dependent on incident electron energy in the energy range of interest.

Experimental data shows good agreement with the simple theory. The random variations in the data, however, prevent any further quantitative comparison with simple theory. On this basis, for example, it is predicted that glass covers 0.065 in. thick should extend solar cell lifetimes appreciably under 800 kev electron bombardment. The thickness of glass required for complete protection from radiation depends significantly on proton energy; for example, 3 mev protons are completely stopped with 3.5 mil of glass, whereas 12 mev of protons require 38 mil of glass.

Extension of the simple displacement theory currently used to describe radiation damage (Ref. V-A-46), to yield more accurate estimates of solar cell performance under particle bombardment, requires evaluation of the limitations of the theory. The theory does not take into account radiation damage annealing processes.

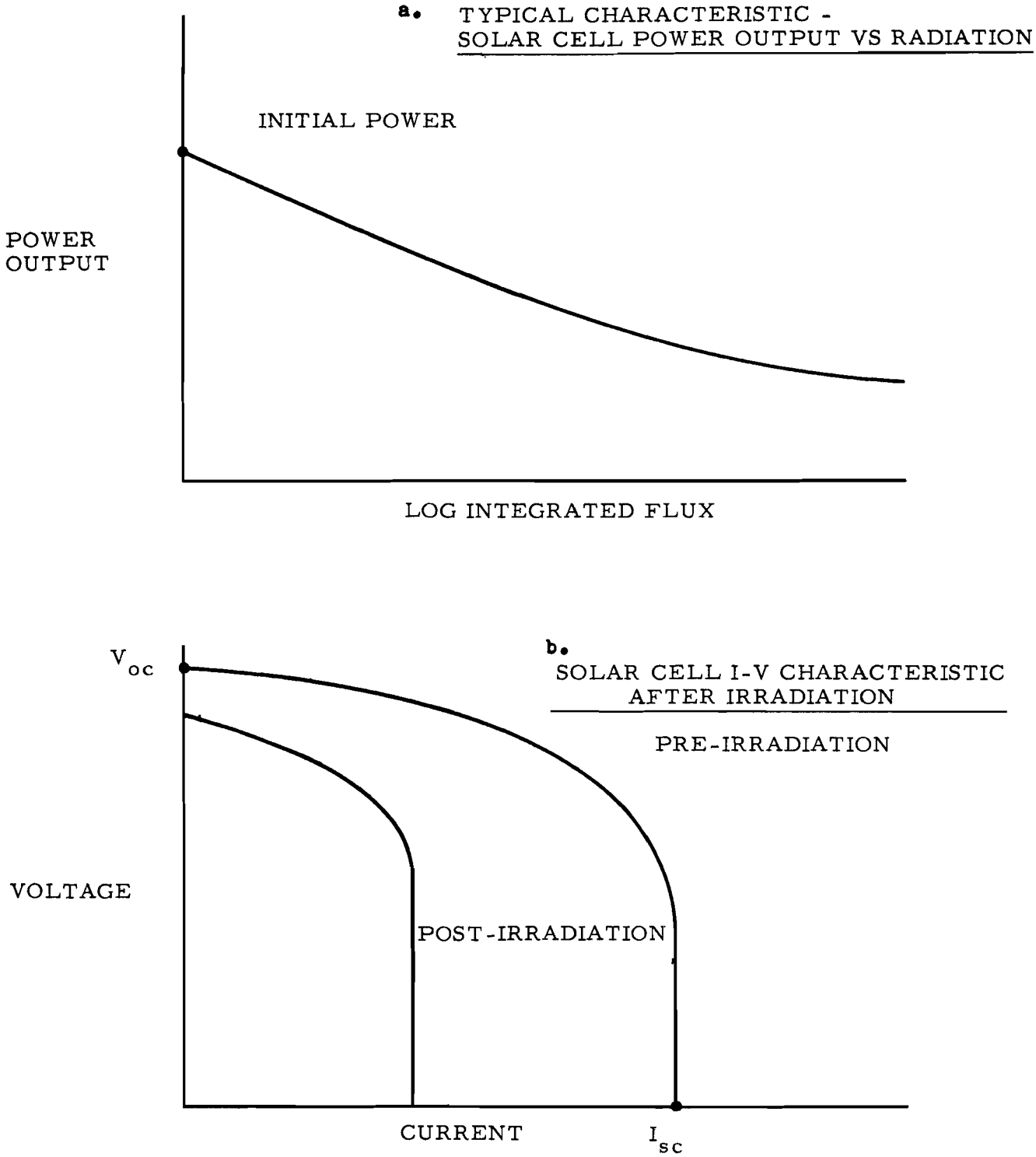

FIGURE V-A-46 TYPICAL SOLAR CELL RESPONSE TO ELECTRON RADIATION

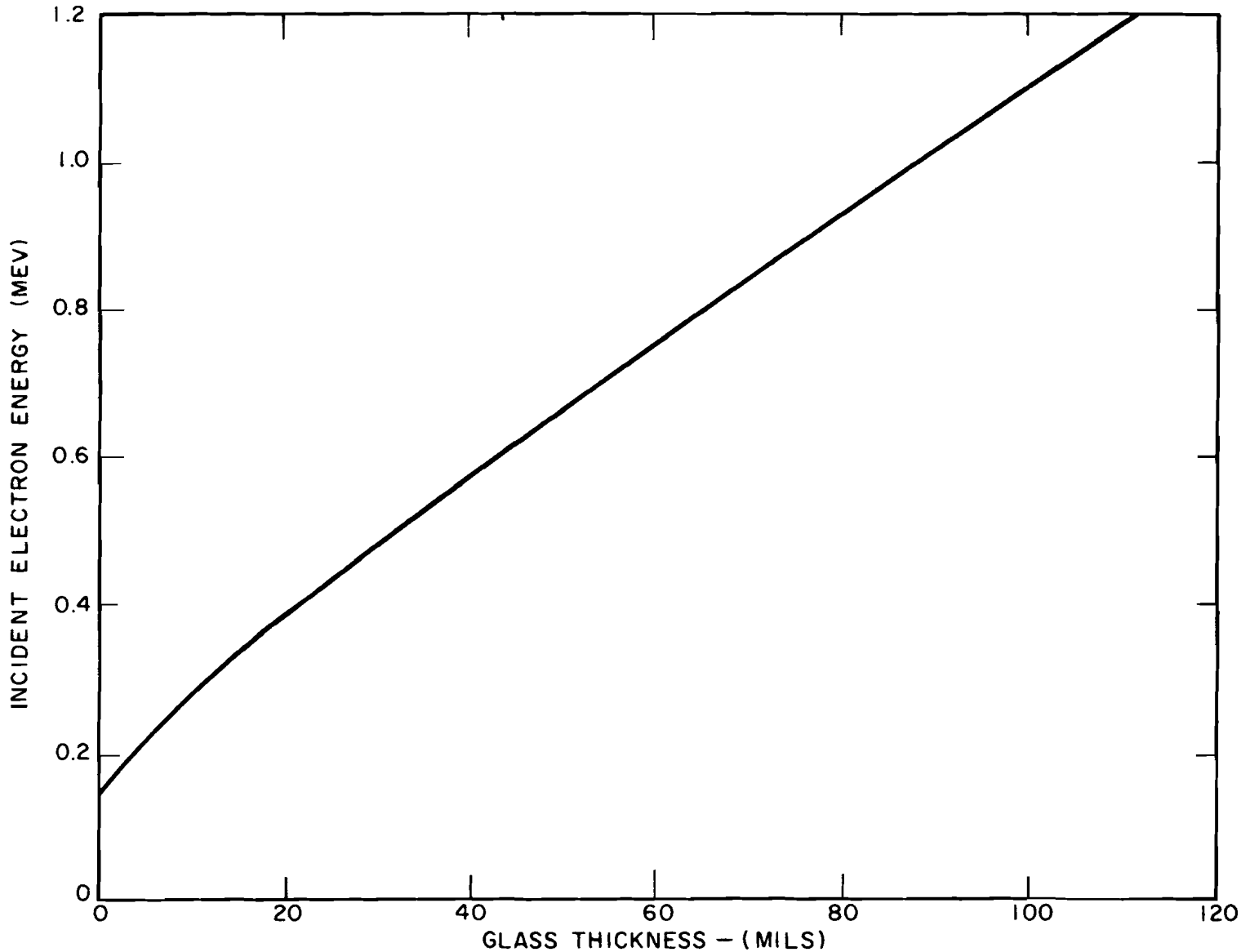

FIGURE V-A-47 GLASS THICKNESS TO REDUCE INCIDENT ELECTRON ENERGY TO MEAN ENERGY OF 145 kev

It has been shown that damage caused by high-energy electron and proton bombardment can be removed by annealing cells at elevated temperatures. The exact temperatures are not well determined, but above 100°C the cells have been found to have much longer useful lives in radiation fields. The Vanguard I vehicle utilized cells which were covered with Vycor windows, resulting in a greenhouse effect causing these cells to reach high equilibrium temperatures. However, this vehicle after more than two years is still transmitting, even though it does encounter substantial amounts of proton and electron radiation. It is thought that the higher temperatures of these cells annealed out any radiation damage as it occurred.

Another limitation of the application of the simple theory is the unknown particle energy spectrum of the Van Allen radiation belt when considering the operation of solar cells in this environment. The integration of the radiation belt particle energy spectrum with the simple theory could have significant effect on the necessary glass cover thicknesses due to the strong energy dependence of the atomic displacement cross-section.

Due to the large number of individual collisions which occur when an electron traverses some given thickness of material, the energy lost in traversing the material is a statistical process, resulting in an effect known as straggling. This straggling produces an electron energy spectrum of degraded energies represented by a mean energy. Thus, the selection of a glass thickness sufficient to reduce electrons of a given incident energy to a mean energy of 145 kev will not completely eliminate atomic displacements since a portion of the electrons will have energies greater than 145 kev.

Considering the relative importance of its limitations, the displacement theory probably provides a valuable estimate for the operation of silicon cells under electron bombardment with estimated accuracies of 25 percent.

However, it is clear that the simple theory becomes inadequate in predicting large extensions of solar cell lifetimes due to the increasing importance of straggling and radiation damage annealing with time. The importance of further experimental and theoretical treatment of the problem is evident.

Glass covers used as filter coatings or protective mechanisms may be discolored by extensive UV and gamma radiation. Several glasses have been demonstrated to be resistant to radiation damage, including quartz and cerium oxide.

The selection of the shielding material thickness represents an optimum compromise between increased weight/unit area for long lifetime or increased area to make up for efficiency reduction. Many satellite missions will spend a small percentage of their orbit passing through the Van Allen radiation, with a consequent decrease in the necessary glass weight. It should be noted that the cells will require protection on the rear side also. The trade off is discussed further in Volume IX.

3.3 Solar Plasma

In interplanetary space, i.e., within the solar system, the particles are predominantly of solar origin. The solar corona consists of out-streaming gas which at the earth's distance from the sun is estimated to be between 10^2 and 10^3 protons/cc and an equal number of electrons, both moving with a velocity of about 500 km/sec. under quiet conditions. During solar flares, densities of 10^4 or perhaps 10^5 protons and electrons per cc moving with a velocity of as high as 1500 km/sec can be expected. The proton kinetic energy in this stream then varies between 2 and 20 kev., while the electron kinetic energy is well below the silicon cell damage threshold.

The proton energy, while above the damage threshold, is sufficiently low to be stopped with glass of a few mils thickness. The glass cover, however, will be spattered. It is not known whether a sever transmission loss will result due to a clouded surface. Sandblasted glass has demonstrated a 15 percent transmission loss and this loss should be included in estimating required cell array area.

3.4 Electromagnetic Radiation

Radiation damage studies on silicon solar energy converters were undertaken by **Loferski** and Rappaport (Ref. V-A-3). Based on their work, the estimated lifetime of silicon solar cells for various components of cosmic ray flux was as follows:

Type of Radiation	Estimated Lifetime in Years
Protons	3.6×10^4
Alpha particles	1.4×10^5
Electrons	10^8
Ultraviolet radiation	85
X-Rays	6.7

The approximate gamma doses at which various devices (including solar cells) are affected are shown in the flux-dose plot of Figure V-A-48, which is based on experimental studies of Enslow, et al (Ref. 28). The figure shows the gamma dosages required to cause 50 percent derating of the solar cell at various fluxes. As shown, direct gamma radiation from the sun will not seriously degrade cell performance for a number of years.

The amount of secondary radiation resulting from bombardment of the cell or glass surface is unknown. Reiffel (Ref. I-B-6) has estimated radiation

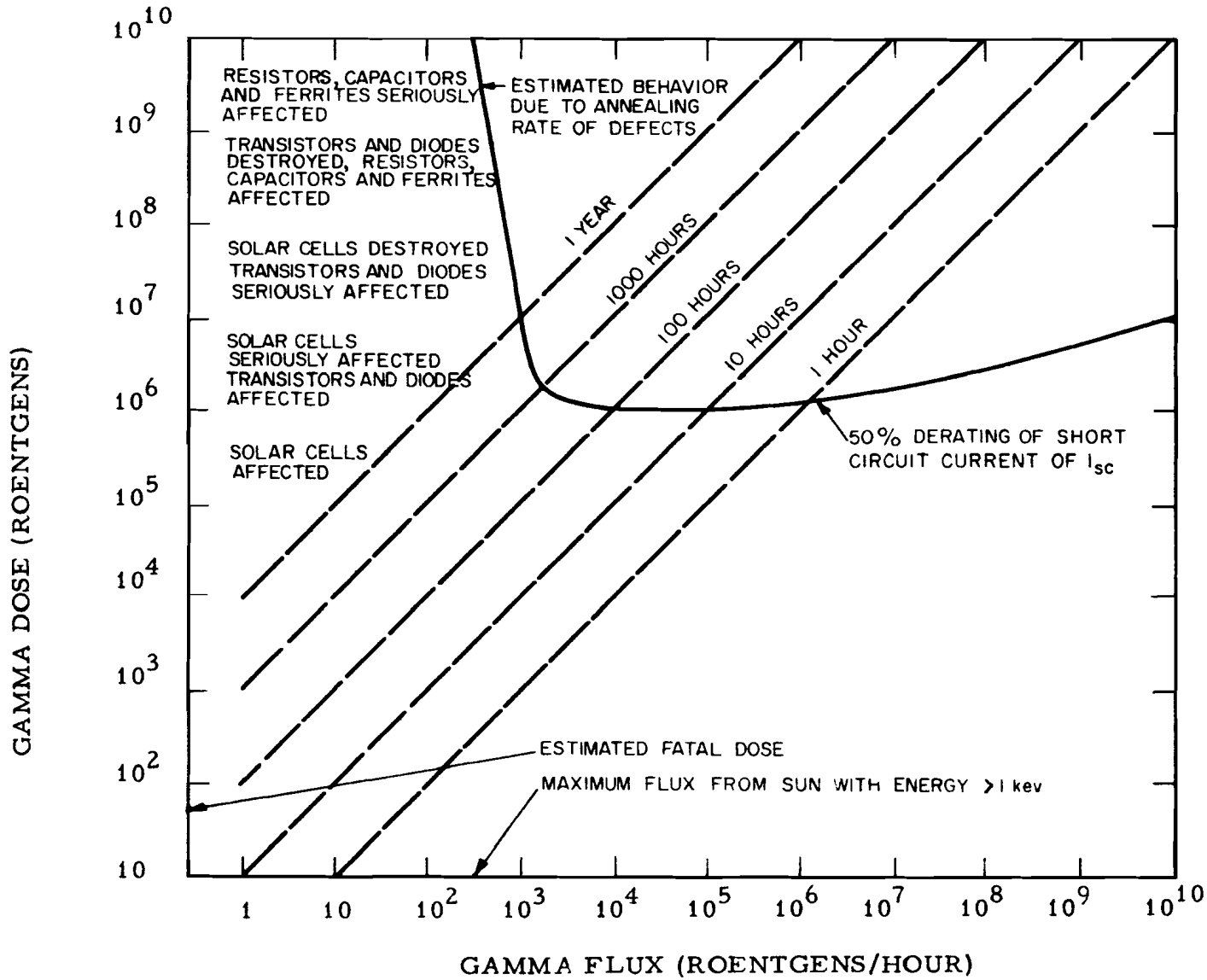

FIGURE V-A-48 FLUX-DOSE PLOT FOR SILICON SOLAR CELLS UNDER GAMMA IRRADIATIONS

doses on the order of 5×10^5 rad/sec, assuming the kinetic energy of the particle is entirely converted to short wavelength radiation. A gamma radiation dose of 10^5 rad will begin to affect solar cell performance. After 10^7 rads the output power would be reduced to approximately 50 percent of its initial value. However, the secondary radiation is likely to be of low energy, easily stopped by a glass cover. The problem will remain unanswered until a thorough evaluation of the solar plasma hazard has been accomplished.

4.0 STRUCTURAL DESIGN OF PHOTOVOLTAIC CELL ARRAYS

A variety of structural design approaches have been used in the photovoltaic systems designed to date. Many of the features of these designs have been dictated by requirements of other parts of the vehicle system. In this subsection, some of the structural features common to most systems are discussed, and specific examples are given.

4.1 Substrate Materials

Solar cell panels are made by supporting the cells and their interconnecting leads on a rigid substrate. The substrate material may itself be rigid or may obtain its rigidity from a supporting frame structure. Among the materials suitable for substrates are the following:

a. Double-faced aluminum honeycomb sheet which provides an extremely high strength to weight ratio.

b. Lightweight framework support of aluminum, magnesium, titanium, or steel, which has more favorable thermal conduction properties than honeycomb.

c. Non-metallic structural materials such as, fiberglass and pressed composition materials, which are electrically insulating and have low thermal conductivities.

d. Non-rigid substrate materials such as fiberglass cloth and foils, which are extremely lightweight but must be supported on rigid frameworks.

e. The actual surface of the vehicle may be used as the substrate, a technique which depends for success upon favorable vehicle shape, size, and temperature characteristics.

4.2 Cell Mounting Techniques

Several techniques are used for mounting solar cells onto the panel substrate. The most frequently used techniques consist of soldering the cells into shingles and bonding the shingles to the substrate surface. These shingles, shown pictorially in Figure V-A-49, are rigid in themselves but must be protected from stresses which may break the soldered bonds. The contacts will support moments of up to 0.3 or 0.4 inch pounds. When the shingles are mounted on an electrically conductive surface, an insulating adhesive must be used, and the cells must not be allowed to come in contact with the conductive surface.

A number of adhesives have been employed in bonding the cells to the substrate. Both epoxies and silicones have been found which meet the severe environmental rigors of space. Adhesives used must survive vacuum, frequent temperature changes (with satellites) and radiation. The adhesive should not absorb moisture or freezing and evaporation problems will result. Spectrolab, Inc. uses its own trademarked adhesive Solabond in its applications. The Jet Propulsion Laboratory has selected General Electric's RTV-60, a silicone-rubber adhesive for its Ranger vehicle.

An alternative technique to the shingle mode of construction is to fabricate modules of parallel-connected cells, as shown in Fig. V-A-50. The cells are mounted flat on the substrate material with their strip contacts facing the center. These modules become essentially a single cell of ten times the area of a single cell. The cells may be soldered to the metallic substrate using their own solder contacts.

The glass covers for the cells are usually bonded directly to the cell surface. Again, both epoxies and silicones

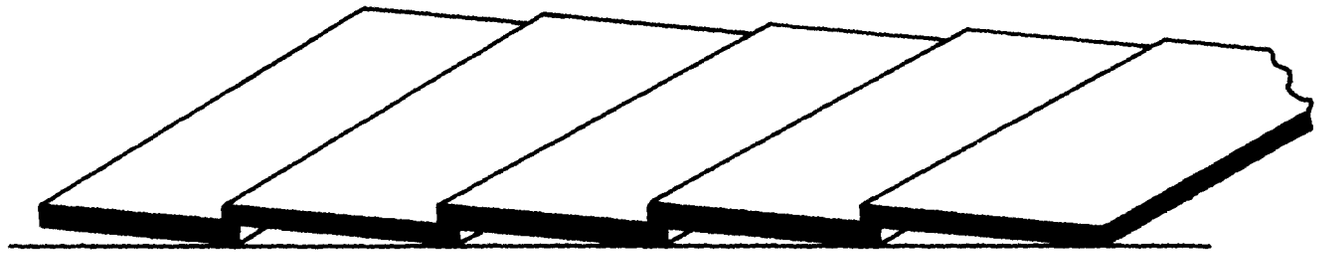

FIG V-A-49 A FIVE-CELL, SERIES SHINGLE

FIGURE V-A-50 A 10-CELL PARALLEL SUBMODULE

have been used for this job. For example, the Jet Propulsion Laboratory uses 15E Furine in the Ranger panels.

Some difficulty is experienced in finding an adhesive which combines sufficient bonding strength and proper optical characteristics with ability to meet the environmental conditions of space. It has been suggested that large coated glass windows could be held mechanically over the cells. The space between the glass and cells would be filled with a material whose optical properties match the filters to the cells and are not degraded by the environment--a material easier to find than an ideal adhesive.

Two representative examples of panel structural design include the following:

a. Tiros - For simplicity, five-cell shingles on RCA's Tiros were mounted directly onto fiberglass boards, which were attached to the vehicle, as shown schematically in Figure V-A-51. A typical printed circuit board had 18 five-cell shingles. The shingles were mounted into small wells integrally molded into the casting while the printed circuitry connecting the cells in series was buried in the lamination of the board.

b. Pioneer V and Explorer VI - The first fully instrumented payloads to be solar powered were the "paddlewheel" vehicles, Pioneer V and Explorer VI, designed and built by the Space Technology Laboratories. The paddlewheel configuration, shown in Figs. V-A-52 and V-A-53 was chosen so that the solar cells could be thermally isolated from the instrumentation and still keep the required number of cells in this nonoriented vehicle.

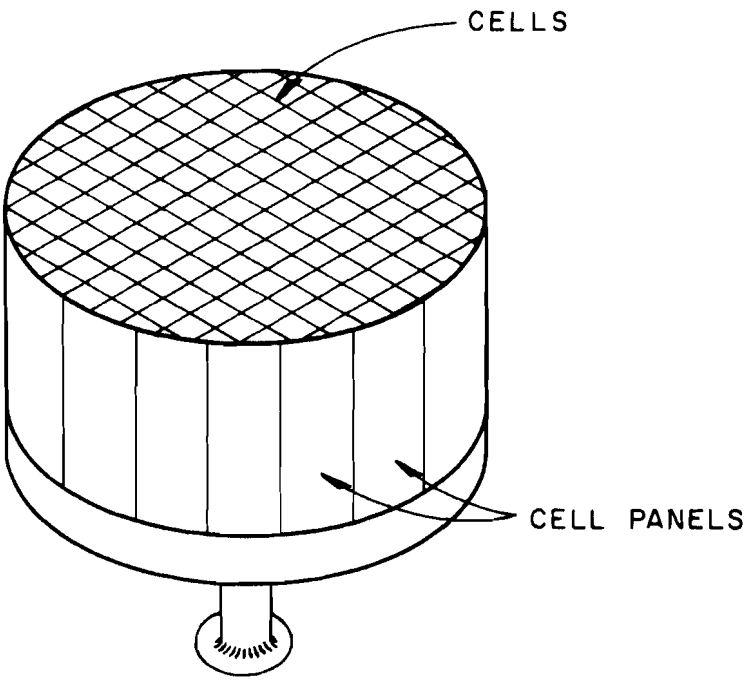

FIGURE V-A-51 PANEL CONFIGURATION OF TIROS VEHICLE

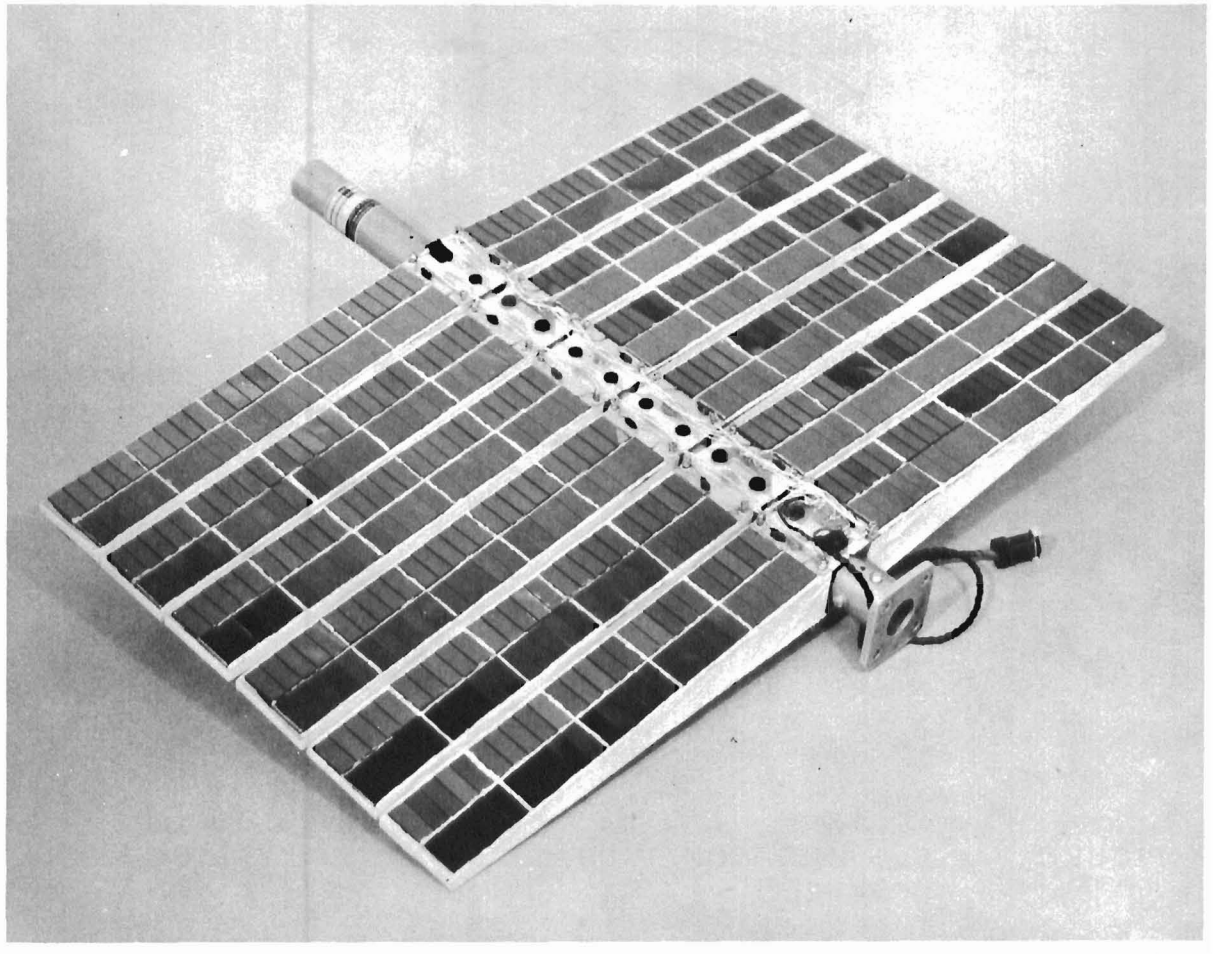

FIGURE V-A-52 A PADDLE FROM PIONEER V

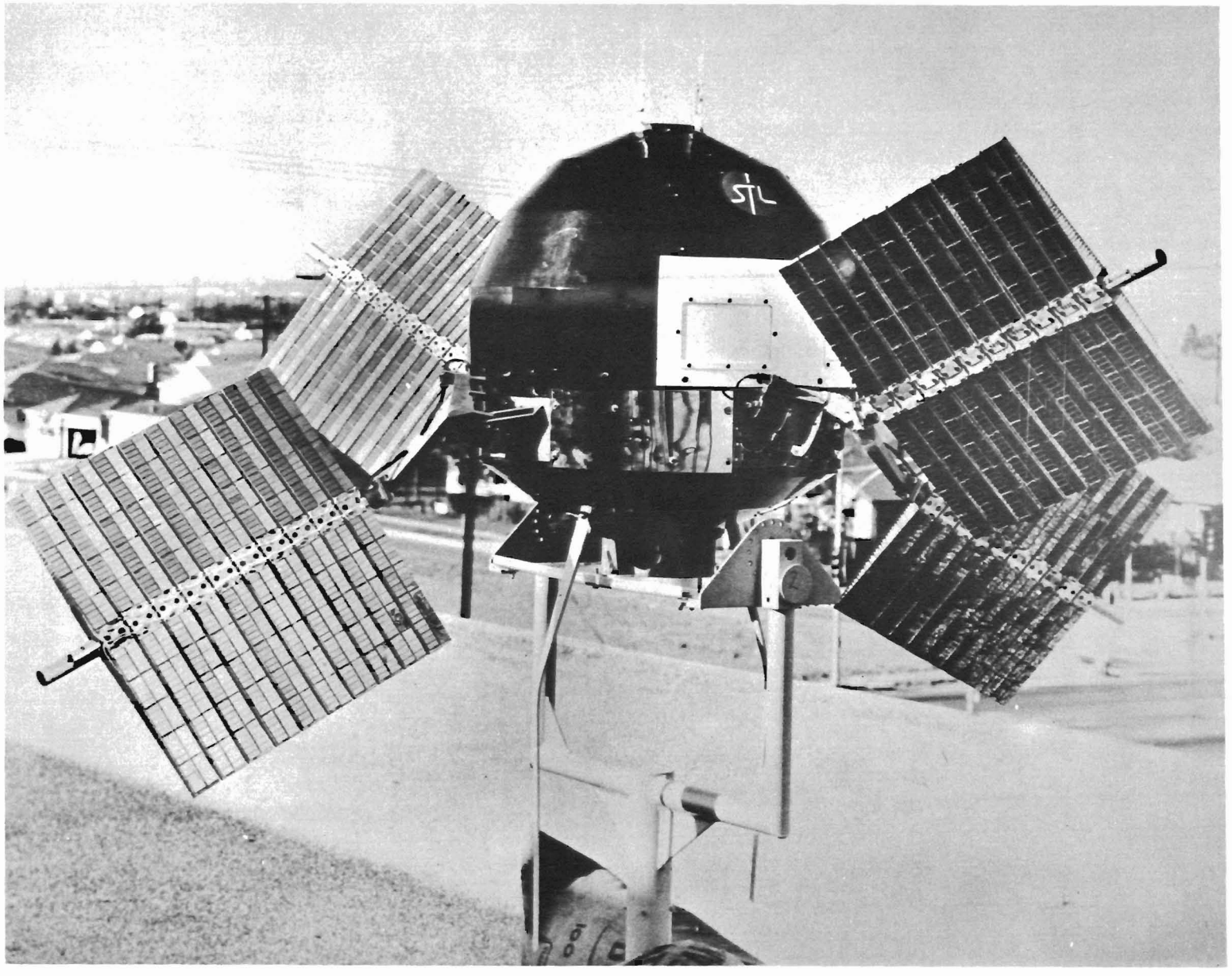

FIGURE V-A-53 EXPLORER VI SATELLITE Payload of Explorer VI satellite shows the orbiter with solar cell paddlewheels extended

to a minimum. The geometry of this system, discussed in subsection 2.0, minimizes variation of output with angle of incidence.

Each paddle is fabricated from wedge-shaped sub-modules. Ten five-cell shingles are bonded to each wedge with Spectrolab's Solabond adhesive. The wedge-shaped substrate is fabricated from aluminum honeycomb with thin anodized facings. Each wedge weighs approximately 0.15 pounds.

The weight of a solar cell structure will depend significantly on the protection required from the radiation hazard. For example, the use of glass covers about 50-mil thick and a corresponding amount of material on the rear surface results in densities of large, flat, extended solar collectors on the order of 2 lb/ft^2, with .2 lb/ft^2 consumed by the solar cells. General Electric estimates that without the protective measures, panel weight could ultimately be decreased to .3 lb/ft with current solar cells. A lightweight structure could, for example, be composed of a framework of magnesium structural members, over which is stretched a flexible wire grid where the cells are attached.

More standard structural techniques are incorporated in the Ranger solar cell panels which consist of a flat trapezoidal structure (30 in. x 11 in. by 6 ft.) using 4340 cells per panel. The cells and their support weigh 0.7 lb/ft^2 while the entire panel weight is 20 lb for an area of 10 ft^2. The basic support is provided by aluminum honeycomb with 12-mil facing, and a 6-mil glass cover and filter is used.

4.3 Optimum Series-Parallel Arrangement of Cells

The optimum series-parallel arrangement of cells in a large array is determined by considerations of reliability and panel configuration. In general cell failures, whether from environmental damage or fabrication errors, result in open-circuits rather than short-circuits. Thus, if the effect of a failure is to be minimized the basic groupings should be of cells in parallel. However, most solar cell users prefer the basic shingle subgroup of Figure V-A-49 either because of its more efficient utilization of panel area or because they have a limited amount of panel area under uniform illumination.

As a rule of thumb, it may be said that the most reliable series-parallel circuit is designed by (1) finding the number of junctions n required to be in series to produce the needed output voltage, (2) finding the number of cells m which cover the largest uniformly illuminated panel area, and (3) making parallel-connections of $\frac{m}{n}$ cells and connecting n of these submodules in series to make the uniformly illuminated panel.

The reliability is not generally increased greatly after the number of parallel cells in a submodule exceeds ten.

5.0 USE OF CONCENTRATING MECHANISMS

The use of concentrators for measuring the solar flux incident on the cell surface can significantly increase the power output per unit cell area. In this subsection, the effect of cell performance on panel design when using solar concentrators is discussed, along with possible advantages of the system. Additional discussion concerning the concentrator design, system weight and cost, and other factors in system design are discussed in Volume IX.

The optimum concentration ratio is a compromise between decreased efficiency at high temperatures and increased power per unit area incident on the cells and is selected to accomplish minimization of vehicle weight and/or minimization of vehicle cost.

Techniques of cell temperature control are discussed in subsection 3.0. The most useful technique for lowering equilibrium cell temperature lies in control of the spectral surface characteristics of the panel and/or the concentrator reflective surface. Spectrally selective techniques which offer only a small advantage at unconcentrated insolance generally are much more attractive at higher insolances. The filters on the reflective surface optimally have the reverse characteristics of the solar cell filters (i.e., for silicon, high reflectivity from 0.45 to 1.13μ, and low reflectivity over the rest of the solar spectrum). Difficulties in using an interference type filter on the reflecting concentrator include the extreme grazing angles of incidence (and loss of spectrally selective properties) and the lack of structural rigidity of the thin, lightweight concentrators. The analysis here assumes only a cell filter.

As an illustration of the advantages available in systems using solar concentrators, consider the following design:

a. System is fully oriented.

b. A flat, solar cell panel configuration will be used, with large thermal conductivity from one side to the other.

c. The efficiency of the solar cells varies with temperature, as shown in Figure V-A-54, and does not vary significantly with insolence.

d. Spectral coatings are available with the characteristics of Figures V-A-25a, V-A-25b, and V-A-25c of subsection 2.1.4. These coatings have been shown to have absorptivities of 0.8, 0.75, and 0.58 to the solar spectrum.

The available spectral coatings will be compared with an ideal coating whose absorptivity is zero for wavelengths outside the region of solar cell response. The over-all absorptivity of such a coating is 0.58.

The expression for equilibrium temperature of the panel is, neglecting the energy transformed to electric power,

$$T = \left(\frac{\alpha^1 CH}{\sigma \epsilon^1} \right)^{1/4} \qquad \text{(A-26)}$$

where α^1 = the net absorptivity of the panel as defined in Section 2,

ϵ^1 = the net emissivity

C = concentration ratio

H = solar constant.

A family of curves in Figure V-A-35 shows equilibrium temperature vs. concentration ratio for several combinations of filters and ratios of cell-covered panel area to uncovered panel area. It is assumed that the panel area uncovered by cells is coated to give it an absorptivity of 0.1 and an emissivity of 0.95. It is further assumed that the emissivity of the ideal cell filter is 1.0 and of other filters is 0.9. The characteristics of the filters are as shown in Table V-A-6.

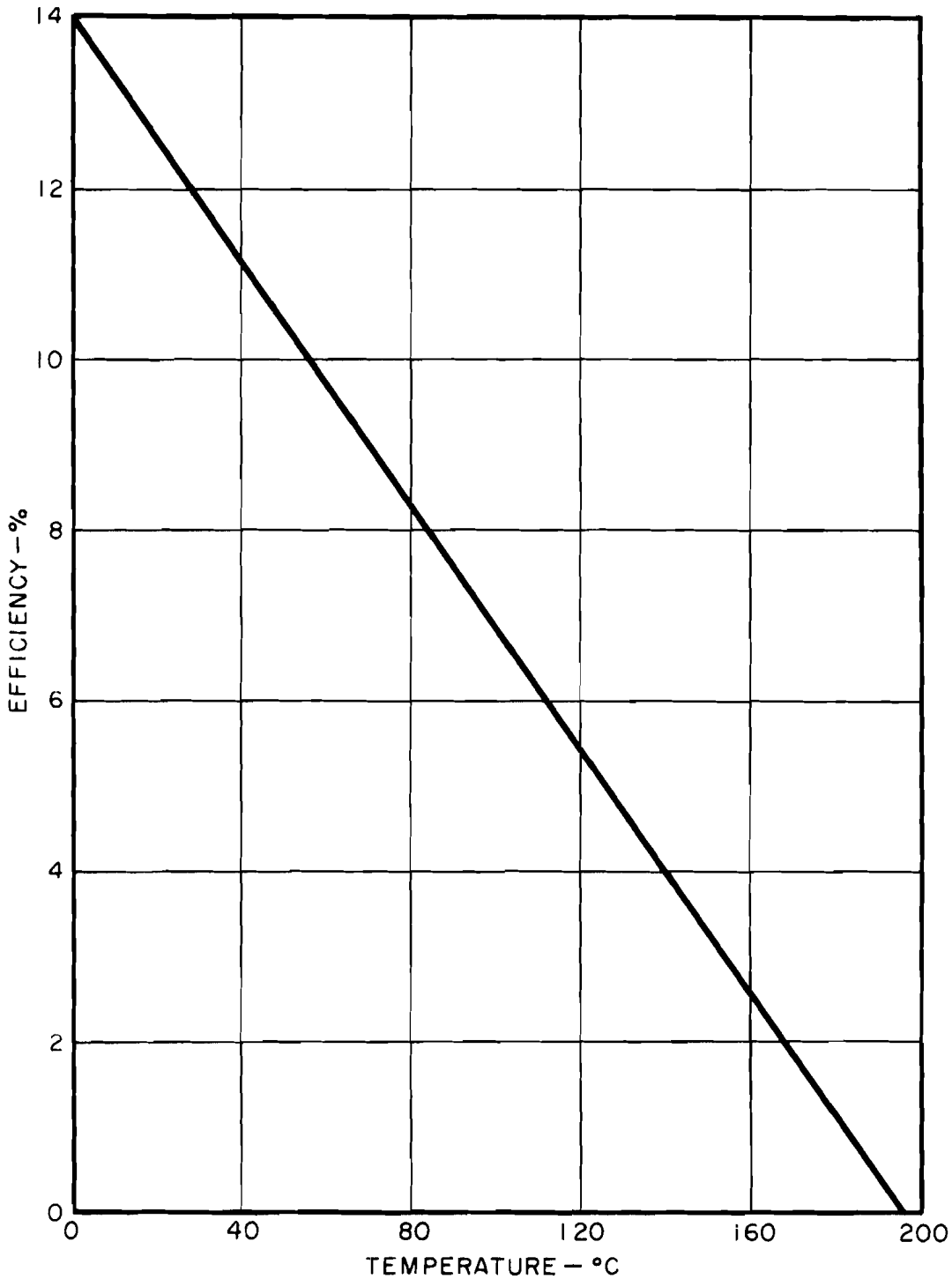

FIGURE V-A-54 EFFICIENCY VS. TEMPERATURE OF A SILICON SOLAR CELL

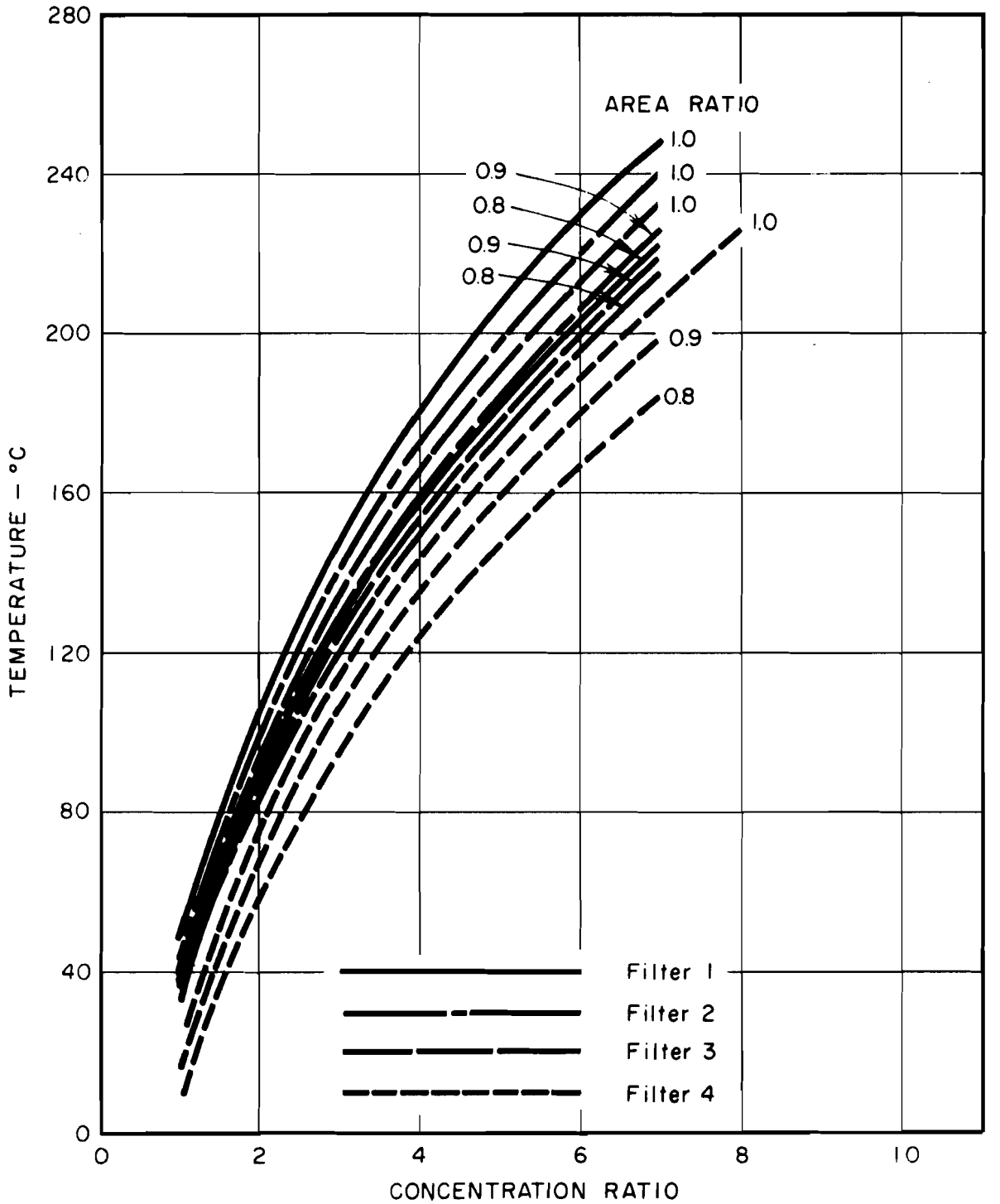

FIGURE V-A-55 TEMPERATURE VS. CONCENTRATION RATIO

TABLE V - A - 6
CHARACTERISTICS OF FILTERS

Filter	Absorptivity	Emissivity	Comment
1	0.8	0.9	Blue filter now in use.
2	0.75	0.9	Red-Blue filter now available.
3	0.60	0.9	Red-Blue filter available later.
4	0.58	1.0	Absolute ultimate filter.
Metal coating	--	0.95	To be used on panel underside.
Top surface coating	0.1	0.95	To be used on panel topside that is not covered by cells.

Equilibrium temperature curves of a flat, oriented cell panel covered with such filters are shown in Figure V-A-55 for various ratios of cell area to panel upper surface area. A good measure of the effectiveness of a concentrator system is the product of the cell efficiency and the concentration ratio. This parameter, called the performance factor, gives the relative output of the cells assuming efficiency varies only with temperature and does not vary greatly with incident intensity.

Figure V-A-56, showing the performance factor vs. concentration ratio, is plotted using Figures V-A-54 and V-A-55. Note that with filter 2, the best currently available, the optimum performance of the cells under concentration is 1.25 times that without concentrators if the surface area is totally covered with cells. If the surface area is only 0.9 or 0.8 covered with cells, the improvement is a factor of 1.30 or 1.32.

These factors are derived on the basis of currently available hardware. With the improved red-blue filter now being developed, as

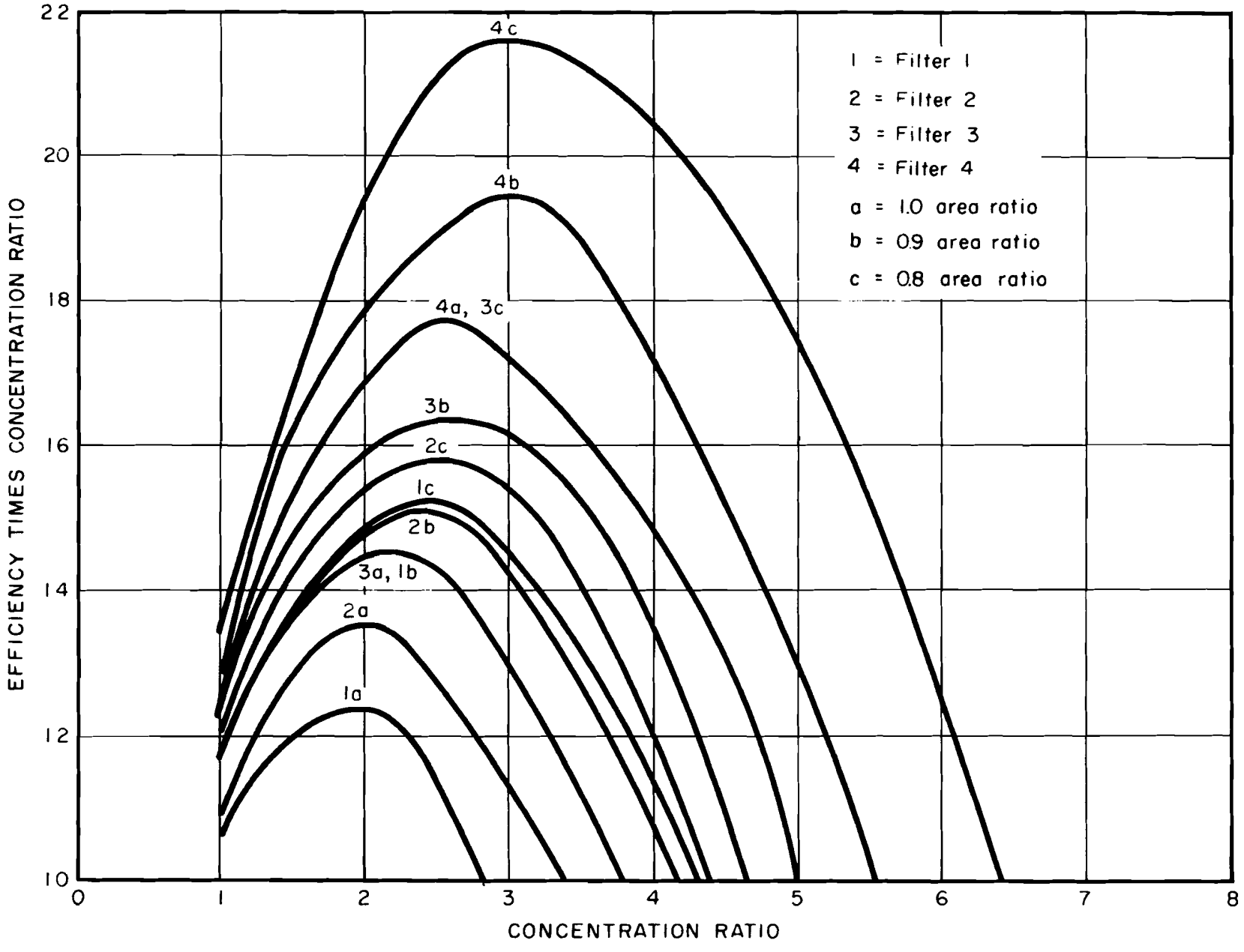

FIGURE V-A-56 PERFORMANCE FACTOR VS. CONCENTRATION RATIO

discussed in subsection 2.1.4, the improvement factor can approach 1.45. Finally, with filter 4 (the theoretical ultimate), the improvement factor approaches 1.6.

Therefore, it is concluded that concentrators can reduce the required cell and panel area by 1/4 to 1/3. With a 1 kw power supply, this implies a cell cost reduction of $50,000 to $100,000. Nevertheless, the added area, weight, cost, and reliability problems of the concentrator must be balanced against possible weight and cost savings resulting from concentrator utilization.

6.0 FUTURE CELL PERFORMANCE

It is reasonable to expect that performance characteristics of photovoltaic energy conversion systems will improve with future developments. In this sub-section, some of the new concepts in photovoltaic devices, in both early and advanced stages of development, are presented, together with a representative, but not complete, listing of active organizations.

6.1 New Devices in or Near Production

6.1.1 Gridded Cells

Recently, a new type solar cell has been placed on the market by both Hoffman Electronics and The International Rectifier Corporation. The new type of contact employed on these cells is shown in Figure V-A-57. The grid contact on the surface effectively reduces the internal series resistance of the cell. Because of this decreased resistance, the optimum operating voltage of the cell will be substantially greater than with nongridded cells. A typical characteristic of a high-efficiency gridded cell is compared in Figure V-A-58 with that of a high-efficiency nongridded cell. Note that the gridded cell has a more nearly flat characteristic in the low voltage portion of the curve due to its lower series resistance.

At present, Hoffman and I. R. C. are producing 13 percent efficient gridded cells in quantity. It is possible to purchase both gridded and nongridded 12 percent cells. The practice seems to be to price the cells according to their efficiency whether or not they are gridded.

Since the gridded contacts are usually only 1 to 2 mil in thickness, there appears to be no added difficulty in bonding glass cover slides to the cell surface.

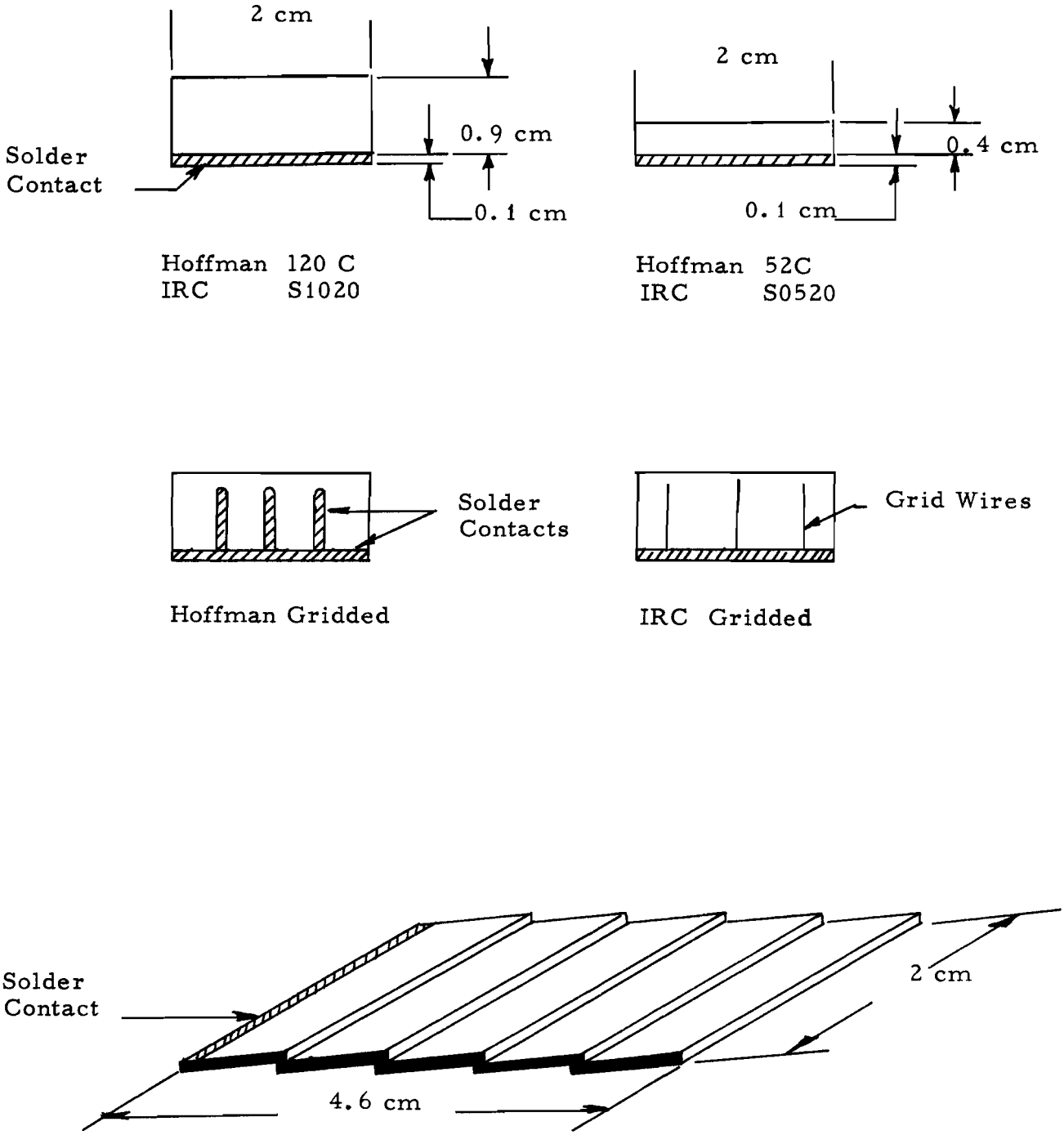

FIGURE V-A-57 POPULAR CELL TYPES

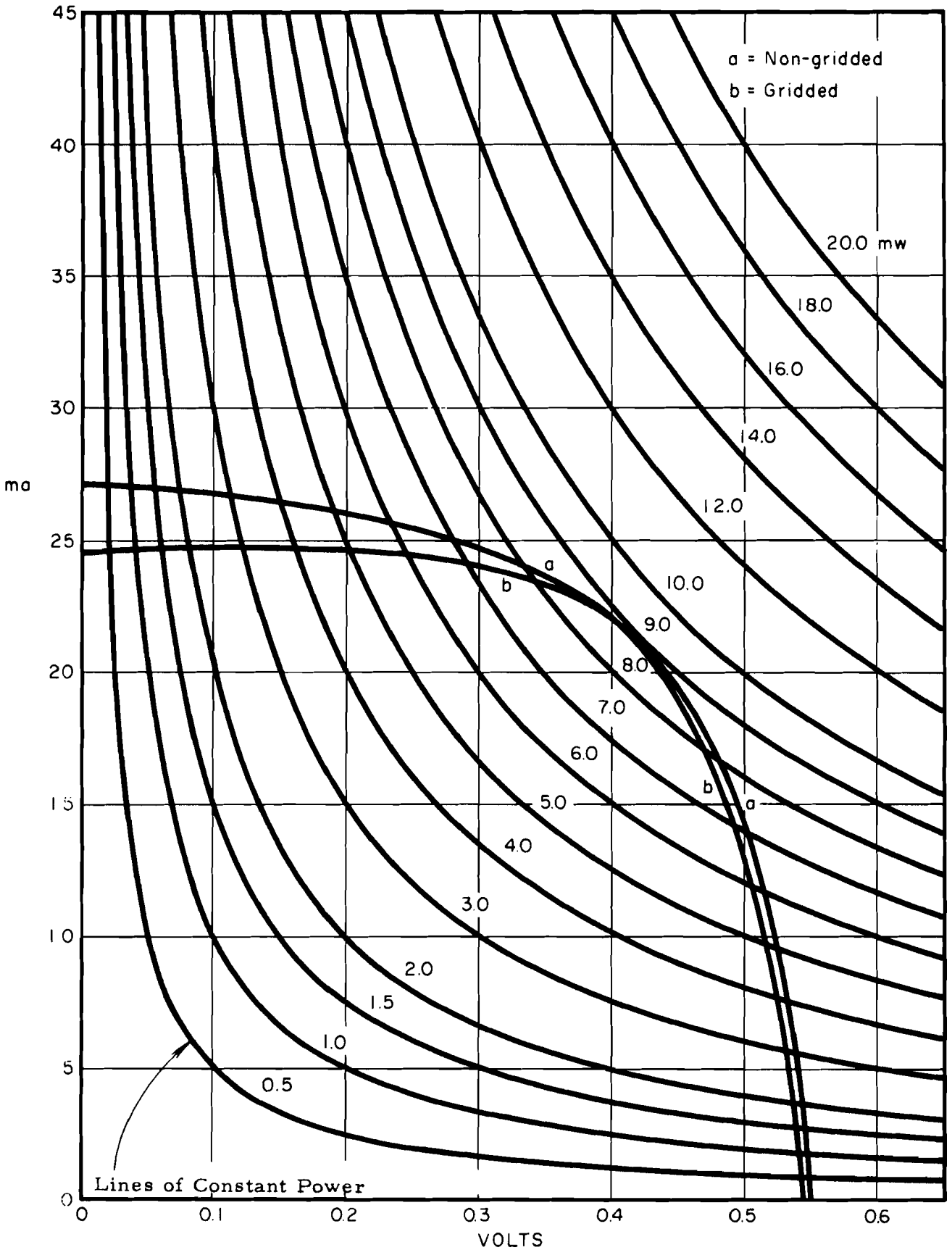

FIGURE V-A-58 CHARACTERISTICS OF TYPICAL GRIDDED AND NON-GRIDDED SILICON CELLS OF EQUAL EFFICIENCY

6.1.2 Large-Area Cells

The availability of the grid-type contacts makes it quite possible to make larger area, high-efficiency cells. The Hoffman Electronics Corporation is presently engaged in a developmental program for the fabrication of cells up to 2- by 10 cm in size. Such cells could be somewhat less expensive per watt than the present size cell and could prove to be more efficient because of reduced edge effects. Additionally, use of such cells should reduce the expense of panel fabrication.

6.1.3 High-Efficiency Silicon Cells

A number of organizations including Hoffman, International Rectifier, and Transitron are engaged in programs designed to produce higher efficiency single-junction silicon cells. The approaches used include the following:

a. Improving the purity and crystal perfection of the silicon material.

b. Using an improved diffusion process designed to increase the lifetime of the diffused material.

c. Improving the cell surface to reduce reflection.

d. Using better ohmic contacts and improved grid structures.

Currently, 13 percent efficient cells are available, and 15 percent cells are observed occasionally. It is quite probable that the ultimate maximum efficiency for an average production model of a silicon photovoltaic converter will be about 15 percent. Future increases in efficiency will utilize some of the more exotic photovoltaic systems now being developed.

6.2 Cells Under Development

A great deal of effort is presently being expended in the United States to develop some new photovoltaic systems which will prove to have advantages

over conventional silicon cells. This work, being supported for the most part by the federal government, is outlined below.

6.2.1 Spherical Cells

The Hoffman Electronics Corporation (under contract to USASRDL) is attempting to develop large-area solar energy converters which consist of small spherical silicon cells. The small silicon spheres, typically 3 mm in diameter, are diffused and embedded in plastic, as shown in Figure V-A-59. Successive plating, lapping, and plating operations produce the finished, large-area solar converter. The investigators have shown that approximately 95 percent of the incident radiation can be absorbed with this geometry; and, if they can make the efficiency of the spheres comparable with that of wafers, a large-area solar "cell" can be made whose efficiency is comparable with that of conventional cells. Experimentally, 10-percent efficiency has been achieved with a 2 cm^2 cell.

6.2.2 Graded Gap and Composite Cells

Since a semiconducting material of a specified band-gap is best suited to converting only a narrow portion of the solar spectrum, considerable effort is being expended toward the development of solar cells incorporating more than one photovoltaic material. Such cells appear in two forms. The composite form incorporates two or more separate materials into one cell, with the incident radiation being split up and directed to the material best suited for each part of the spectrum. Graded gap cells are essentially fabricated from a single crystal which is integrally composed of more than one material. The basic theory of such cells is developed in section 7.0.

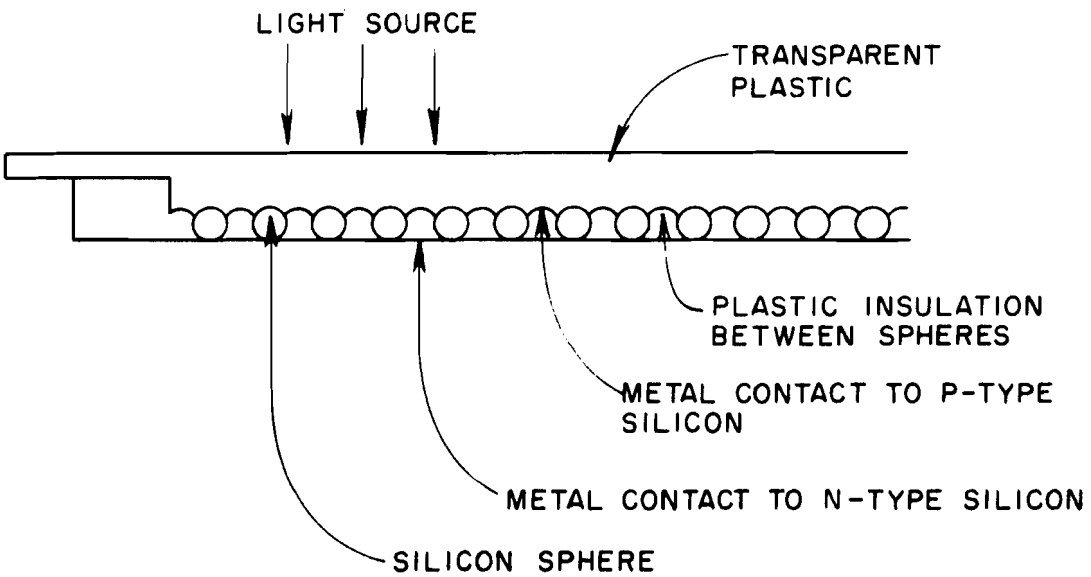

FIGURE V-A-59 CROSS-SECTIONAL VIEW OF LARGE AREA SOLAR CELL COMPOSED OF SILICON SPHERES

Two basic approaches are being used toward the development of composite energy gap cells. Electro-Optical Systems, Inc., under contract to USASRDL, is studying a reflection type cell in which the solar spectrum is divided into two parts by a dichroic mirror, one part being directed to a high energy gap cell and one to a low energy gap cell. The basic geometry of the device is shown in Figure V-A-60.

Theoretical calculations indicate that the optimum material for the high energy gap material is 1.65 ev and that the optimum for the low energy gap material is 1.1 ev. The materials being developed for the high-energy gap cell are aluminum antimonide and cadmium selenide. If one of these materials can be brought to a state of perfection approaching that of silicon, this composite cell could yield efficiencies approaching 20 percent.

An extensive materials development program, in progress at the Harshaw Chemical Company, is designed to produce materials suitable for a stacked or layered composite cell. The basic geometry of this cell type is shown in Figure V-A-61. The device depends for its success upon a material transmitting, as a window, all radiation whose energy is less than its band-gap. Then, by stacking cells, one on top of the other in order of increasing band-gap, a great portion of the incident spectrum can effectively be utilized.

The most difficult problem, one that is circumvented in the reflector configuration, is that of making the materials pure enough so that they will in fact transmit the appropriate portions of the incident spectrum sufficiently well to justify this mode of operation. The Harshaw people (under contract to USARDL) have been developing CdS, ZnSe, ZnTe, CdSe, CdTe, and

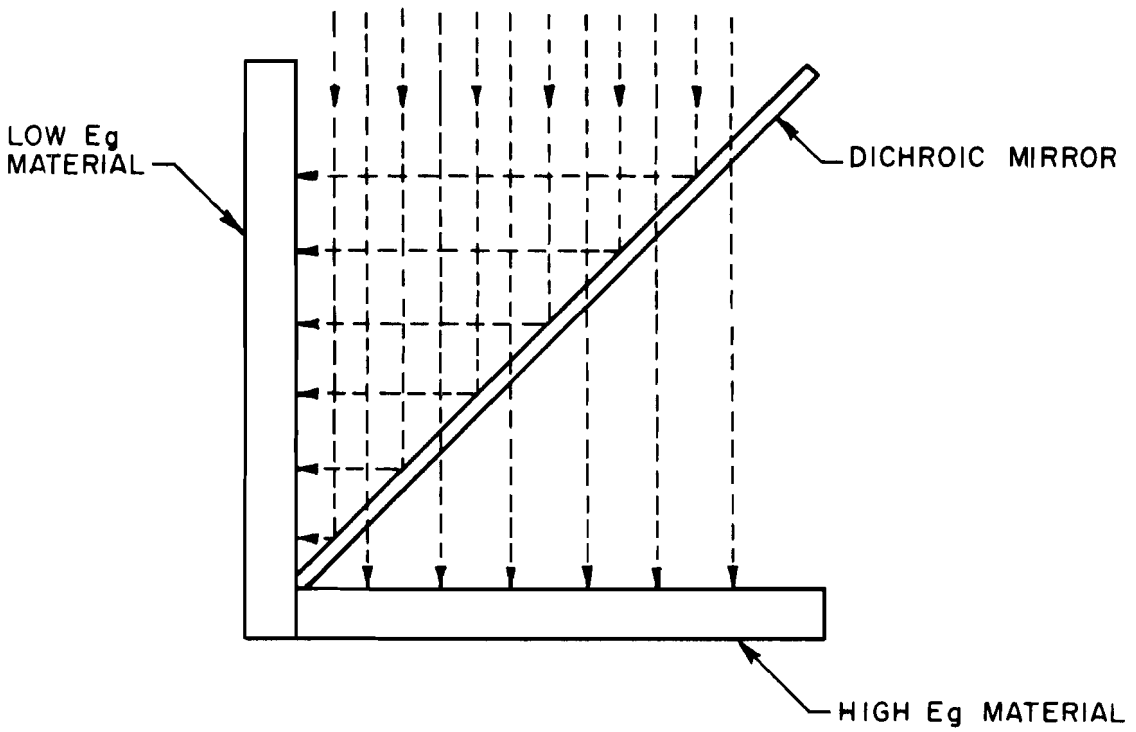

FIG V-A-60 REFLECTIVE COMPOSITE SOLAR CELL

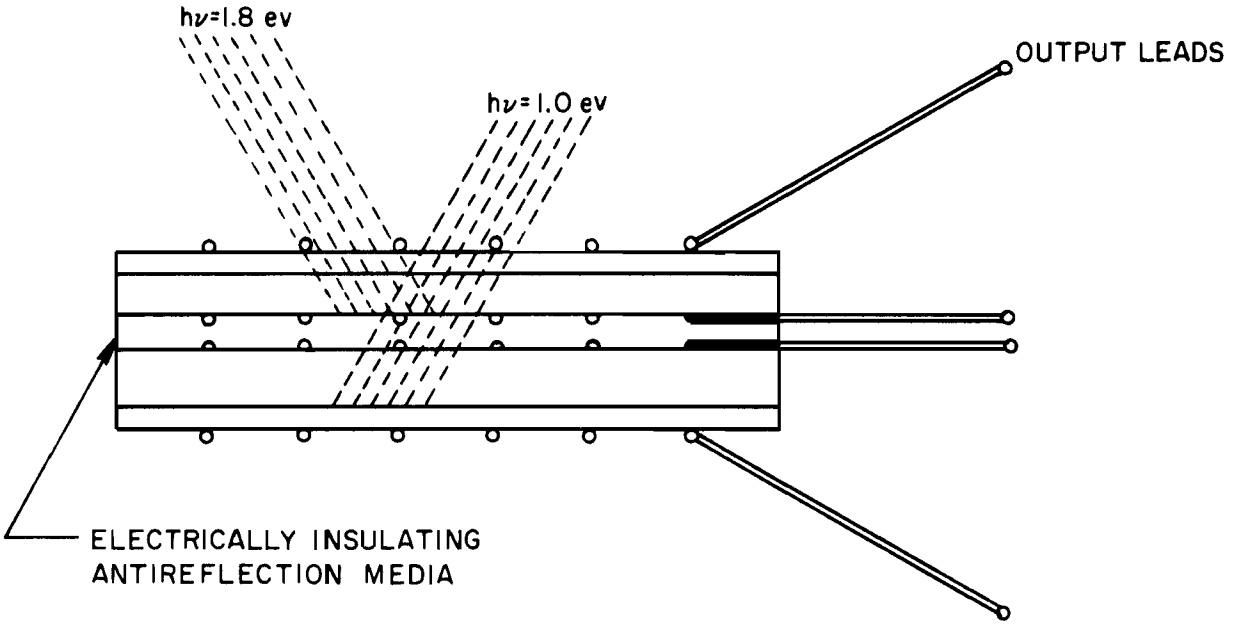

FIG V-A-61 TYPICAL COMPOSITE ENERGY GAP SOLAR CELL

ZnS for use in such devices. However, at this time, efficient solar cells have only been made with CdS. Such composite cells can, in theory, approach efficiencies of 30 percent.

Graded gap cells have been proposed in several different forms. A graded gap might be made by vapor, depositing one semiconductor onto another, or by pulling a crystal from a melt whose constitution is changed during the pulling operation. The theory of such devices can be quite involved and is discussed in Section 7.0. The primary purpose of the varying gap is to utilize the best photovoltaic properties of more than one material in a single p-n junction cell.

The Eagle-Picher Research Laboratories are presently engaged in a study, sponsored by USASRDL, designed to construct a multiple band-gap cell made up of GaP and GaAs. The physical design of the cell is shown in Figure V-A-62 and the distribution of band-gap, in Figure V-A-63. It is hoped that the cell would have as much current available at the junction as a GaAs cell (1.35 ev band-gap) with the higher voltages theoretically available in a GaP cell (2.2 ev band-gap). The maximum theoretical efficiency of such a cell would appear to be 20 to 30 percent. The approach currently used consists of diffusing phosphorus into a GaAs wafer to a predetermined depth and then diffusing a dopant (usually cadmium) into the GaP-GaAs wafer. Solar cells have been made with this technique which showed the approach to be valid, and it is quite possible that such cells will soon exceed in efficiency the maximum efficiency obtained with single gap GaAs cells.

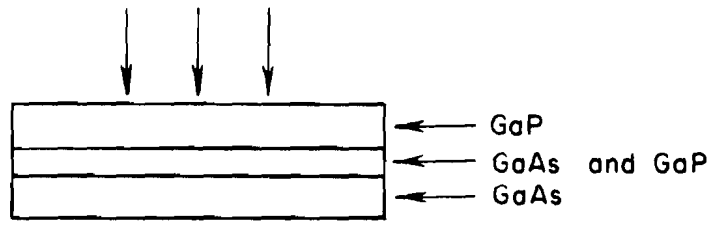

FIGURE V-A-62 A GALLIUM PHOSPHIDE - GALLIUM ARSENIDE CELL

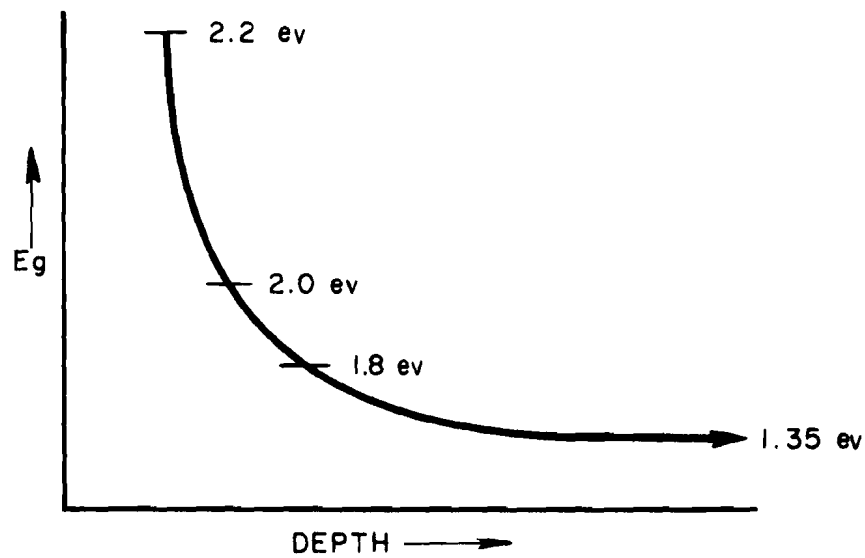

FIGURE V-A-63 ENERGY BOND VARIATION IN THE GALLIUM PHOSPHIDE-GALLIUM ARSENIDE CELL

The Harshaw Chemical Company is also attempting the fabrication of a type of graded gap cell in their composite cell study. They are presently investigating ZnTe-CdS and CdTe-CdS junctions.

6.2.3 High-Temperature Cells

Several programs are in progress directed toward development of cells which will be more efficient than silicon cells at elevated temperatures. It might be expected that, at increasing temperatures, the optimum energy gap of a photovoltaic cell will increase. Wysocki and Rappaport (Ref. V-A-7) predict that the maximum efficiencies of various band-gaps are as shown in Figure V-A-64, assuming I_o is made up of a diffusion part and a recombination current.

However, such predicted efficiencies cannot account for performance degrading effects which are not functions of the band-gap such as low mobilities, low lifetimes, and extreme technical difficulties in producing large area single crystals. Thus, several high temperature semiconducting materials are being investigated, including CdS, GaAs, and CdTe. Measured data on cells fabricated from GaAs and CdS are shown in Figure V-A-65. It appears at this time that much work needs to be done to bring these materials to a level of development comparable with silicon. A discussion of the developmental programs is given below.

6.2.4 CdS Cells

It is interesting to note that efficient cadmium sulfide solar cells were reported (Ref. V-A-8) at about the same time as the first silicon solar cells. Since that time, a great deal of effort has been expended by several laboratories -- including Harshaw Chemical Company, Clevite Corporation, Armour Research Foundation,

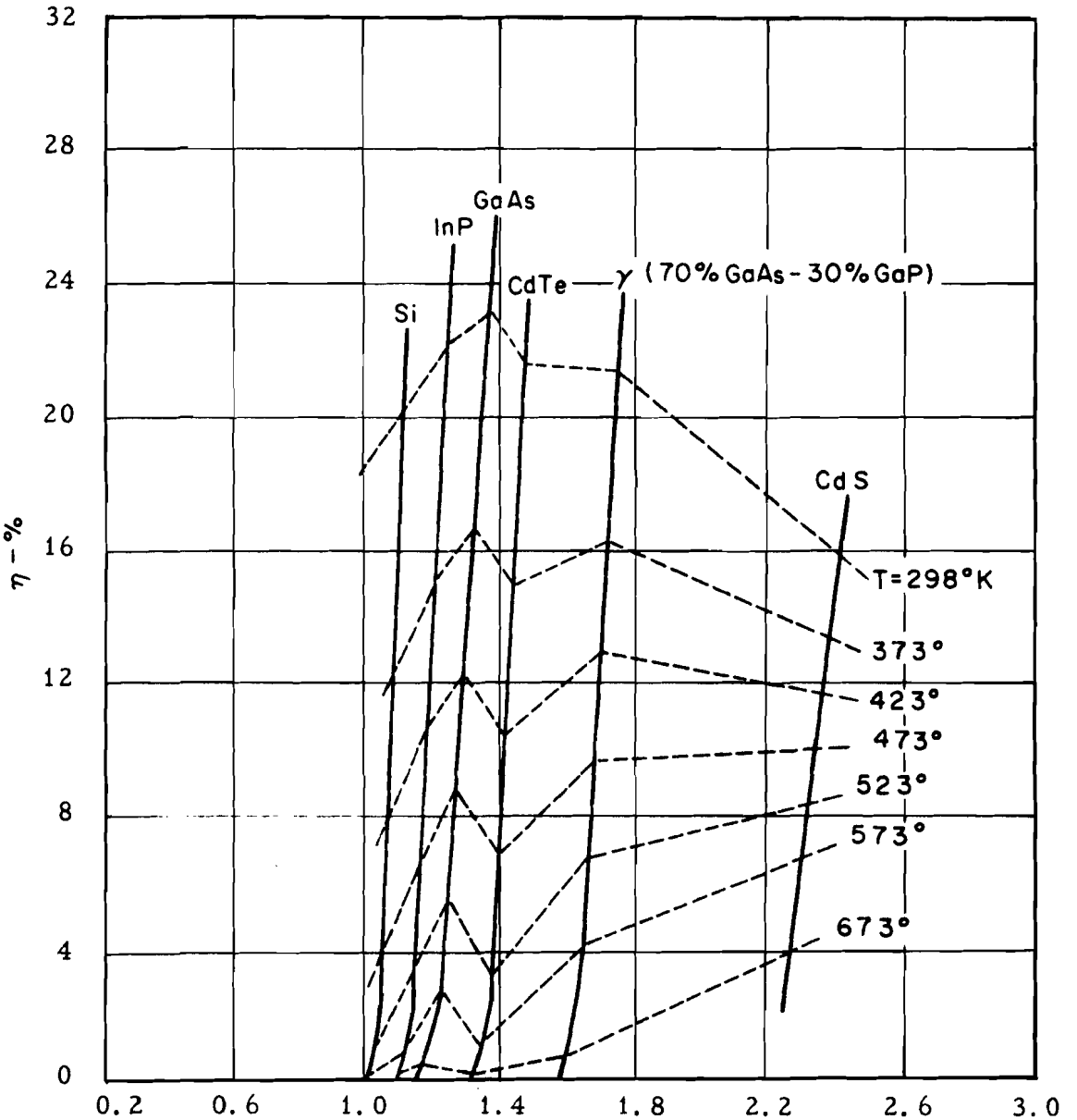

FIGURE V-A-64 EFFICIENCY VS. ENERGY GAP

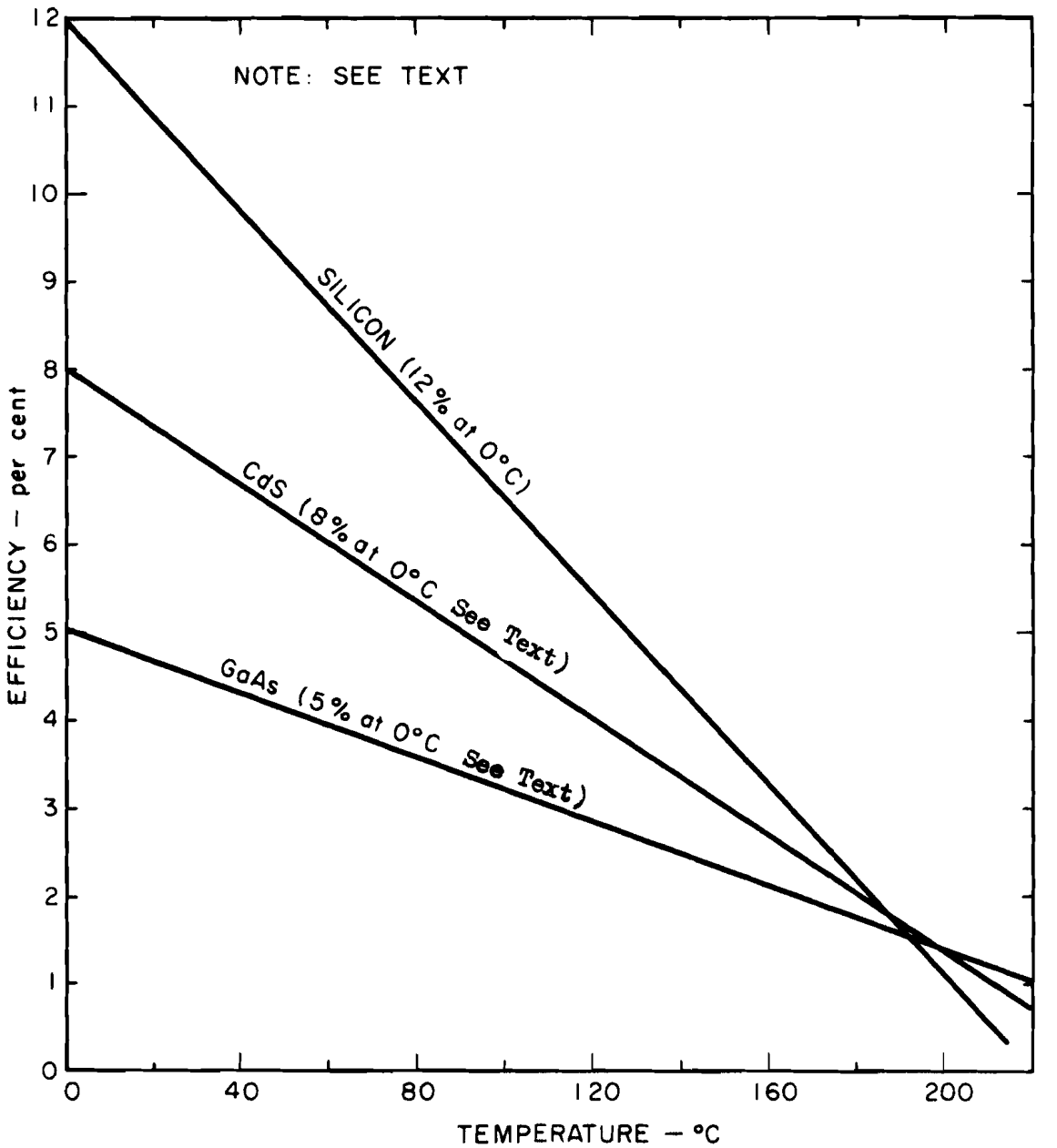

FIGURE V-A-65 EFFICIENCY VS. TEMPERATURE

Eagle-Picher Laboratories, and WADD -- toward the development of improved CdS cells. At the present time, the best cells are about 7 percent efficient, with the average somewhat lower.

The CdS solar cells that have been developed do not utilize the same physical processes that p-n junction silicon cells use. Instead of generating a voltage across a p-n junction, the CdS cells are constructed so that a barrier layer appears at a contact (usually copper). The voltage is then generated across this barrier layer. Barrier layers of this type are much more readily made than p-n junctions, a fact that explains why CdS cells would be made with efficiencies comparable to silicon cells at a time when the metallurgy of CdS was much less developed than that of silicon. Even now, there is no conclusive evidence available that a p-n junction has ever been made in CdS.

As might be expected, the spectral response of the CdS cell is not that which would be found in a p-n junction cell in a material with the band-gap of CdS (2.4 ev). The response (see Figure V-A-66) is more indicative of a material of band-gap 1.3 ev. Williams and Bube (Ref. V-A-9) suggest that the barrier layer effect results from the photo-emission of electrons from the upper metal into the CdS crystal.

Because the band-gap effectively is 1.3 microns in this solar cell, its efficiencies could, with expected great improvement in the purification and growth of the crystals, approach or slightly exceed that of silicon cells. At their present state of development, CdS solar cells offer no advantages over silicon cells to compensate for their lower efficiencies. However, their rate of efficiency degradation with temperature,

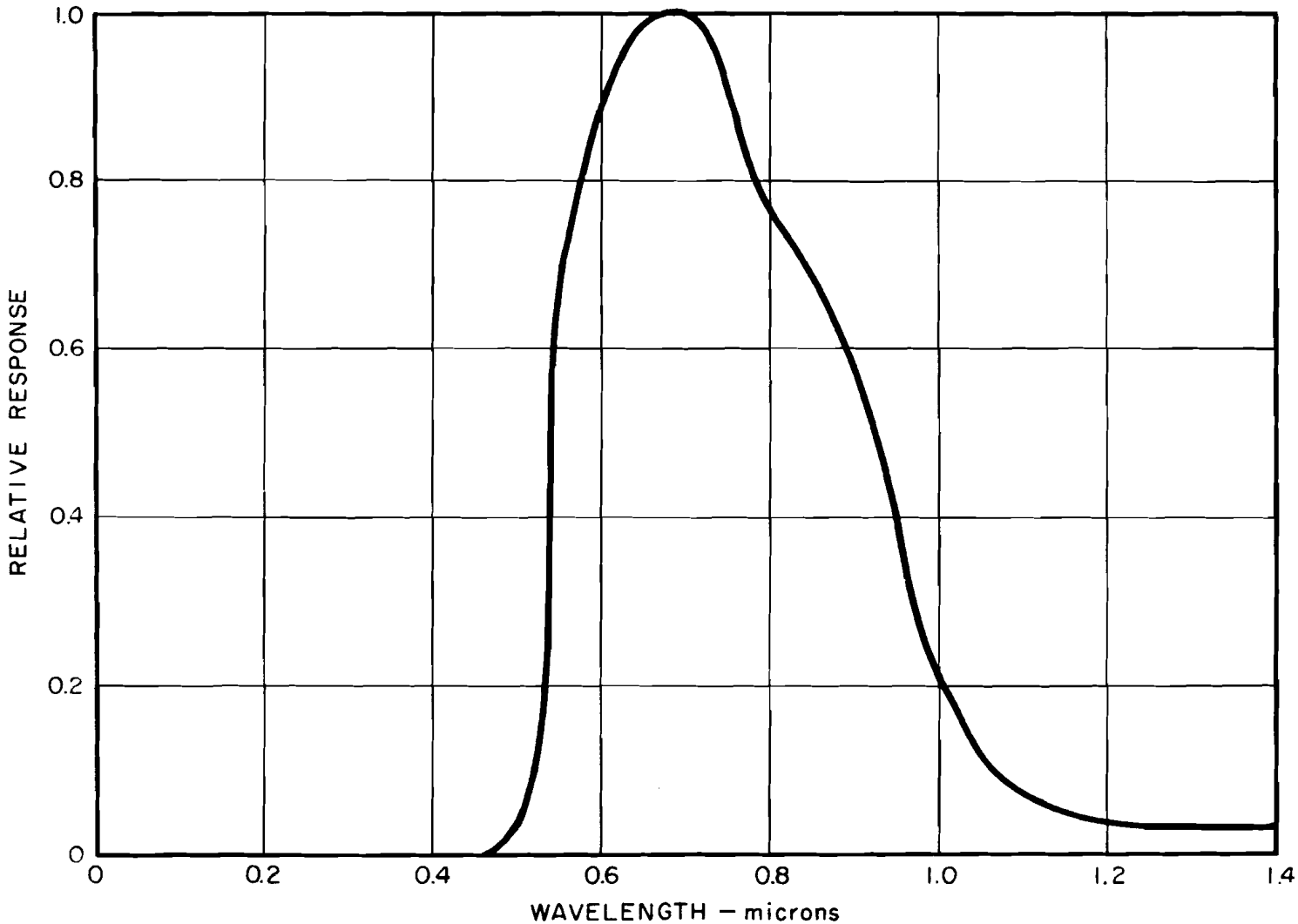

FIGURE V-A-66 RESPONSE OF A CdS CELL

as shown in Figure V-A-65, appears to be lower than with silicon cells, indicating that CdS cells may, with improvement, be useful in high-temperature applications.

6.2.5 GaAs Cells

The intermetallic semiconductor gallium arsenide (energy gap of about 1.4 ev) has been the subject of an extensive development program at the RCA laboratories in Princeton with the hope of producing solar cells with improved high-temperature operating characteristics. The work, sponsored by the Signal Corps, has resulted in successful fabrication of GaAs solar cells with efficiencies of 5 percent, at room temperature. However, the metallurgical problems have proved to be quite severe; and large area crystals, suitable for solar cells, have been found to be difficult to produce. Also, actual high-temperature characteristics of the cells have not proved to be as favorable as the early theoretical estimates indicated, as shown in Figure V-A-65. It is possible that a major breakthrough in purification and growth of GaAs crystals could improve the high-temperature performance of GaAs cells sufficiently to warrant their use in systems where high temperatures cannot be avoided. However, at the present, it is not clear what the ultimate properties of GaAs cells will be.

6.2.6 CdTe Cells

A program has recently been instituted by the Armour Research Foundation, under contract to USASRDL, for the development of CdTe as a solar cell material. This material, with a band-gap of 1.4 ev, offers promise of yielding cells with improved high-temperature characteristics. Because it is in an early stage of development, no solar cells have been made. However, this II-VI material has favorable lifetime

and mobility properties, and successful p-n junctions have been made. Some work on this material in the Soviet Union (Ref. V-A-10) has produced successful solar cells of efficiencies up to 5 percent.

6.2.7 Polycrystalline Cells

It has been suggested that large-area solar cells could be made from polycrystalline material, since the area of silicon crystals is presently limited. If reasonable quantities of photovoltaic material, the great expense of solar-to-electrical power conversion could be reduced. Possibly very large solar collector-converters could be made by depositing the photovoltaic material directly on large area panels. Although such devices are not likely to be soon available, considerable research is being conducted on the basic properties of thin films. Both inorganic and organic materials are being considered.

The General Electric Company, Semiconductor Department, (under contract to USASRDL) is engaged in an effort to develop large area lightweight cells. They are presently considering techniques for the deposition of thin films of semiconducting silicon, with hopes of achieving photovoltaic conversion efficiencies of 5 to 10 percent.

It is well known that certain organic compounds exhibit photovoltaic characteristics. If the properties of these compounds could be improved to enable reasonable solar-to-electrical energy conversion efficiencies to be reached, they should prove to be ideal materials for large-area, thin, lightweight solar cells. A large number of organizations are studying organic photovoltaic materials, including Brooklyn Polytechnic Institute, University of California at Berkeley, National Carbon Company, Ohio State University,

New York University, and the Franklin Institute. Among the materials being considered are ethylene diamine tetracetic acid, phenosaframine, proflavin, anthracene, and phthalocyanine.

6.2.8 Large-Area, Single Crystal Cells

If large-area single crystal silicon were available, considerable expense would be saved in the fabrication of large-area solar panels. The Grace Chemical Company (through a contract to USASRDL) is presently attempting to develop a continuous process for growing large, single-crystal sheets of silicon. This process, if successful, would make fabrication of efficient, large-area cells economically feasible.

6.2.9 Radiation Resistant Cells

It has been suggested (Ref. V-A-11) that through special design of the p-n junction, silicon solar cells could be made which are considerably more resistant to electron and proton radiation than currently available cells. However, at this time, no developmental work on such cells is in progress.

6.3 Summary and Conclusions

In summary it is estimated that:

a. Silicon solar cells will remain the most effective photovoltaic energy conversion devices for at least three more years.

b. Intermetallic cells will probably appear in two or three years which will yield better high-temperature efficiencies than silicon cells.

c. Ultimately, multienergy gap materials will appear which yield better all around efficiencies (20 percent) than silicon cells but which will in all probability find only limited application because of innately higher (by a factor of two to five) fabrication costs.

d. Photovoltaic materials developed within three to five years, will enable the fabrication of large-area, low-cost, low-efficiency (three to five percent) solar energy collector-converters. These materials could conceivably be either organic semiconductors or polycrystalline thin films.

Unless such advances do occur in the development of photovoltaic devices, the use of such devices in space-power system will almost surely be reduced when other energy sources (e.g. thermionic, thermoelectric, or nuclear) are developed.

7.0 BASIC THEORY

This subsection presents a general theoretical description of solar cells, of both the conventional single-junction, single-energy gap type and of the multiband-gap devices now under development. Subsection 7.1 describes an idealized, simplified picture of the solar cell for readers not familiar with semiconductor theory and defines some of the more important nomenclature. In subsection 7.2 a detailed derivation of the solar cell characteristic equation is given, while in subsection 7.3, is presented the theory of composite and multigap cells.

7.1 Basic Semiconductor Concepts

If a metal is described as a solid in which some of the electrons associated with the constituent atoms are always free to move about the solid and if an insulator is described as a material in which all the electrons are firmly bonded to the atoms and cannot move about the crystal, a semiconductor may be described as a material in which none of the electrons are free at absolute zero temperature but in which more and more are free at higher and higher temperatures.

In a semiconductor, the electrons are bonded to the atoms by a relatively small energy called the band-gap or forbidden energy gap, E_g. As the temperature rises, the average energy of the electrons rises and with it the number of electrons at each instant possessing enough energy to be free. The conductivity of a semiconductor, therefore, increases with temperature.

The average energy of the electrons in a material at temperature T is described in terms of the quantity kT where k is Boltzman's constant. The quantity $\exp\left(\frac{E}{kT}\right)$ then simply relates an energy to the thermal electron energy. This quantity is seen often in semiconductor equations.

An electron may also be given sufficient energy to become free through interaction with a photon, where the electron absorbs all the energy of the photon, $h\nu$. Obviously, for this to occur the photon energy, $h\nu$, must be greater than the gap energy of the electron, E_g.

Another unique characteristic of semiconductors lies in the existence of holes. When an electron is excited and freed, a vacancy is left in the atom from which the electron was excited. In the presence of an electric field a bound electron can, under the forces of the field, easily be moved from its own atom to an adjacent atom possessing such a vacancy. The vacancy in effect propagates in a field in a direction opposite to that of the electrons. It is characteristic of most semiconductors that these vacancies, called holes, move in a field almost as readily as electrons and act very much like positively charged electrons.

If an atom of foreign material is present in a semiconductor crystal a number of effects can occur. Two are of paramount importance in semiconductor devices:

a. The impurity atom can, when integrated into the crystal structure, have one extra electron which is very readily excited into a free state.
b. The impurity atom can, when integrated into the crystal, present a vacancy or a hole to the crystal.

Crystals containing many impurities of the first type will have one free electron and one free hole from each thermally excited electron and one free electron from each impurity atom. Because such crystals have more free electrons present than free holes, they are called n-type. Conversely, materials of the second type, which have more free holes than electrons, are called p-type.

Crystals which have a substantial number of impurity atoms present, referred to as being heavily doped, conduct current almost exclusively by only one type of charged carrier, either electrons or holes.

7.1.1 A Description of Parameters

A number of the parameters utilized in semiconductor theory which are referred to in this text are defined and discussed below.

a. Intrinsic carrier concentration, n_i. If a semiconductor is not doped, it has no impurities. The number of holes and electrons per unit volume is equal and is called the intrinsic carrier concentration.

b. Minority and majority carrier concentration. In a doped crystal, there are more carriers of one type present per unit volume than of the other type. The concentration of carriers of the majority type is signified by n_n and p_p for n- and p-type material, respectively; whereas the concentration of the minority type is signified by p_n and n_p in n- and p-type material.

c. Mobility. The mobility of holes and electrons, μ_p and μ_n, respectively, describes the ease with which the carriers move under an applied field. It is described by the average carrier velocity divided by the applied field, usually in cm^2 per volt sec.

d. Diffusion coefficient. If a gradient of concentration of carriers exists in a crystal, the carriers will tend to diffuse just as heat will diffuse under a temperature gradient. The diffusion coefficient in semiconductors, usually given in cm^2 per sec , plays the same role as the diffusion coefficient in the temperature diffusion equation.

e. Lifetime. When a carrier is thermally excited into the free state, it will remain in this state for a finite length of time. After a time defined as the lifetime -- τ_n and τ_p for holes and electrons respectively -- the number of excited holes and electrons will have decayed to 1/e of its previous value. In equilibrium, of course, an equal number of newly excited carriers will keep the total number constant.

f. Diffusion length. If the carriers are diffusing under a concentration gradient and recombining (returning to the unexcited state) at the same time, the average length traveled by the carriers before recombination is called the diffusion length, L_n and L_p for electrons and holes, respectively.

7.1.2 The Semiconductor Junction

Consider now a semiconductor crystal in which the impurity concentration is nonuniform, so nonuniform in fact that the crystal is p-type on one side and n-type on the other. The region of the crystal where the p and n types meet is called the junction. If both p and n-type impurities are present throughout, the junction occurs where their concentrations are equal. The most important concept involved is this -- the potential energy of holes is greater in the n-region than in the p-region, whereas that of electrons is greater in the p-region than in the n-region. The junction then presents a potential barrier to both holes and electrons.

It is easy to understand this effect if one pictures two semiconductor crystals, one p-type and one n-type, being brought together.

The nonequilibrium distribution of carriers (all holes on one side, all electrons on the other) results in a diffusion of carriers across the junction. This diffusion will, however, produce a nonequilibrium charge distribution and a resulting field. This field will cause a current to flow opposite to the diffusion current which, in equilibrium, is equal to the diffusion current. The situation is illustrated below.

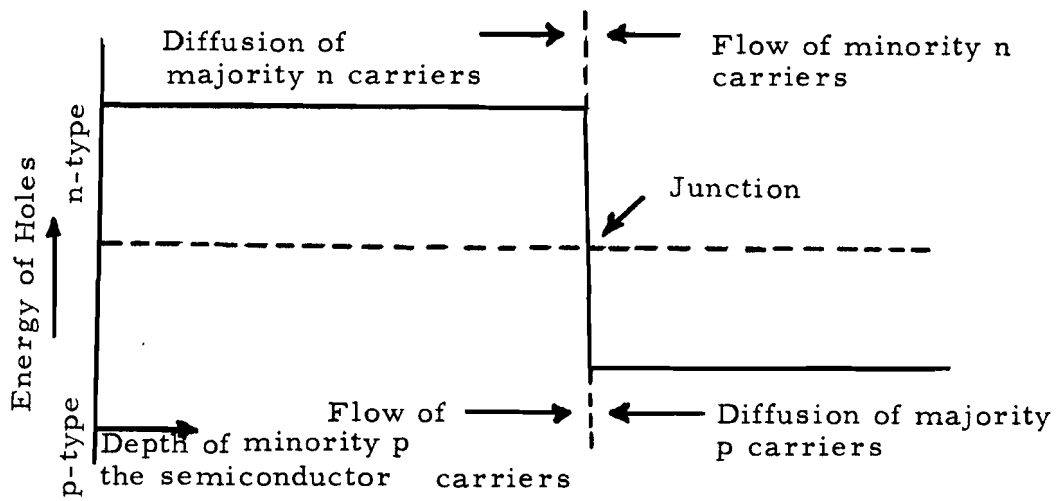

The availability of minority carriers dictates the equilibrium conditions. The flow by diffusion of majority carriers cannot exceed that of minority carriers, or the junction potential barrier will rise until the flow of majority carriers is reduced to equal that of the minority carriers. This equilibrium current is referred to as the saturation current, I_o. Note that the potential gradient between the p and n regions is concentrated in a region very close to the junction, called the depletion region. Any minority carriers reaching this region are swept across the junction by the fields present in the depletion region. Increasing the intensity of the fields will not increase this current, since all minority carriers reaching the junction are already swept across.

However, the converse is true with majority carrier flow. These currents are limited by the junction barrier. Therefore, decreasing the junction barrier will sharply increase the majority carrier flow. The rectifying properties of semiconductor junctions now become apparent. If no field is externally applied across the semiconductor junction, the net current flowing across the junction is zero. In fact, the potential barrier referred to above cannot be measured externally because of similar, exactly equal and opposite, potential barriers which will appear in the contacts made to the semiconductor for measurements.

When an external potential difference is applied in such a direction as to cause minority carrier flow, the fields in the depletion region will increase. However, as was seen above, the minority carrier flow will not increase, and will remain equal to I_o. The majority carrier current, equal in equilibrium to I_o, will be further reduced by the increased potential barrier, so that the maximum current seen externally is I_o.

If a field is applied in the majority carrier direction, however, the situation is quite different. The barrier will be lowered, and the majority carrier current will increase sharply with voltage, exponentially in fact, so that it equals

$$I_m = A \exp (\alpha V) \tag{A-27}$$

where A and α are constants and V is the externally applied voltage. Since for zero voltage $I_m = I_o$, A must be I_o. Fermi-Dirac statistics predict that α is q divided by kT where q is the electronic charge and k is Boltzman's constant.

It has thus been shown that the current voltage characteristic of a junction is given by

$$I = I_m + I_n \tag{A-28}$$

where I_m is the majority carrier current and I_n is the minority current or

$$I = I_o \exp (qV/kT) - I_o \qquad \text{(A-29)}$$

which is called the ideal diode equation.

7.1.3 The Solar Cell

Suppose, now, photons of energy greater than E_g (the gap energy of the material) impinge upon a semiconductor junction. As was mentioned previously, the photons will excite new p and n carriers; that is, each photon will excite one minority and one majority carrier whether in the p or in the n region. Any of these minority carriers that reach the junction will be swept across by the fields. The potential barrier across the junction will then be lowered, so that enough additional majority carriers will flow to just equal the additional minority carrier flow from the photons. However, the situation is far different from what it was before for the decrease in the potential barrier can be seen externally. In fact, the situation is described by the circuit shown below:

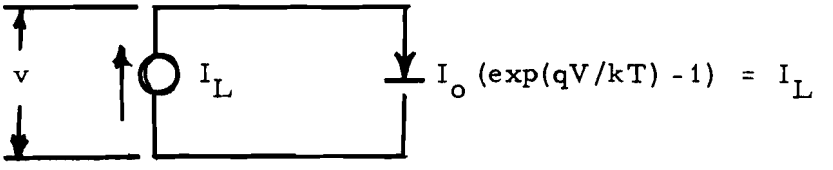

The diode represents the junction before the photon-generated minority carrier current appeared. The current generator represents the photon-generated current. The voltage V appears externally, can be measured, and is just sufficient so that the diode current of Equation A-29 just equals the added, photon-generated, minority carrier current.

If, now, the semiconductor junction is short circuited, the junction potential barrier can only be that which normally is present under dark conditions--that which cannot be measured externally because of the compensation barriers in the contacts. The current generated by I_L, the photon-generated minority carrier current, then must all flow through the external short circuit to be I_o. Finally, if the external circuit is a resistance, the equivalent circuit becomes

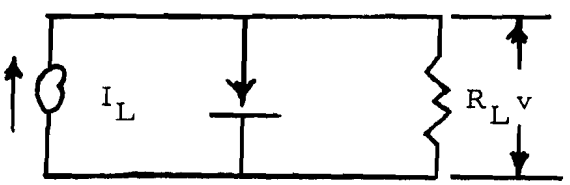

The photon-generated current is divided between the diode and the resistor. As the current in the diode is given by Equation (A-29), the current in the external load is I_L minus the diode current, or

$$I = I_L - I_o \left[\exp \quad (qV/kT) \quad -1\right] \qquad \text{(A-30)}$$

This is the fundamental idealized solar cell operating equation. Detailed expressions for I_L and I_o, in terms of the photon intensity and the semiconductor parameters, are derived in subsection 7.2.

7.2 Derivation of the Solar Cell Current-Voltage Characteristic

In this subsection, the solar cell characteristic equation is derived using the diffusion and continuity equations. The resulting equation will contain expressions for I_L, the photon-generated junction minority carrier currents and I_o, the saturation current or dark current, in terms of the parameters of the semiconductor, the shape and form of the cell, and the incident radiation.

7.2.1 The Solar Cell Model

Consider the solar cell to be a flat wafer, rectangular in cross sections as shown in Figure V-A-67. Photons of energy $h\nu$ enter the surface at $x = -a$, generating carriers in either the p or n regions. These carriers then move toward the junction to form the junction current.

Solar cells are manufactured from slices of silicon typically 20 mil thick, containing a uniformly distributed concentration of n-type impurity atoms. The wafers are then heated in an atmosphere of p-type impurity atoms, so that the p-type atoms diffuse into the surface. The concentration of p-type atoms near the surface is much greater than that of the n-type atoms, so the material near the surface has become p-type, whereas the material further down in the material has remained n-type. The depth at which the diffused concentration of p-type material equals that of the n-type material is defined as the junction. The situation is illustrated in Figure V-A-67b.

Knowledge of the nature of the function describing the decrease in diffused impurity concentration with depth is very important in deriving expressions for solar cell characteristics. The function can be derived and is, for most diffusion processes, an error function complement (Ref. V-A-12).

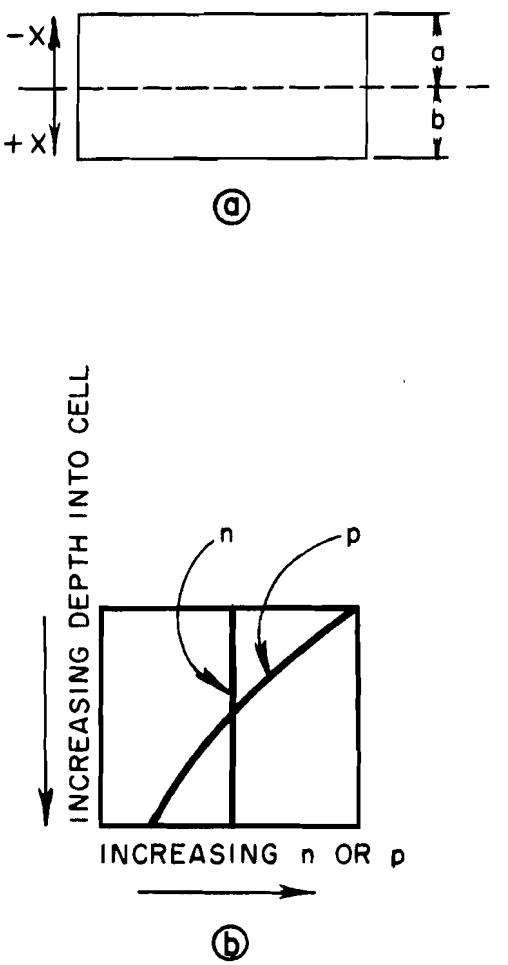

FIGURE V-A-67 THE SOLAR CELL MODEL

For a few processes, not usually found in solar cell work, the function is an exponential.

The error function complement is as difficult to deal with analytically as the exponential is easy. For this reason, and because the exponential very well approximates the error function complement over the range of values of interest, the variation of impurity distribution with depth is, in this analysis, assumed to be an exponential.

Before a differential equation can be solved for the carrier distribution within the cell, boundary conditions must be assumed. The surface characteristics of a semiconductor are usually described by a velocity called the surface recombination velocity. Since surfaces cause excited electrons and holes to recombine much more rapidly near the surface than they do in the bulk material (i.e., the lifetime of carriers near the surface is much less than in the bulk), there is a net flow of carriers to the surface and effectively out into oblivion. The surface recombination velocity is a measure of the rate of this flow and will be the boundary condition for the current at the surface. The equilibrium concentration of minority carriers ignoring the surface is n_p or p_n for p and n type material, respectively; q is the charge of the carriers; and n or p is the equilibrium concentration of minority carriers. When surface effects are considered the minority carrier current at the surface, into the surface is (Ref. V-A-13),

$$\begin{aligned} I_n &= q\, S_n\, (n-n_p) \qquad \text{(n material)} \\ I_p &= (-q)\, S_p\, (p-p_n) \qquad \text{(p material)} \end{aligned} \tag{A-31}$$

where S_n and S_p are the surface recombination velocities.

At the junction, x = 0, the boundary condition is

$$\begin{aligned} n &= p_n \exp(qV/kT) \\ p &= n_p \exp(qV/kT) \end{aligned} \tag{A-32}$$

where n and p are the actual minority carrier concentrations very near the junctions. These equations are derived from the fact that when majority carriers flow across the junction as a result of an applied voltage (or a photon-generated voltage), the majority carriers on one side of the junction become minority carriers on the other side of the junction, thus increasing the minority carrier density.

The final condition to be specified is that of the incoming radiation. It is assumed that the concentration of incident photons absorbed through the surface of energy greater than E_g is N_o per unit area per unit time and that the absorption length of the photons in the material does not vary with wavelength. These assumptions are not justified by experiment but are made so that the resulting differential equation will not have wavelength as a parameter.

7.2.2 The Mathematical Solution

One of the important characteristics of semiconductors is that the product of the concentrations of holes and electrons is a constant. If n_i is the concentration of holes and electrons in intrinsic material, this constant then is seen to be n_i^2. The parameter n_i is a function of temperature and of the gap energy of the material and is predicted to be of the form (Ref. V-A-13),

$$n_i^2 = b\, T^3 \exp\left[-qE_g/kT\right] \tag{A-33}$$

where b is not a function of temperature.

For the solar cell model described above, it was assumed that the concentration of p-type impurity atoms was of the form

$$P = P_o \exp\left[-(x+a)\ \beta\right] \tag{A-34}$$

where β is some constant and P_o is the concentration on the surface (x = -a). Then, let it be assumed that each impurity atom provides one p-type carrier (hole), so that the variation of majority carriers (holes) in the p-region is also given by Equation A-34. Finally, since the product of the electron and hole concentration in the p-region is equal to n_i^2, the minority carrier (electron) concentration in the p-region is, from Equation A-34,

$$n_p = \frac{n_i^2}{P_p} = \frac{n_i^2}{P_o} = \exp\left[(x + a)\beta\right] \tag{A-35}$$

It can be shown (Reference V-A-13) that a gradient of carrier concentration produces an electric field equal to

$$E_p = \frac{kT}{qp_p} \frac{dp_p}{dx} \tag{A-36}$$

Thus, from Equations A-36 and A-34

$$E_p = \frac{-kT}{q} \beta \ . \tag{A-37}$$

Since the n-type impurities do not have a gradient, the field in the n-region, E_n, is zero.

Now, currents flow in a semiconductor due to both fields (drift currents) and concentration gradients (diffusion currents). From the definition of mobility the rate of drift carrier flow is simply the carrier concentration times the field times the mobility; whereas, the rate of diffusion carrier flow is, from the definition of the diffusion coefficient, the concentration gradient times the diffusion coefficient. The total minority carrier currents, then, are the sums of drift and diffusion currents and are

$$I_p = q\,\mu_p\,p\,E_n - q\,D_p\,\frac{\partial p}{\partial x} \qquad \text{(A-38)}$$

$$I_n = q\,\mu_n\,n\,E_p + q\,D_n\,\frac{\partial n}{\partial x}$$

It can be shown that (Reference V-A-13)

$$D_p = \frac{KT}{q}\,\mu_p \text{ and } D_n = \frac{KT}{q}\,\mu_n\,. \qquad \text{(A-39)}$$

This relationship, derived by Einstein, might be expected because both the diffusion coefficients and the mobilities are measures of the ease with which carriers move through the crystal.

From Equations A-37, A-38, and A-39

$$I_n = q\,D_n\,(-\beta n + dn/dx)$$

$$I_p = -q\,D_p\,dp/dx \qquad \text{(A-40)}$$

The continuity equation dictates that the divergence of current must equal the net rate of creation of charge within a point. If n is total electron density in the p-region and τ_n is the average electron lifetime, the rate of loss of electrons by recombination is n/τ_n. If n_p is the electron density under equilibrium (due only to thermal generation) the rate of thermal generation, g_n, must be equal to n_p/τ_n so that, from Equation A-35

$$g_n = (n_i^2/P_o\,\tau_n)\,\exp\,[(x+a)\beta] \qquad \text{(A-41)}$$

The continuity equation, then, may be written, if f_n is the rate of photon generation of carriers, as

$$f_n + g_n - n/\tau_n + \frac{1}{q} \nabla \cdot I_n = 0 \qquad \text{(A-42)}$$

Assuming that each absorbed photon generates one electron-hole pair, the rate of photon generation is equal to the rate of photon absorption. The number of photons penetrating to a depth x is

$$N(x) = N_o \exp\left[- \left(\frac{a+x}{a_p}\right)\right] \qquad \text{(A-43)}$$

Where a_p is the absorption length and is, in general, a function of wavelength, then

$$f_p = - \frac{d\,N(x)}{dx} = \frac{1}{a} N_o \exp\left(- \frac{a+x}{a_p}\right) \qquad \text{(A-44)}$$

Finally, from Equations A-40, A-41, A-42, and A-44

$$\frac{d^2n}{dx^2} - \beta \frac{dn}{dx} - \frac{n}{\tau_n D_n} = - \frac{1}{D_n} \left[\frac{n_i^2}{P_o \tau_n} \exp \beta(a+x) + \frac{N_o}{a_p} \exp\left(- \frac{a+x}{a_p} \right)\right] \qquad \text{(A-45)}$$

The quantity $\tau_n D_n = L_n^2$ is the diffusion length.

The boundary conditions are

$$\text{at } x + -a, \quad \frac{1}{q} I_n = S_n (n-n_p) \qquad \text{(A-46)}$$

where S_n is the surface recombination velocity on the p-side, and at x = 0,

$$n = p_n \exp(qV/kT) = n_p \exp(qV/kT) = \frac{n_i^2}{P_o} \exp(\beta a) \exp(qV/kT) \qquad \text{(A-47)}$$

Solving Equation A-45 subject to the boundary conditions in Equations A-46 and A-47 and inserting the resulting expression for n into Equation A-40, the junction current

due to electrons is

$$I_{jn} = I_{on}(\exp(qV/kT) - 1) - I_{Ln} \tag{A-48}$$

where

$$I_{on} = \frac{qn_i^2 \exp(\beta a) L_n}{P_o \tau_n} \left[\frac{1/L_n + \beta/2 \left(\frac{S_n L_n}{D_n} \right) \tanh\left(a\sqrt{\beta^2/4 + 1/L_n^2} \right) + \frac{S_n L_n}{D_n}}{\sqrt{\beta^2/4 + 1/L_n^2}} \right] \Bigg/ \left[\frac{S_n/D_n + \beta/2}{\sqrt{\beta^2/4 + 1/L_n^2}} \tanh\left(a\sqrt{\beta^2/4 + 1/L_n^2} \right) + 1 \right] \tag{A-49}$$

and

$$I_{Ln} = \frac{qN_o \exp\left(\frac{-a}{a_p}\right) L_n/a_p}{1 - (L_n/a_p)^2 - \frac{\beta L_n^2}{a_p}} \left[\frac{1/L_n + \beta/2 \, L_n \left(\frac{S_n}{D_n} + \beta \right) \tanh\left(a\sqrt{\beta^2/4 + 1/L_n^2} \right) + \frac{S_n L_n}{D_n} + \beta L_n}{\sqrt{\beta^2/4 + 1/L_n^2}} \right] \Bigg/ \left[\frac{S_n/D_n + \beta/2}{\sqrt{\beta^2/4 + 1/L_n^2}} \tanh\left(a\sqrt{\beta^2/4 + 1/L_n^2} \right) + 1 \right]$$

$$- \left[\frac{\left(\frac{L_n}{a_p} - \frac{S_n L_n}{D_n} + \beta L_n \right) \exp(a/a_p + a\beta/2) - \operatorname{sech}\left(a\sqrt{\beta^2/4 + 1/L_n^2} \right)}{\frac{S_n/D_n + \beta/2}{\sqrt{\beta^2/4 + 1/L_n^2}} \tanh\left(a\sqrt{\beta^2/4 + 1/L_n^2} \right) + 1} + \frac{L_n}{a_p} \right] \tag{A-50}$$

Using a similar technique, the junction current due to carrier generation in the n-region may be derived. The model used in this analysis assumes a uniform impurity density in the n-region. For this reason, the drift current may be neglected, and the junction current from the n-region is due entirely to diffusion. It is then seen in a fashion exactly analogous to that shown above that the junction current due to diffusion is

$$I_{jp} = I_{op}(\exp(qV/kT) - 1) - I_{Lp} \tag{A-51}$$

$$I_{op} = \frac{q L_p n_i^2}{\tau_p n_n} \left[\frac{\tanh \frac{b}{L_p} + \frac{L_p S_p}{D_p}}{\frac{L_p S_p}{D_p} + 1} \right] \tag{A-52}$$

and

$$I_{Lp} = \frac{qN_o \exp^{(-a/a_p)} L_p/a_n}{1 - (L_p/a_n)^2} \left[\frac{\tanh \frac{b}{L_p} + \frac{L_p S_p}{D_p}}{\frac{S_p L_p}{D_p} \tanh b/L_p + 1} \right.$$

$$\left. \frac{\left(\frac{S_p L_p}{D_p} - \frac{L_p}{a_n} \right) \exp -b/a_n \operatorname{sech} \frac{b}{L_p}}{\frac{L_p S_p}{D_n} \tanh \frac{b}{L_p} + 1} - \frac{L_p}{a_n} \right] . \tag{A-53}$$

It has been shown by Sah et al. (Ref. V-A-14) that the forward current in higher energy gap semiconductor p-n junctions (higher than approximately 1 ev) with low lifetimes and resistivities contains a significant contribution from generation and recombination of carriers in the space charge region. Thus, to Equations (A-48) and (A-51) might be added a term such as:

$$I_j = I_o (\exp(qV/kT)-1) - I_L + I' \Big| \tag{A-54}$$

where the added term I' accounts for the space charge region current. Sah et al. predict that

$$I' = 2(kT/qE) q n_i \exp(qV/2kT)/2\gamma \tag{A-55}$$

where

E = the field intensity in the space charge region

γ = the carrier lifetime

Thus, for certain materials, i.e. silicon, the I' term in Equation A-54 dominates and

$$I_j = I'_o \exp(qV/2kT) - I_L \qquad (A - 56)$$

over a large portion of the characteristic. However, the short circuit current is still described quite well by Equations A-50 and A-53.

Wolf and Prince (Ref. V-A-2) have derived a comparable expression neglecting the drift field in the p-region and assuming S_n to be infinite because of the contact covering the back side of silicon cells. Then, assuming the absorption coefficient (the reciprocal of α) shown in Figure V-A-68, they have calculated the total fraction of excited carriers to reach the junction as a function of wavelength of the incident light. This parameter, called the collection efficiency, is plotted in Figure V-A-69, for a specific solar cell. If the fraction of collected carriers is plotted as a function of the power in the incident monochromatic light, the theoretical solar cell response characteristic is obtained. Wolf and Prince have compared the theoretical response with the experimental (Figure V-A-70) and have shown that excellent agreement is obtained.

Thus, it may be concluded that the preceeding analyses are indeed valid for silicon cells and that they may be applied to comparable cells of other semiconducting materials.

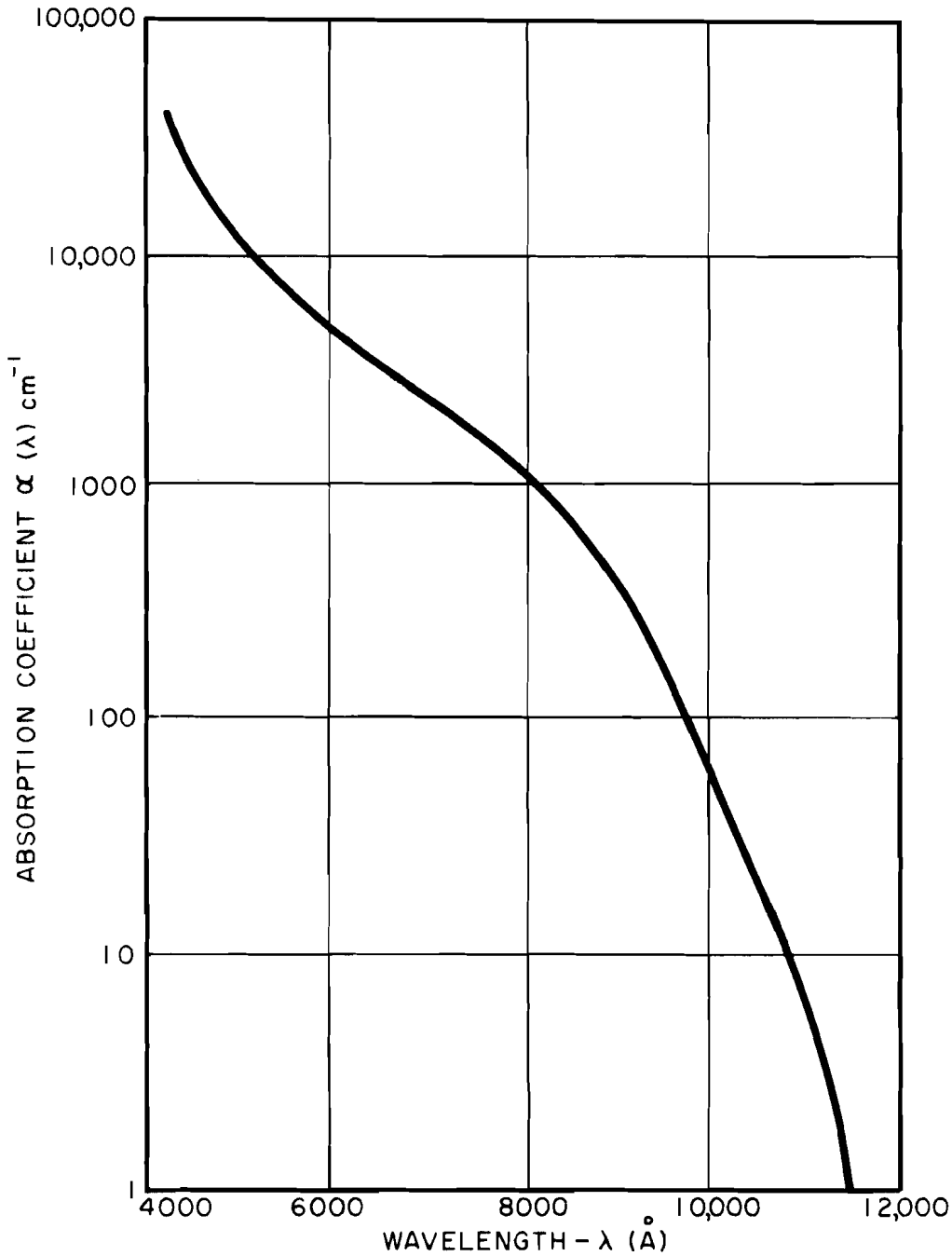

FIGURE V-A-68 ABSORPTION COEFFICIENT α OF SILICON AS A FUNCTION OF WAVELENGTH.

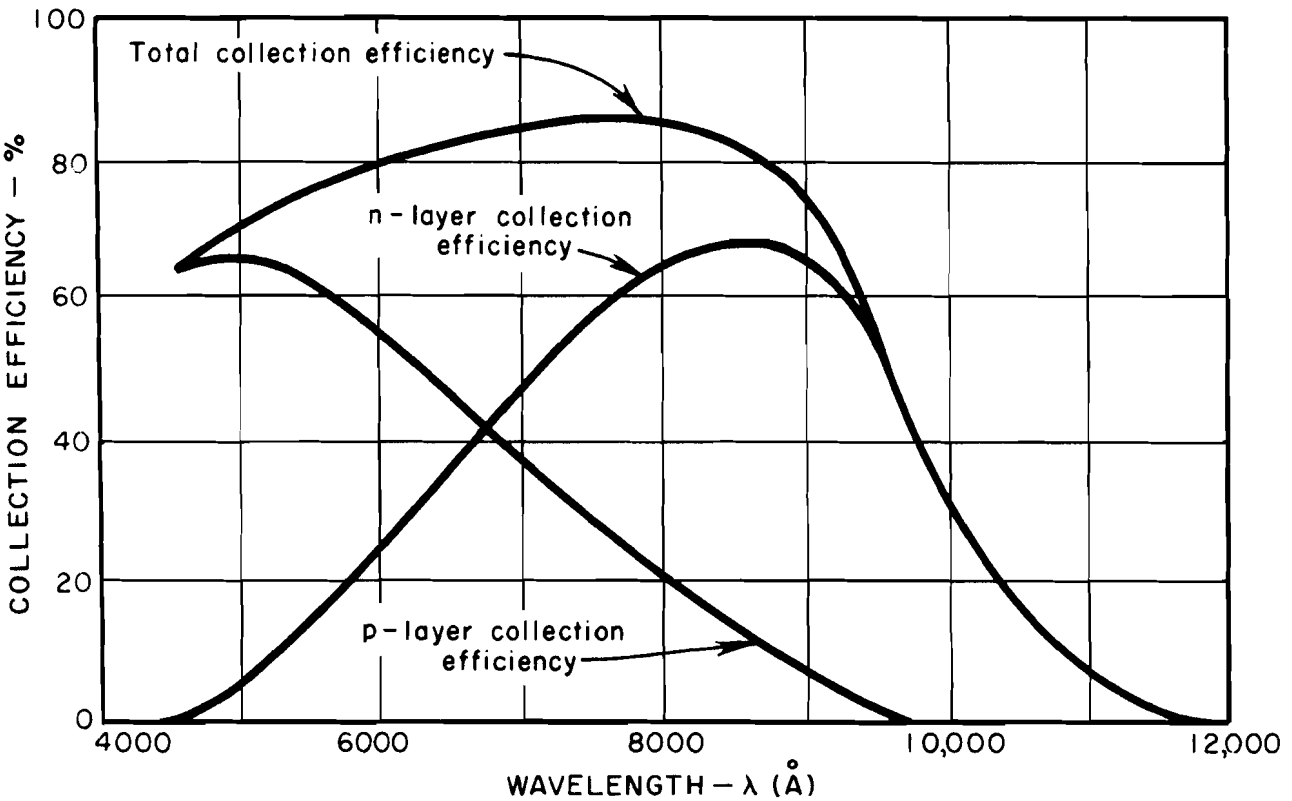

FIGURE V-A-69 COLLECTION EFFICIENCY $\gamma(\lambda)$ AS A FUNCTION OF WAVELENGTH, CALCULATED FOR SOLAR CELL NO. 3-329

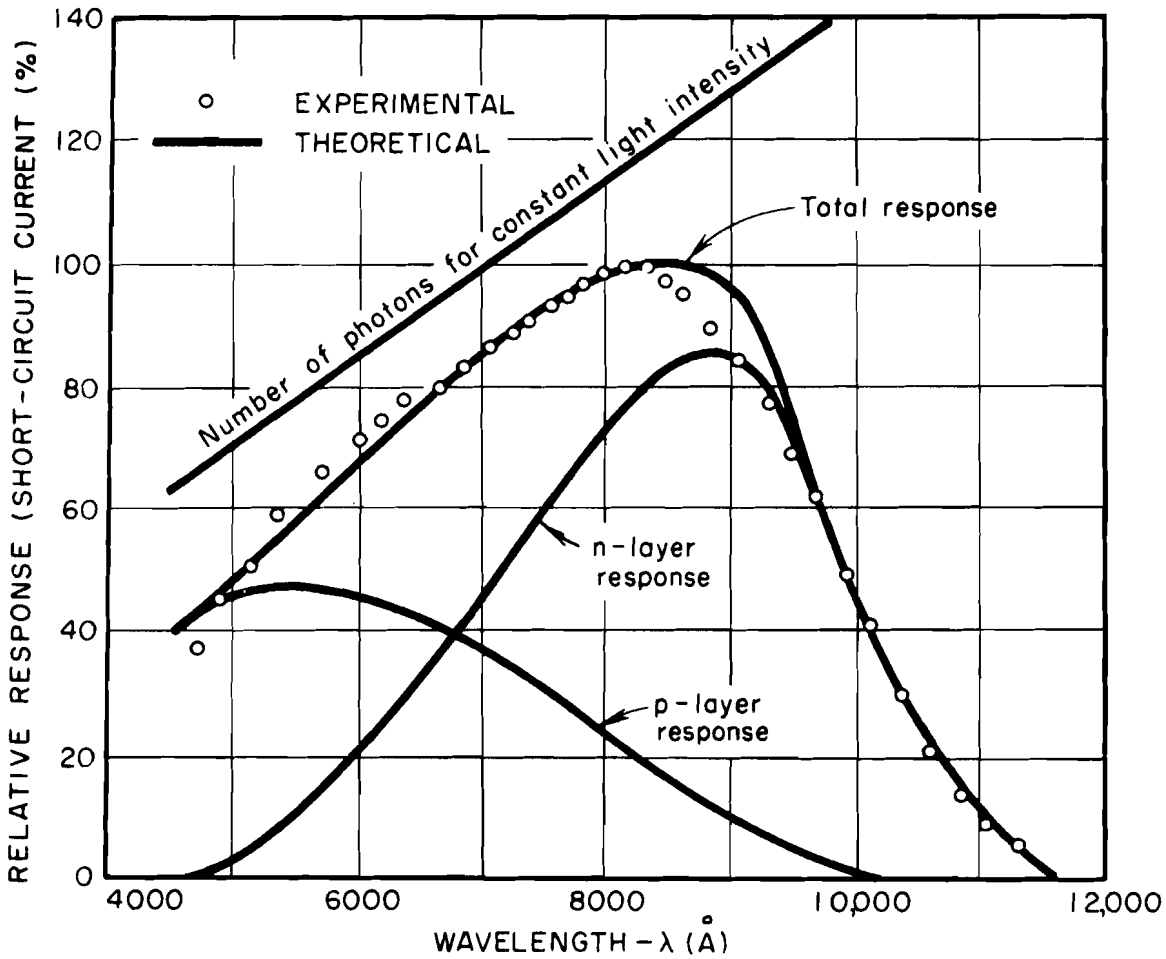

FIGURE V-A-70 SPECIAL RESPONSE OF SOLAR CELL NO. 3-329

7.3 Theory of Composite Cells

Any single energy gap semiconductor material can convert only a relatively narrow portion of the entire solar spectrum into electrical carriers with nearly unit photon efficiency. Photons with energy lower than the energy gap will not excite hole-electron pairs in the semiconductor, whereas higher energy photons will convert part of their energy to heat and become absorbed nearer to the surface of the solar cell. In the silicon solar cell the spectral efficiency (that is, the fraction of the total energy contained in the solar spectrum which is actually imparted to the carriers) is somewhat less than 50 percent. The spectral efficiency of the solar cell can, however, be increased by providing the capability of converting photons into electrical carriers at more than one energy gap.

In principle, a single energy gap semiconductor material is transparent to photons with energy less than the energy gap of a semiconductor material. Actually, this is true only for relatively pure and well-developed semiconductor materials, such as germanium and silicon. Since the ideal semiconductor material will transmit energy at wavelengths longer than the cutoff wavelength, it is feasible to consider a stacked photovoltaic energy converter in which the high-energy photons are converted at the top of the stack and the low energy photons are converted in layers below.

It is advantageous to utilize a higher energy gap semiconductor material along with silicon in the fabrication of a multilayered photovoltaic cell. Silicon, gallium arsenide, aluminum antimonide, and gallium phosphide are semiconductors whose band-gap energies make them appear particularly attractive for solar converters. Each of these materials can convert solar energy into electrical energy efficiently in a narrow wavelength near their absorption edge,

while the unabsorbed radiation of longer wavelength is transmitted through the material. Several combinations of semiconductor materials for possible multi-layered semiconductor solar cells are given in Table V-A-7.

For a composite cell construction using stacked semiconductors, it is essential that the high energy gap components transmit the long wavelength radiation and that the surfaces between the cells be treated to minimize reflection and scattering. Thus,both surfaces of all cells in the composite structure must be prepared as optical flats and treated with antireflection coatings such as silicon monoxide, arsenic trisulfide, or magnesium fluoride. The III-V intermetallic compound semiconductors such as gallium arsenide or indium phosphide, are reported to have low carrier lifetimes, as well as high optical absorption coefficients. The physical causes for these undesirable characteristics are believed to lie in the purity and crystalline perfection which are attainable in the intermetallic compounds. Characteristically, these materials have a high vapor pressure constituent and manifest instability in certain environments. Since minority carrier lifetime and optical absorption coefficients are at least as important as energy gap in the stacked form of composite solar cell configuration, these materials may prove to be limited in their application to this type of converter.

An advantageous two-semiconductor composite solar cell could be made by mounting the cells at right angles to each other and using a dichroic mirror to direct the longer and shorter wavelengths to the proper cells, as shown previously.

In this type of battery, the solar radiation is incident on the dichroic mirror at an angle of 45°, and the dichroic is fabricated in such a manner as to transmit the higher energy photons to one cell while reflecting those of low energy to the other. It becomes immediately obvious that the optical

TABLE V-A-7

POSSIBLE COMPOSITE PHOTOVOLTAIC CELLS

	Layer Materials	Energy Gap (eV)	Cutoff Wavelength (microns)
Cell No. 1.			
	GaP	2.4	0.5
	AlSb	1.6	0.78
	GaAs	1.35	0.92
	Si	1.1	1.1
Cell No. 2.			
	AlAs	2.16	0.57
	CdSe	1.84	0.68
	GaAs	1.35	0.92
	Si	1.1	1.1
Cell No. 3.			
	GaP	2.4	0.5
	CdTe	1.45	0.86
	Si	1.1	1.1
	GaSb	0.69	1.8

transmission of the high energy gap cell no longer affects the operation of the lower energy gap cell. The over-all efficiency of the solar battery now depends only upon the transmission and reflection characteristics of the dichroic mirror. Such mirrors can be made to transmit approximately 95 percent of the energy in the shorter wavelengths while reflecting approximately 95 percent of the energy in the longer wavelengths.

In view of the limited transmission of most intermetallic semiconductors, it was felt that this type of solar battery might prove to be more efficient than the previously discussed stacked type of composite battery.

7.3.1 The Optimum Materials for a Composite Solar Cell

A theoretical determination of the optimum materials for a composite solar cell requires knowledge both of the band-gaps of the available materials and of the ability of the materials to convert efficiently those portions of the incident spectrum lying within their excitation ranges.

The band-gaps of many intermetallic semiconductors are well known. However, information as to which intermetallics are capable of actually converting photon energy into electrical energy efficiently is not readily available. Considerable work has been done to fabricate solar cells from Si, Ge, CdS, GaAs, and perhaps a few other materials. The work done, however, undoubtedly can be improved upon, and new work can conceivably bring new materials into the technology of solar cells.

For this reason, in this analytical study, all materials will be assumed to have potentially equal mobilities, diffusion lengths, and surface recombination velocities. In other words, the optimum materials are chosen solely on the basis of the incident spectrum, the band-gap of the material, and the probable I_o of the material.

7.3.2 Optimization of the Spectrum Efficiency of a Composite Cell

The spectrum efficiency of a composite cell can be maximized by maximizing the total spectral energy which is actually absorbed by the excited carriers. In general, a hole-electron pair, excited in a semiconductor of band-gap E_g, by a quantum of energy $h\nu$, greater than E_g, absorbs from this quantum, energy E_g. If $N(\lambda)$ is the number of quanta per unit wavelength per unit time in the wavelength increment $d\lambda$, the integrated power absorbed by the semiconductor may be found by summing the number of quanta of energy greater than E_g and multiplying by E_g.

The case of an ideal composite cell will be considered. It will be assumed that the cell is composed of two semiconductors of band-gaps E_{g1} and E_{g2} where $E_{g1} < E_{g2}$. It is further assumed that the incident spectrum is divided into two parts so that all radiation for which $E_{g1} < h_\nu < E_{g2}$ is directed to and absorbed by the cell of band-gap E_{g1}, and all radiation of $H > E_{g2}$ is directed to and absorbed by the cell of band-gap E_{g2}. The integrated power absorbed by the excited carriers in the two cells is, then

$$P = E_{g2} \int_{E_{g2}}^{\infty} N(\lambda)d\lambda + E_{g1} \int_{E_{g1}}^{E_{g2}} N(\lambda)d\lambda \qquad \text{(A-57)}$$

7.3.3 A Graphical Solution for the Optimum Spectrum Efficiency

This equation may be evaluated graphically for various assumed values of E_{g2} and E_{g1} with the aid of a plot of the solar photon distribution, as is shown in Figures V-A-71 and V-A-72. A plot for this case is shown in Figure V-A-73. The lower and higher energy gaps of the composite cell

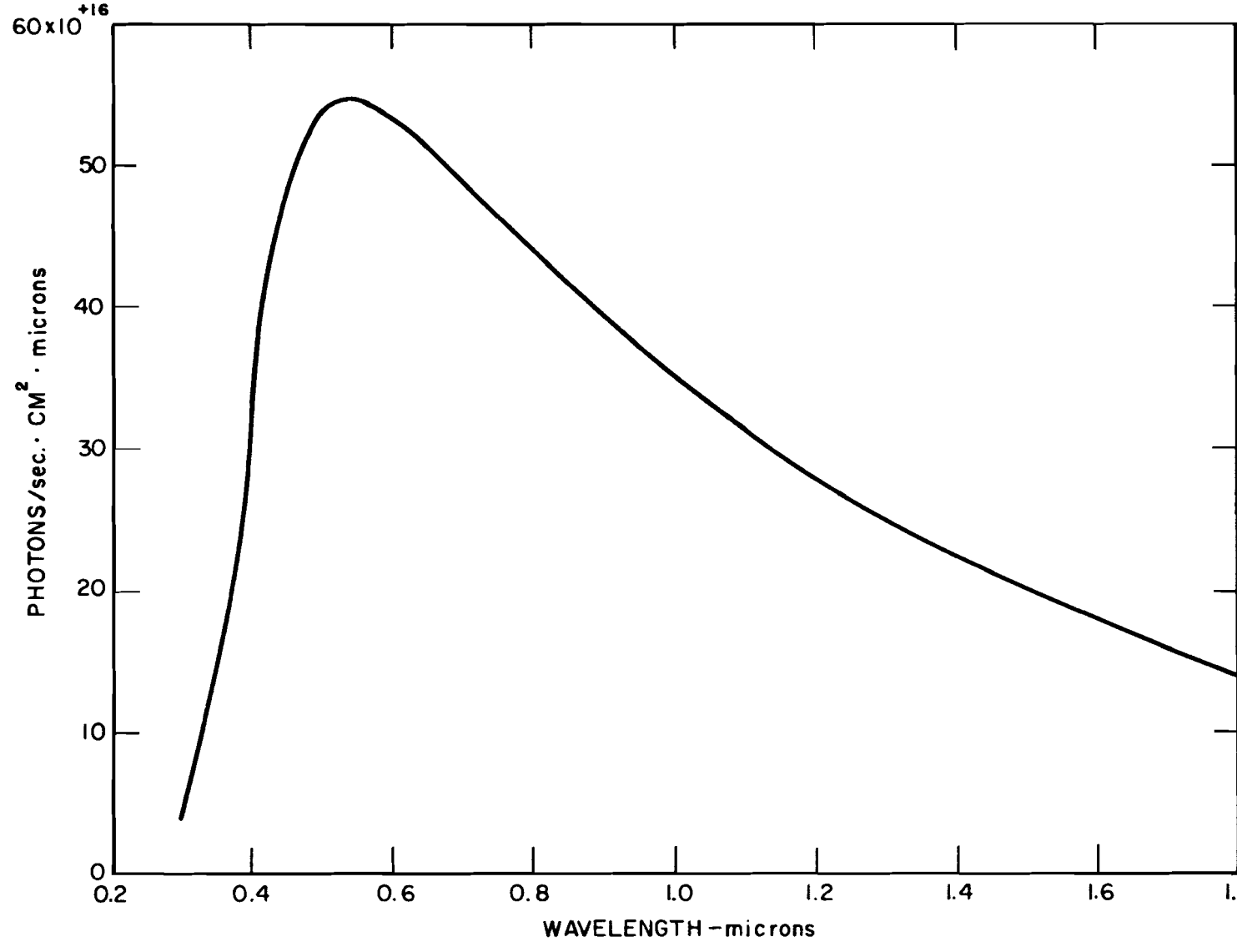

FIG V-A-71 PHOTON DISTRIBUTION IN THE ABSORBED SOLAR SPECTRUM

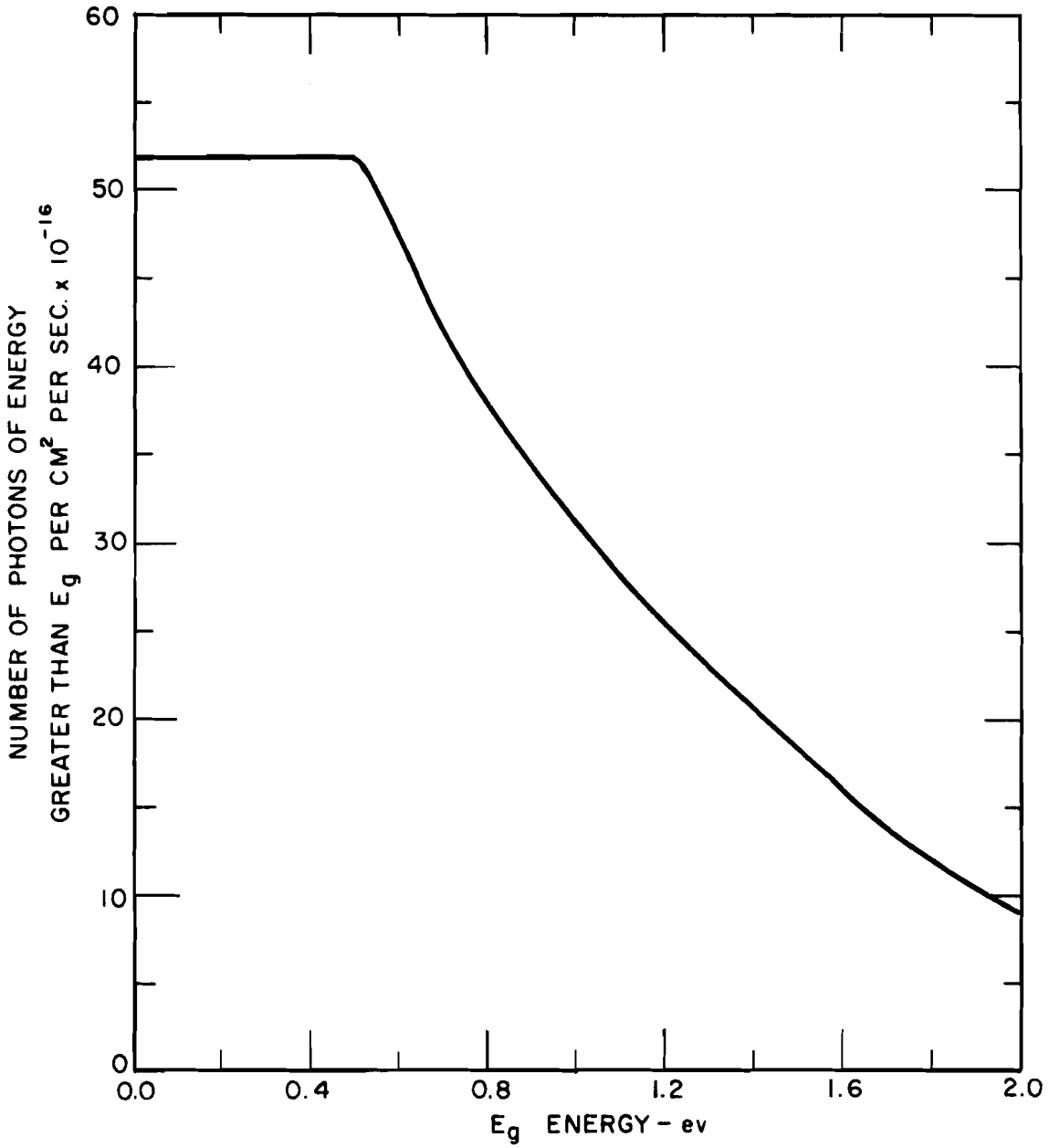

FIGURE V-A-72 PHOTON DISTRIBUTION VS. ENERGY

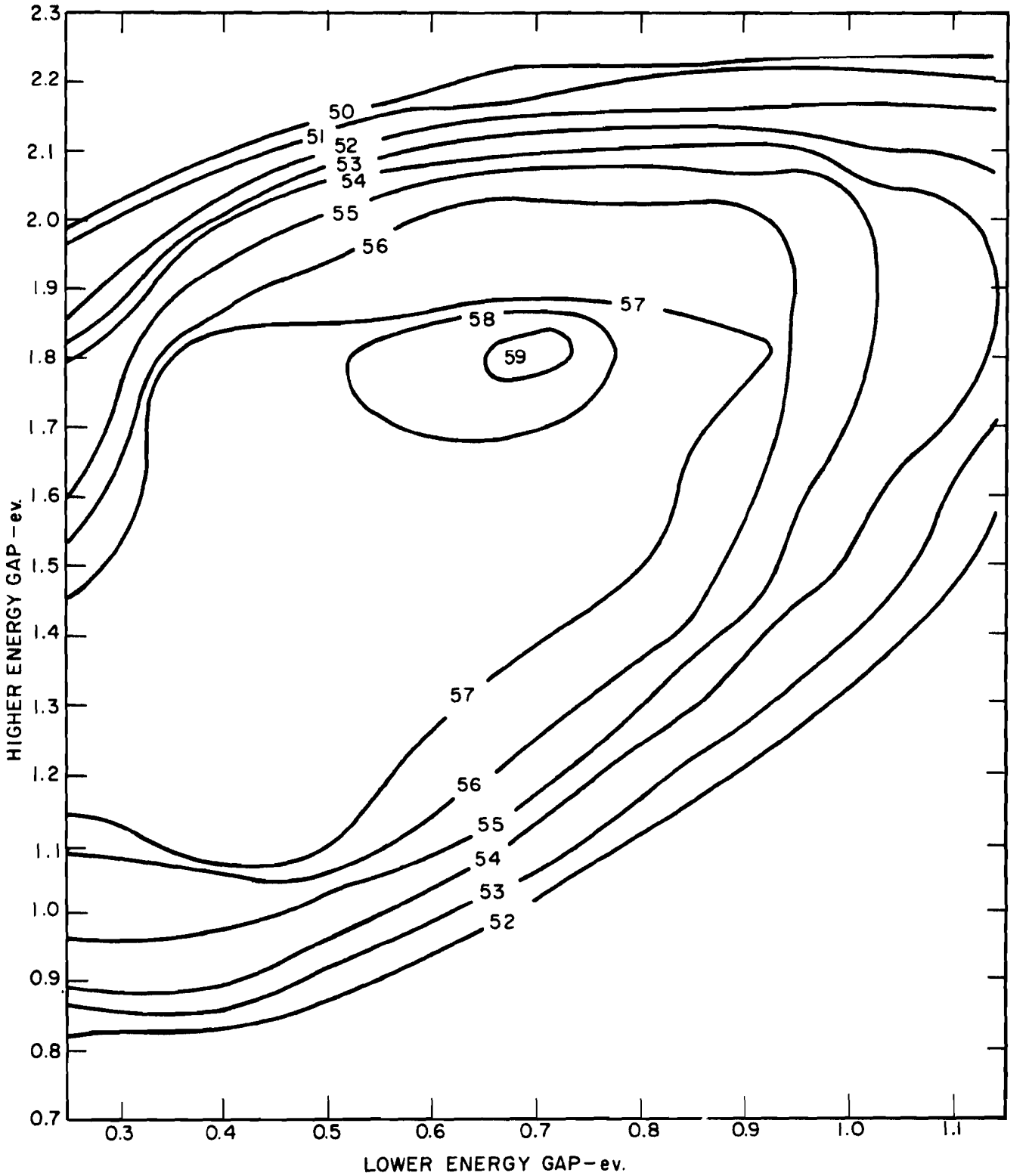

FIGURE V-A-73 THEORETICAL EFFICIENCY CONTOURS FOR A COMPOSITE SOLAR CELL OF TWO DIFFERING SEMICONDUCTORS AS FUNCTIONS OF THE BAND SEPARATIONS

are plotted on the x and y axes, respectively, and curves of constant spectral efficiency are shown. The spectrum efficiency is simply the spectral power absorbed by the carriers divided by the integrated incident spectral power.

Note that the highest spectrum efficiency occurs for a composite cell made from cells of band-gaps of 0.7 ev and 1.9 ev. It may be seen from Fig. V-A-70 that variations of the lower gap up to 1.0 ev and of the higher gap through the range from 1.0 to 2.0 ev are possible while still keeping the spectrum efficiency greater than 55 percent (which is nine-tenths of the maximum spectrum efficiency). It must be understood, however, that variations in the two gaps cannot be made independently.

7.3.4 Determination of Optimum Band-Gaps Considering Leakage Currents

In general, the leakage current, I_o, increases as the band-gap decreases, and any increase in I_o has a detrimental effect on the performance of a solar cell, since it causes a reduction in the open-circuit voltage and output power. For this reason, it is necessary to consider I_o in determining true optimum band-gaps for a composite cell.

Let the following equation describe solar cell operation

$$I = I_L - I_o \left[\exp (qV/kT) - 1 \right], \tag{A-58}$$

where I_L is the total current produced by the photon excitation, V is the junction voltage, and I is the junction current. It can be seen that the junction is effectively shunted by a diode of characteristic

$$I_o \left[\exp (qV/kT) - 1\right] . \tag{A-59}$$

In general, I_o is very small, and the situation can be approximated by writing

$$I = I_L - I_o \exp (qV/kT). \tag{A-60}$$

The power delivered by the junction is

$$P = IV = V \left[I_L - I_o \exp(qV/kT) \right]. \tag{A-61}$$

For maximum power,

$$d(IV) = IdV + VdI = 0 \tag{A-62}$$

or

$$\frac{dI}{dV} = - \frac{I}{V} . \tag{A-63}$$

But

$$\frac{dI}{dV} = \frac{qI_o}{kT} \exp (qV/kT). \tag{A-64}$$

Thus, for maximum power

$$\frac{q V}{k T} \exp (qV/kT) = I_L/I_o - \exp (qV/kT) \tag{A-65}$$

or

$$(1 + q V/kT) \exp (qV/kT) \approx \left(\frac{qV}{kT}\right) \exp \frac{qV}{kT} = \frac{I_L}{I_o}. \tag{A-66}$$

Thus,

$$\frac{qV}{kT} = \ln\left(\frac{I_L}{I_o}\right) - \ln \left(\frac{qV}{kT}\right). \tag{A-67}$$

As a first approximation let $qV/kT = \ln\left(\frac{I_L}{I_o}\right)$

then,

$$\frac{qV}{kT} \approx \ln\left(\frac{I_L}{I_o}\right) - \ln \ln\left(\frac{I_L}{I_o}\right) \tag{A-68}$$

Now, the power, P, is equal to IV so that,

$$I = I_L - I_o \exp (qV/kT) = I_L - I_L/\ln(I_L/I_o) \tag{A-69}$$

$$= I_L \left[1 - 1/\ln (I_L/I_o)\right] . \tag{A-70}$$

Therefore,

$$P = IV = \frac{kT}{q} I_L \ln\left(\frac{I_L}{I_o}\right) \left\{1 - 1/\ln(I_L/I_o)\right\} \qquad (A-71)$$

$$= \frac{kT}{q} I_L \left\{\ln\left(\frac{I_L}{I_o}\right) - 1\right\} \approx \frac{kT}{q} I_L \ln\left(\frac{I_L}{I_o}\right). \qquad (A-72)$$

A relationship relating I_o to E_g must now be assumed. The semiconductor theory of Shockley (Ref. V-A-13) predicts that $I_o \approx \exp(-qE_g/kT)$. This relationship has been verified for a few materials of low band-gaps. It is, therefore, assumed that $I_o = I_F \exp(-qE_g/kT)$. I_F is independent of E_g and is assumed nearly equal for all materials.

Then,

$$P = \frac{kT}{q} I_L \left\{\frac{qE_g}{kT} + \ln\left(\frac{I_L}{I_F}\right)\right\} \qquad (A-73)$$

$$= I_L E_g + \frac{kTI_L}{q} \ln(I_L/I_F) \qquad (A-74)$$

$$= I_L \left\{E_g - \frac{kT}{q} \ln(I_F/I_L)\right\} . \qquad (A-75)$$

This expression relates the maximum output power of the cell to $I_L E_g$, the power delivered to the collected carriers, and to a wasted fraction of power, $I_L (kT/q) \ln (I_F/I_L)$. Let this be written in the form

$P_{max} = I_L(E_g - E_w)$ where $I_L E_w$ is the wasted power.

Applying this relationship to the band-gap optimization and assuming E_w constant for various materials, we have

$$P_{max} = (E_{g2} - E_w) \int_{E_{g2}}^{\infty} N(E_g)dE + (E_{g1} - E_w) \int_{E_{g1}}^{E_{g2}} N(E_g)dE \qquad (A-76)$$

and following the procedure of Section 2. 2. 1

$$P_{max} = \frac{52 \times 10^{16}}{1.8} \left\{ (E_{g1} - E_w)(E_{g2} - E_{g1}) + \right. \tag{A-77}$$

$$\left. (E_{g2} - E_w) \cdot (2.2 - E_{g2}) \right\} . \tag{A-78}$$

Differentiate to maximize the power with respect to the band gaps:

$$\frac{\partial P}{\partial E_{g1}} = E_{g2} - 2E_{g1} + E_w = 0 \tag{A-79}$$

$$\frac{\partial P}{\partial E_{g2}} = E_{g1} - 2E_{g2} + 2.2 = 0. \tag{A-80}$$

The solutions

$$E_{g1} = 0.74 + 2/3E_w \tag{A-81}$$

$$E_{g2} = 1.5 + 1/3E_w.$$

E_w must be determined experimentally, but it is worthwhile to make some **speculations** at this point. If one assumes, for example, that silicon is the optimum material for the lower energy gap, then

$$E_{g1} = 1.1 = 0.74 + \frac{2}{3} E_w,$$

and

$$E_w = 0.54 \text{ ev} \tag{A-82}$$

$$E_{g2} = 1.5 + \frac{1}{3} E_w = 1.68.$$

If everything else is ideal, so that the efficiency of the cell depends only on the spectrum efficiency and the amount of wasted power corresponding to E_w, then one can calculate the power output for a composite cell for which $E_{g1} = 1.1$ ev, $E_{g2} = 1.68$ ev, and $E_w = 0.54$ ev. This power turns out to be 25×10^{16} ev/cm^2 sec. Taking the ratio of this to the total incident solar power, 68×10^{16} ev/cm^2 sec, one gets an upper limit on efficiency of 37 percent. On the same basis, a

single silicon cell would have an efficiency of 23 percent, and a single germanium cell 7.5 percent. These values for silicon and germanium are close enough to experimental values to indicate that the theory given here can and should be used as a guide in the selection of semiconductor materials for composite solar cells.

7.4 Theory of Variable Band-Gap Cells

The design of conventional single energy gap solar cells usually involves a compromise between two conflicting goals. The first goal is to maximize carrier collection: that is, to maintain conditions so that the maximum number of the photon-excited carriers will actually reach the junction and become part of the useful cell output. The second goal is to minimize the junction saturation current, I_o, and thereby increase the output voltage of the solar cell, for

$$V = \frac{kT}{q} \ln \frac{I_L - I}{I_o} \tag{A-83}$$

where

k = Boltzman's constant

T = absolute temperature

q = electronic charge

I_L = current collected at the junction

I = output current delivered to the load

I_o = saturation current.

In general, the saturation current tends to decrease with the increasing forbidden gap, E_g, of the semiconductor. At the same time, carrier generation tends to occur more and more near the surface of the semiconductor, as the energy gap increases. Because the most important source of carrier recombination in large area photocells is the surface recombination, moving the region of carrier generation closer to the surface will only result in

increasing the fraction of carriers lost to surface recombination, thereby decreasing the fraction of carriers reaching the junction.

One possible way of getting around the conflicting interests imposed on the energy gap is to utilize variation of energy gap in the design of the solar cell. That is, the solar cell may consist of more than one semiconductor element.

These two types of cells are characterized by the portion of the cell in which the greater part of the carrier generation occurs. They are referred to as front-surface cells, and back-surface cells.

In the front-surface cell, shown in Fig. V-A-74, the radiation is absorbed mainly in the region on which it impinges, that is, in the p-region on a p-n diffused solar cell. The carriers then drift or diffuse to the junction to become part of the collected current. The saturation current I_o, is controlled almost entirely by the characteristics of the back region, or the n-region in a p-n diffused cell, because the n-region is much thicker than the front region. The expected collection efficiency in a cell where surface recombination controls the collection efficiency approaches 50 per cent. The over-all efficiency of the cell may, however, be increased if a considerably higher energy gap semiconductor is used for the back or n-region of the cell than is used for the front or p-region of the cell.

This higher energy gap material would substantially reduce the saturation current, I_o, and therefore increase the output voltage of the cell. Theoretically, the gap of the back region semiconductor could be raised until the contribution to I_o from the back region is reduced to the same order of magnitude as the contribution from the front region. Experience shows, however, that a semiconductor with a gap of approximately 2.0 ev might offer the lowest I_o available. Data are inconclusive on the further decrease of I_o with increasing band gap.

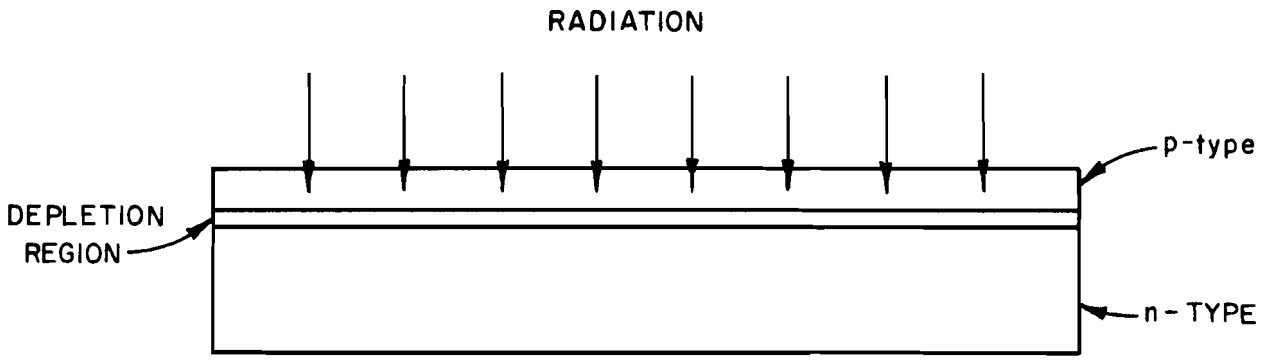

FIGURE V-A-74 FRONT SURFACE CELL

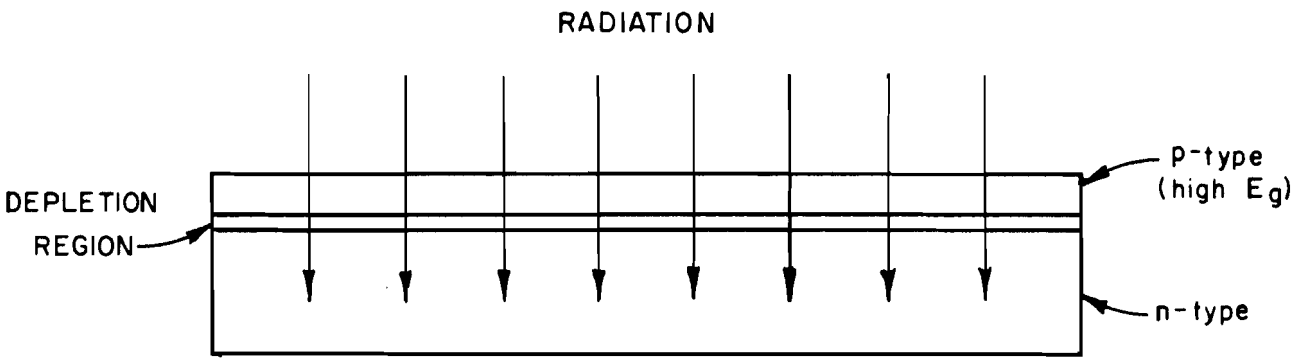

FIGURE V-A-75 BACK-SURFACE CELL

Since, if the saturation current could be reduced to a low enough level, the voltage output of the cell could be raised to very nearly the band gap voltage, E_g, the maximum theoretical efficiency of such a cell appears to be near 50 percent. More practical estimates of the theoretical efficiency of such cells would, however, have to await experimental tests of graded gap solar cells.

The second type of solar cell, the back-surface cell (Fig. V-A-75) is that in which the major part of the carrier generation occurs in the back region or in the n-region of a p-n diffused cell. Such a cell could be made if the front region were a high band-gap semiconductor so that it were almost transparent to the greater part of the solar radiation and if the back region were a lower band gap semiconductor, in which the radiation would generate carriers. This type of configuration could practically eliminate carrier recombination caused by low surface lifetime; and, if volume lifetime were sufficiently high and the carrier generation were sufficiently near the junction, practically all the generated carriers would reach the junction. However, this same lower band-gap semiconductor would also contribute all of the saturation current. The saturation current would, therefore, be relatively high compared with that in the front region type cell. Calculations show that varying the band gap within the back region itself would have little effect on the high I_o expected, and, therefore, the front-surface cell should be investigated.

In summary it should be emphasized that while theoretical prediction of semiconductor device behavior must be used as a guide in directing the experimental efforts to develop new devices, frequently it is found that ultimate device behavior is significantly different from that predicted.

However, it may be concluded that the composite cell, and graded gap cell, are sufficiently promising in theory to justify considerable experimental effort on their development.

REFERENCE LIST

V-A-1. Kuiper, G. P. The Earth as a Planet. Chicago: University of Chicago Press, 1954.

V-A-2. Prince, M. B., and Wolf, M. "New Developments in Silicon Photovoltaic Devices," J. of the Brit IRE, Vol. 18 (October 1958), p. 583.

V-A-3. Loferski, J., and Rappaport, P. "The Effect of Radiation on Silicon Solar Energy Converters," RCA Rev., Vol. 19, December 1958.

V-A-4. Chow, K. T., and Lodi, E. A. (Lockheed Missile Systems Division) "Proton Damage to Solar Cells," AIEE Paper No. CP 60-1081.

V-A-5. Fraser, J. C. (General Electric Co.) "Electron Irradiation of Silicon Solar Cells," AIEE Paper No. CP 60-1094.

V-A-6. Downing, R. G. (Space Technology Laboratories) "Electron Bombardment of Silicon Solar Cells," STL-TR-60-0000-04057, EM 10-5.

V-A-7. Wysocki, J. J., and Rappaport, P. "Effect of Temperature on Photovoltaic Solar Energy Conversion," JAP, Vol. 31, (March 1960), p. 571.

V-A-8. Reynolds, D. C., et al. "Photovoltaic Effect in Cadmium Sulfide Crystals," Phys. Rev. (1954), pp. 533-534.

V-A-9. Williams, R., and Bube, R. "Photoemission in the Photovoltaic Effect in Cadmium Sulfide Crystals," J. of Appl. Phys., Vol. 31 (June 1960), p. 968.

V-A-10. Vadakov, Yu, et al. "A p-n Junction Photocell Made of Cadmium Telluride," Soviet Physics Solid State, Vol. 2 (July 1960), p. 1.

V-A-11. "Proceedings of the Symposium on Solar Cell Power Systems for Space Vehicles," Washington, D. C., May 3-4, 1960.

V-A-12. Snits, F.M. "Formation of Junction Structures by Solid-State Diffusion," Proc. of IRE, Vol. 46 (June 1958), p. 1049.

V-A-13. Shockley, W. "Electrons and Holes in the Semiconductors," Von Nostrand, 307, 1950.

V-A-14. Sah, C. T., et al. "Carrier Generation and Recombination in p-n Junctions and p-n Junction Characteristics," Proc. of IRE, Vol. 95 (September 1957), p. 228.

SELECTED ADDITIONAL REFERENCES

A. GENERAL SEMICONDUCTOR THEORY:

1. Dunlap, W. C. An Introduction to Semiconductors, New York, 1957.
2. Kittel, Charles. Solid State Physics, New York, 1956.
3. Smith, R. A. Semiconductors, Cambridge, 1959.
4. van der Ziel, Albert. Solid State Physical Electronics, New York: Prentice-Hall, 1957.

B. THEORY OF PHOTOVOLTAIC CELLS:

5. Chapin, et al. "A New Silicon p-n Junction Photocell for Converting Solar Radiation into Electrical Power," JAP, Vol. 25, (1954), p. 676.
6. Goldstein, B. "High-Voltage Photovoltaic Effect," JAP, Vol. 30 (February 1959), p. 155.
7. Lehovec, K. "The Photovoltaic Effect," Phys. Rev., Vol. 74 (1948), p. 463.
8. Loferski, J.J. "Theoretical Considerations Governing the Choice of Optimum Semiconductor for Photovoltaic Solar Energy Conversion," JAP, Vol. 27 (July 1956), p. 777.
9. Nash, H., and Luft, W. "Improved Silicon Photovoltaic Cells for Space Vehicles," Electronic Industries, Vol. 18 (August 1959), p. 91.
10. Pearson, G. L. "Conversion of Solar to Electrical Energy," Amer. J. Phys, Vol. 25 (December 1957), p. 951.
11. Pfann, W., and Van Roosbroeck. "Radioactive and Photoelectric p-n Junction Power Sources," JAP Vol. 25, (1954), p. 1422.

12. Prince, M. B. " Silicon Solar Energy Converters, " JAP, Vol. 26 (May 1955), p. 534.

13. Rappaport, P., et al. "The Electron-Voltaic Effect in Germanium and Silicon p-n Junctions, " RCA Rev., Vol. 17 (March 1956), p. 100

14. Rittner, D. " Use of p-n Junctions for Solar Energy Conversion," Phys. Rev., Vol. 96 (1954), p. 1708.

15. "Transactions of the Conference on the use of Solar Energy, " University of Arizona Press, 1958.

16. Wolf, M. "Limitations and Possibilities for Improvement of Photovoltaic Solar Energy Converters, " Proc. of IRE, Vol. 48 (July 1960), p. 1246.

C. UTILIZATION OF SOLAR CELLS:

17. Acker, et al. "Solar-Cell Power Supplies for Satellites, " Electronics, Vol. 33 (March 11, 1960), p. 167.

18. Cummerow, R. "Use of Silicon p-n Junctions for Converting Solar Energy to Electrical Energy," Phys. Rev., Vol. 95 (1954), p. 561.

19. Elliott, J. F. "Design Considerations for a High Reliability Photovoltaic Solar Energy Converter, " Solar Energy, Vol. 3 (April 1959), p. 34.

20. Escoffery, C., and Luft, W. "Silicon Photovoltaic Cells and the Utilization of Solar Energy, " International Rectifier Corporation, June, 1960.

21. Francis, A. B., and Happ. "Photovoltaic Solar Energy Converters for Space Vehicles -- Present Capabilities and Objectives." Presented at the AIEE Summer and Pacific General Meeting, Seattle, Washington, June 21-26, 1959.

22. Heeger, A. J., and Nisbet. "The Solar Cell -- Conditions for Optimum Performance," Solar Energy, Vol. 3 (January 1959), p. 12.

23. Heeger, A. J., and Nisbet. "The Solar Cell Diode Curve-A Crucial Design Parameter," Solar Energy, Vol. 3, March 1959.

24. Vavilov, et al. " Solar Batteries in Sputniks," Electronics Design, Vol. 7 (September 1959), p. 52.

25. Report of the Joint Meeting on Solar Cell Measurement Standardization, Lockheed Missiles Systems Division, Los Angeles, California, Doc. No. 288184, December 17, 1959.

D. TEMPERATURE EFFECTS ON SOLAR CELLS:

26. Halsted, R. E. "Temperature Considerations in Solar Energy, Battery Development, JAP, Vol. 28 (October 1957), p. 113.

27. Luft, W., and Nash. "Temperature Control of Silicon Solar Cells in Space Environment," Semiconductor Products, Vol. 3 (June 1960), p. 39.

E. RADIATION EFFECTS ON SOLAR CELLS:

28. Enslow, G., and Junga, F. A. "Gamma Radiation Effects in Silicon Solar Cells," Third Semiannual Radiation Symposium Convention Record, October 1958.

29. Junga, F. A., and Enslow. " Radiation Effects in Silicon Solar Cells," IRE Trans on Nuclear Science, June, 1959

30. Loferski, J. J., and Rappaport, P. "The Effect of Radiation on Silicon Solar Energy Converters, "RCA Rev. Vol. 19 (December 1958), p. 536.

31. Loferski, J. J., and Rappaport, P. "Radiation Damage in Ge and Si Detected by Carrier Lifetime Changes: Damage Thresholds." Phys. Rev., Vol. 111 (July 1958), p. 43.

32. Schurf, K. "Photovoltaic Effect Produced in Silicon Solar Cells, by X- and Gamma Rays," J of Res. of Nat. Bur. of Stand, Vol. 64A (July and August 1960), p. 287.

F CELLS OF MATERIALS OTHER THAN SILICON:

33. Goldstein, B. "Properties of Photovoltaic Films of CdTe," Phys. Rev., Vol. 109 (January 15, 1958), p. 601.

34. Jenny, et al. "Photovoltaic Effect in GaAs p-n Junctions and Solar Energy Converters," Phys. Rev., Vol. 101 (February 1956), p. 101.

35. Reynolds, et al. "Photovoltaic Effect in CdS," Phys. Rev., Vol. 96 (1954), p. 533.

36. Reynolds, D. C. "Mechanism for Photovoltaic and Photoconductivity Effects in Activated CdS Crystals," Phys. Rev., Vol. 96 (December 1954), p. 1705.

37. Rothlein, D. J., and Fowler. "Germanium Photovoltaic Cells," Trans IRE, (April 1954), p. 67.

38. Williams, R., and Bube, R. "Photoemission in the Photovoltaic Effect in Cadmium Sulfide Crystals," JAP, Vol. 31 (June 1960), p. 968.

ENERGY CONVERSION SYSTEMS REFERENCE HANDBOOK

Volume V - Direct Solar Conversion

Section B

PHOTOEMISSIVE POWER GENERATORS

W. R. Menetrey
Energy Research Division
ELECTRO-OPTICAL SYSTEMS, INC.

Manuscript released by the author
September 1960 for publication in this
WADD Technical Report 60-699 Energy Conversion Systems Reference Handbook

V - B PHOTOEMISSIVE POWER GENERATORS

CONTENTS

ILLUSTRATIONS

Figures

B PHOTOEMISSIVE POWER GENERATORS

Photoelectric emission occurs when electrons in a material gain enough energy by absorbing incident radiation to escape from the material surface. A current flow is established when these electrons are collected by a second surface and a load is connected between the emitter and collector. Thus, a hypothetical device for converting the sun's radiant energy into electrical power is possible.

A great deal of speculative interest centers on the possibility of large area, light-weight photoemissive generators which, while operating at low efficiency, would nevertheless result in a low specific weight (lb/kw). These future power supplies are typically envisioned as sheets of plastic coated thinly with metal and exposed to the solar radiation. As demonstrated in the following paragraphs, this vision is premature. Until unforeseen technicological breakthroughs are achieved, the photoemissive converter offers little competition to the readily available photovoltaic converter.

1.0 THEORETICAL DESCRIPTION

The energy relations of the converter are shown in Figure V-B-1 where it is assumed that steady state conditions prevail. The cathode and anode are materials having work functions W_c and W_a, respectively. The current I, flowing through R_L, causes the anode Fermi level to be raised above the photocathode Fermi level. A proton of energy $h\nu$ strikes the cathode photosurface and causes an electron to be emitted having an energy

$$E = h\nu = \frac{1}{2} m v_e^2 \qquad \text{(B-1)}$$

The condition for escape from the surface of a photoelectron is

$$\frac{1}{2} m v_e^2 \cos^2 \theta \geq W_c \qquad \text{(B-2)}$$

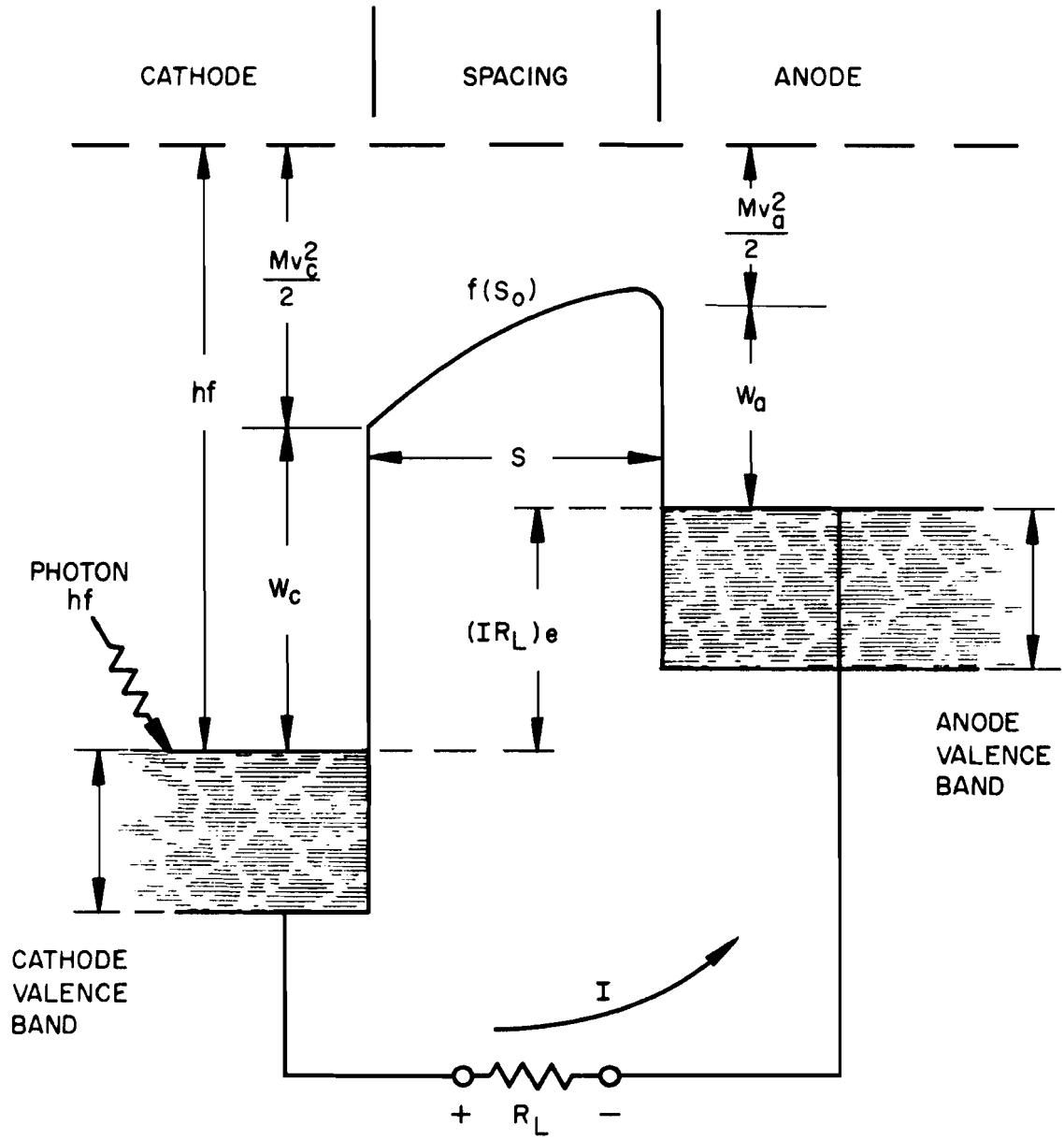

FIGURE V-B-1 PHOTOELECTRIC PHENOMENA

where θ defines the velocity direction of the electron relatiave to the surface normal. Assume that the photoelectrons reaching the surface of the emitter have a isentropic distribution of velocities and that no energy is lost while traveling to the surface. It has been shown that this is approximately the case for volume photoemission (the minor effects of surface photoemission are neglected) and for semiconductor emitters. The photoelectrons satisfying the above condition have directions contained within a cone's apex angle of $2\theta_c$, where

$$\theta_c = \cos^{-1} \frac{W_c}{h\nu} \qquad \text{(B-3)}$$

Since the direction of the electrons reaching the surface is entirely random, the number of these photoelectrons having directions contained within the defined cone is

$$N_1 = N_o \frac{1}{2} (1-\cos \theta_c) = \frac{No}{2} \left(1-\sqrt{\frac{W_c}{h\nu}}\right) \qquad \text{(B-4)}$$

Where N_o is the total number of photoelectrons and N_1 is the number of electrons which are emitted. The quantum efficiency at any given wavelength is by definition the number of electrons emitted per incident photon and is given by N_1/N_o. The quantum efficiency is shown in Figure V-B-2 as a function of wavelength for materials at room temperature with W_c equal to values of .01 to 2.0 electron volts. It can be seen that maximum obtainable quantum efficiency (neglecting possible secondary electron effects) is 50 percent, arising from the fact that emission emanates from one surface of the material and half the photoelectrons will have velocity directed into the material rather than outward.

The electron traverses the cathode to anode spacing and arrives

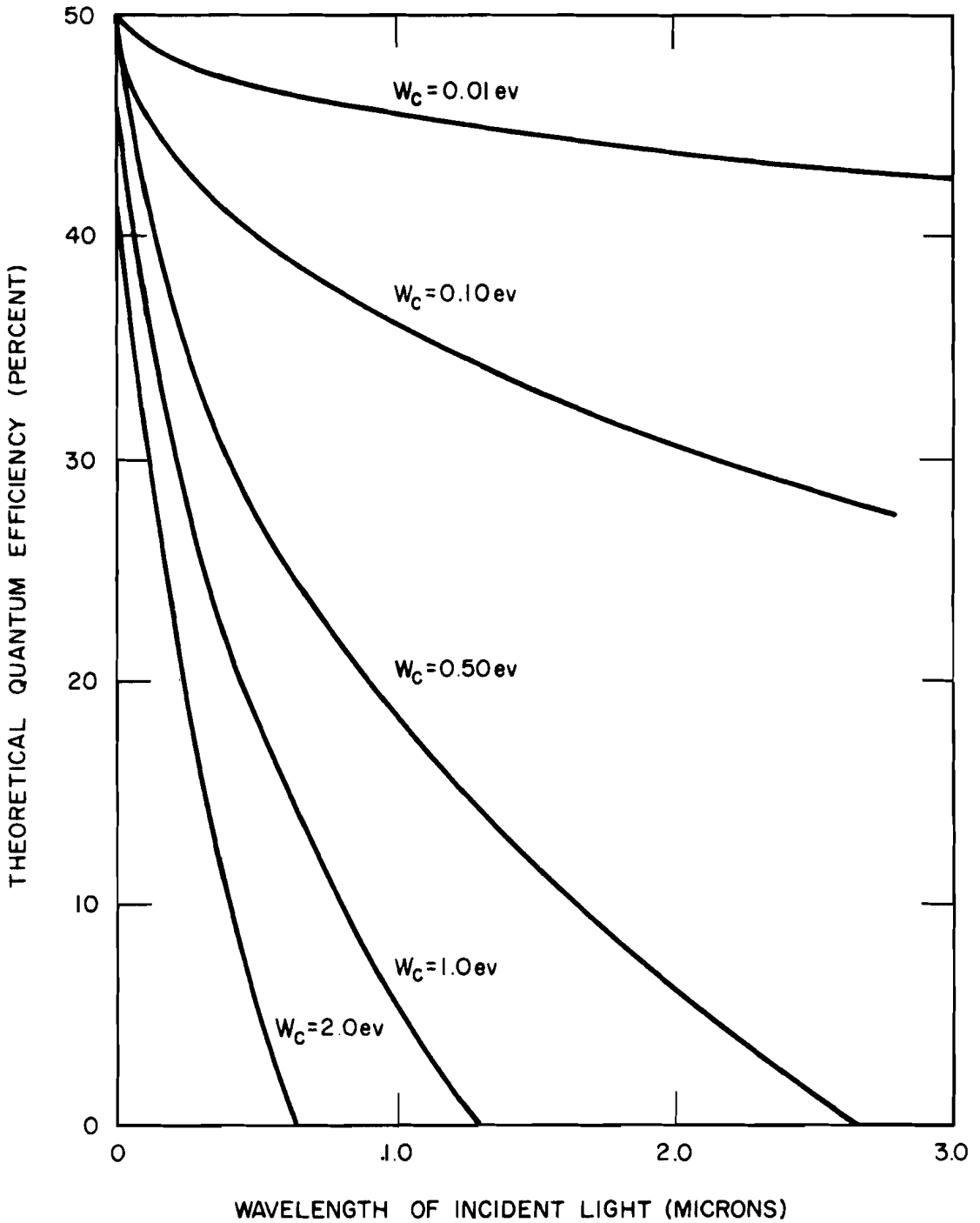

FIGURE V-B-2 THEORETICAL QUANTUM EFFICIENCY FOR PHOTOEMISSION VERSUS WAVELENGTH

at the anode after having expended a total energy of

$$W_a + mv_a^2/2 . \tag{B-5}$$

The energy available to the load per emitted electron is therefore

$$(IR_L)e = h\nu - W_a - mv_a^2/2 \tag{B-6}$$

The energy loss in heating the anode can be considered to be a result of an effective internal resistance of the photo-diode.

If the anode is illuminated by photons, it will also emit electrons, and these electrons will be attracted to the more positive cathode. A reverse current will flow through the load, decreasing the available power output. The anode emission will be particularly large if the anode has a smaller work function than the cathode. Therefore, protons must be prevented from hitting the anode surface, i.e., the anode must be kept in the dark.

The basic energy level diagram of Figure V-B-1 points out three important facts:

a. The anode work function W_a should be minimized in order to convert a larger percentage of the input light energy into useful work.

b. The anode surface should be shielded from the light to prevent reverse current and lower efficiency.

c. The cathode work function W_c does not effect the energy conversion directly but does determine the potential convertible spectral region. It also determines the initial kinetic energy of the photoelectrons emitted into the cathode-anode space and, therefore, the space charge characteristics. Filtering of the

incident light spectrum may be necessary to prevent low energy protons from reaching the photo cathode.

The spectral response of a given material measures the emission current produced by a unit energy of incident light as a function of wavelength. The emissive current is:

$$i_s = \frac{N_1 e}{t} \tag{B-7}$$

where t equals time, the incident power is:

$$P_i = \frac{N_o h\nu}{t} \tag{B-8}$$

therefore the spectral response, i.e., emission current per unit of incident radiant power, is given by:

$$J_p = \frac{i_s}{P_i} = \frac{e}{2h\nu}\left(1 - \sqrt{\frac{W_c}{h\nu}}\right) \tag{B-9}$$

The spectral response curves for an emitter work function of .01 to 2.0 electron volts is shown in Figure V-B-3.

The solar power in the vicinity of the earth's orbit is about 1400 watt/meters^{-2} incident on an area normal to the flux. For a photoelectric converter, the useful portion of the spectrum exists at wavelengths greater than about 2 volts or 0.65 microns, equivalent to 42 percent of the solar flux or about 600 watts/meter^2. The theoretical efficiency of the photoelectric converter can be determined by:

a. Knowing the solar radiation available as a function of the wavelength.

b. Knowing the efficiency as a function of wavelength of the

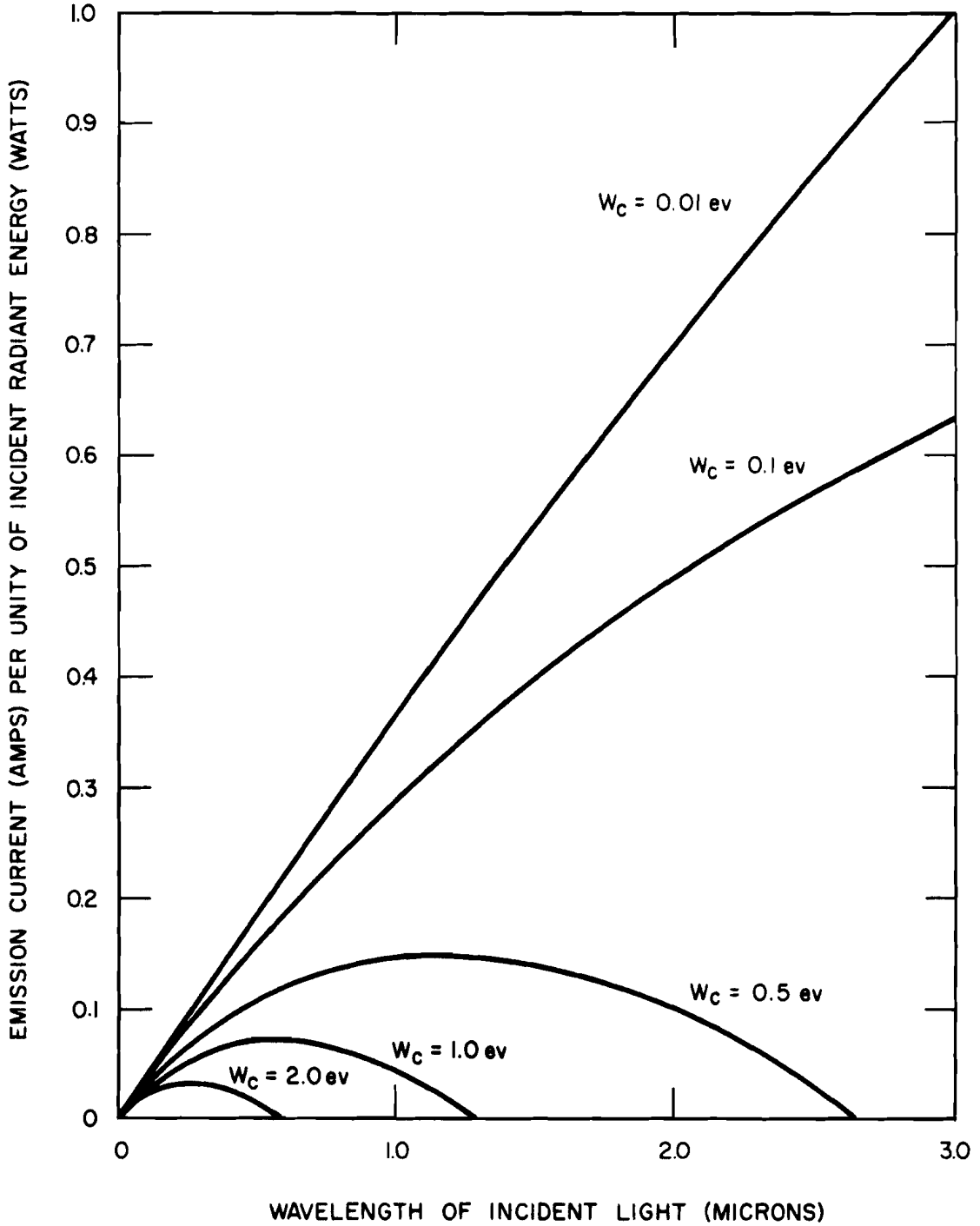

FIGURE V-B-3 THEORETICAL SPECTRAL RESPONSE FOR PHOTOEMISSION

photoemitter surface.

c. Integrating the product of photocathode quantum efficiency and solar radiation, from maximum photon energy to that which produces a photoelectron just energetic enough to reach the anode.

Using these steps, the characteristic operating curve for a photogenerator can be drawn (current density vs. voltage). The characteristic curve for a photogenerator having C_sS_b photocathodes is given in Figure V-B-4. A curve is limited by the solar illumination level to current densities about an order of magnitude below the space charge limit given for a 2 mil spacing photogenerator. A load line may be drawn to describe the devices operating characteristics and must intercept the voltage axis at the value of the anode work function (per electron). Two values for this anode are practical:

a. The same material as the photocathode - C_sS_b with a work function of 1.75.

b. Silver cesium oxide which has the lowest known work function, 1.1 electron volts, and has a very low quantum efficiency.

A load line is drawn in Figure V-B-4 for the cases of maximum power density output. The rectangular areas indicated are proportional to the output power density and are a maximum for that particular slope of the load line. Since maximum power delivery occurs with a matched load, this line also delineates the internal resistance of the generator. The internal resistance shown is extremely low compared with the value for known photocells.

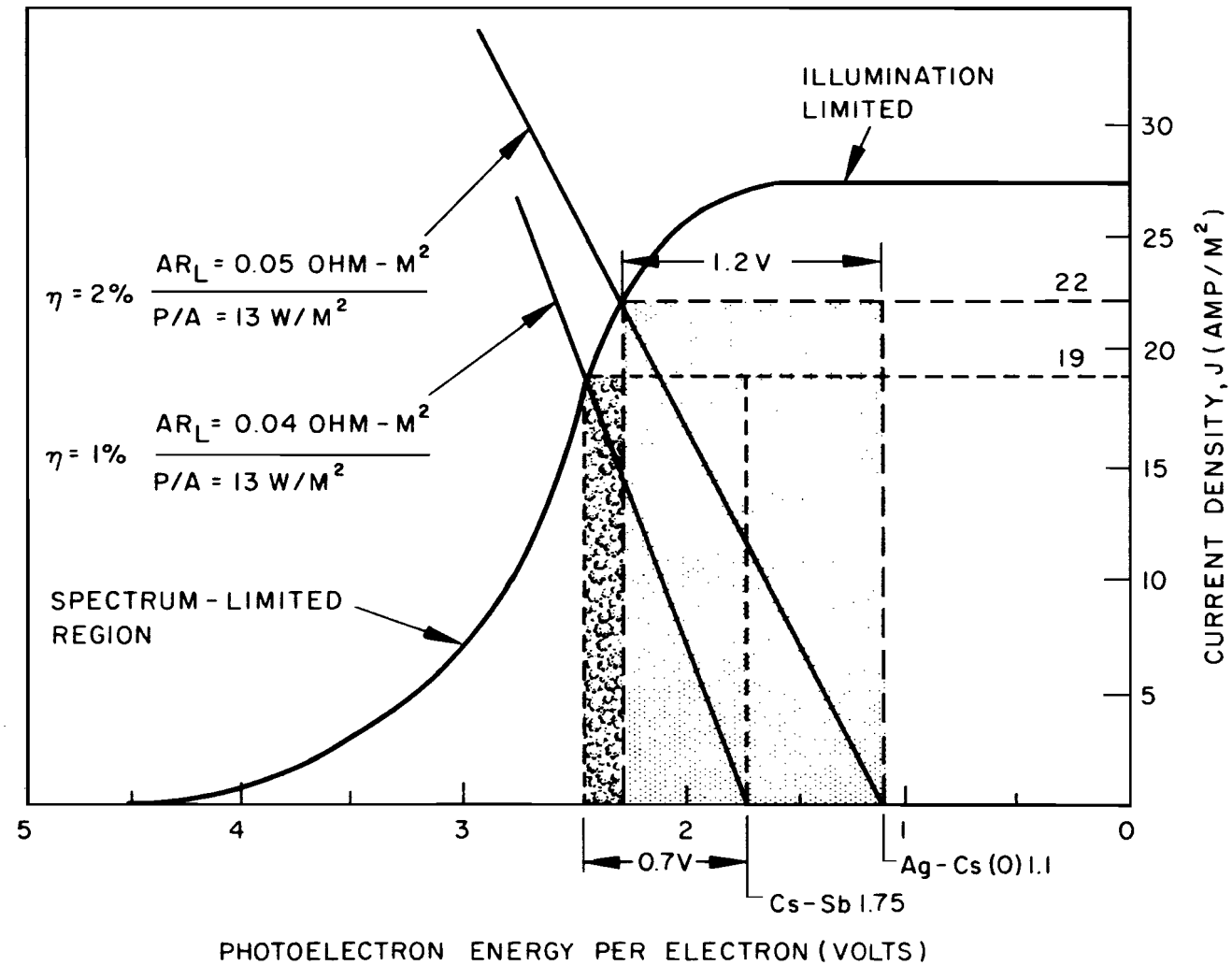

FIGURE V-B-4 THEORETICAL CHARACTERISTIC CURVE
ANTIMONY - CESIUM PHOTOGENERATOR

When a space charge analysis is made, similar to the analysis for a thermionic diode, the space charge limited potential distribution within the cathode-anode space is a maximum value. The anode should optimally be spaced at such a distance that it is at the maximum value point. This maximum point can be specified by a "design current density" (J_o), and is given by

$$J_o = \frac{1}{a^2 d^2} \qquad \text{(B-10)}$$

where $a^2 = 4.25 \times 10^5 \ (h\nu - W_c)^{3/2}$

d = anode-cathode spacing .

As a representative value, assume that the initial photoelectric energy ($h\nu - W_c$) is 0.5 electron volts and the design spacing chosen is 2 mil. Substitution gives a design current density of 350 amp/meter^2 which is much less than the solar illumination limit of 30 amp/meter^2. For a spacing of 150 mil, the design current density is .06 amp/meter^2.

2.0 GEOMETRIC CONFIGURATION

A version of the photoelectric generator currently being developed and tested by Westinghouse Electric (Ref. V-B-4) consists of a photocathode and an anode separated electrically by an insulator and structurally by a piece of fine wire mesh. These are enclosed sandwich-like between two thin sheets of glass which act as the vacuum envelope. The anode is a layer of low work function material evaporated on one side of the screen. The other side of the screen is coated with an insulator so that the screen functions both as a support and spacer. The cathode is formed by evaporating a suitable photoemissive substance onto the glass and a second piece of screen that has previously been sealed or otherwise applied to the glass. This photocathode screen is needed to reduce the resistance of photocathode sensitive layer. A schematic cross

section of the generator is shown in Figure V-B-5. The entire structure can be very thin, and thicknesses of 30 mil are estimated for future devices.

Practical use of the photoemissive generator will require that several cells be placed in a series and that these series circuits be placed in parallel. In series, the current available is that from the cell having the least illumination; therefore, series-connected cells should be mounted on a plane so that illumination is equal, similar to the photovoltaic cell. There is no problem in connecting the cells in parallel, since the illumination limited currents are exactly additive.

Another basic configuration would allow the incident radiation to shine through the anode screen onto the cathode surface. This configuration is not as efficient as absorbing the incident radiation on the back surface because:

a. The cathode is partially shielded,

b. The screen anode will allow many of the emitted electrons to pass through uncollected.

The experimental state-of-the-art is represented by the characteristics of Figures V-B-6 and V-B-7 which represent results using the experimental WX-3964 photogenerator developed by Westinghouse Electric Corporation, Electronic Tube Division. This work has been supported in part by the U. S. Army Signal Research Development Laboratory under Contract No. DA-36-039-SC-85248 and Advanced Research Projects Agency Order No. 80-59. The experimental cell has a spacing of 150 mil (with a space charge limitation of about 6 microamp/centimeter^2) and an emitting surface of 20 cm. As shown, the efficiency was very low. The apparent internal resistance is plotted against the load current ignoring the presence of photoemission from the anode.

CROSS SECTION OF PHOTOGENERATOR

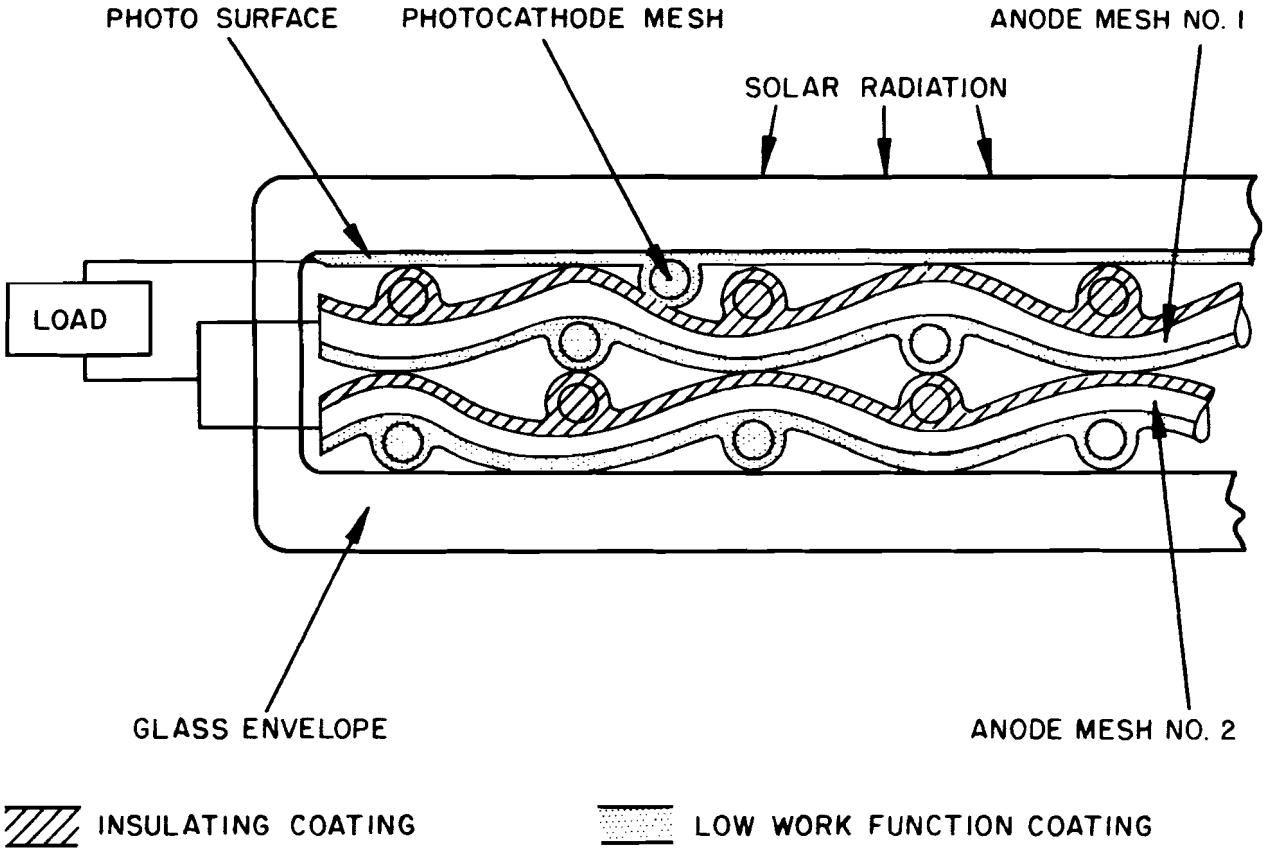

FIGURE V-B-5

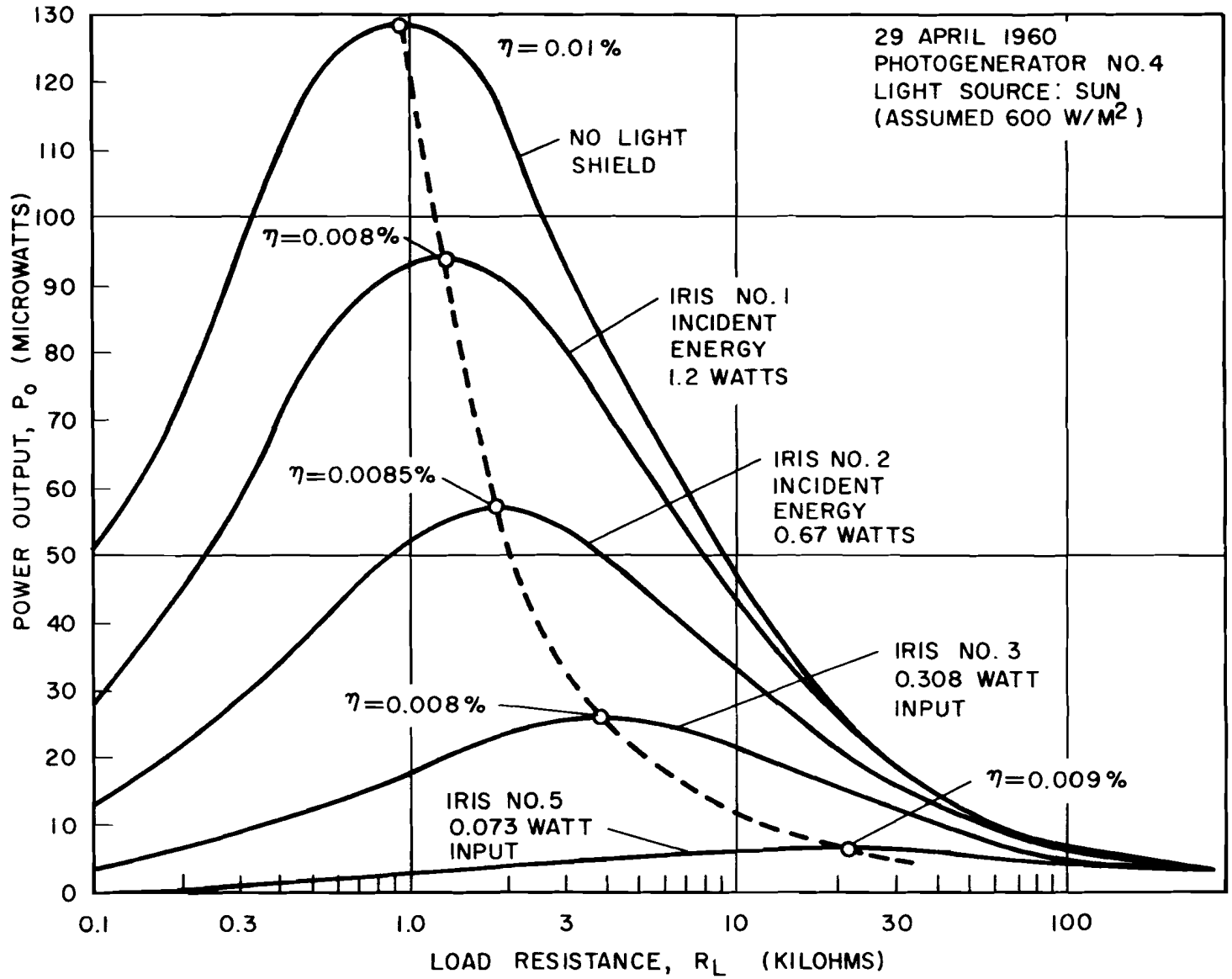

FIGURE V-B-6 PHOTOGENERATOR TESTS

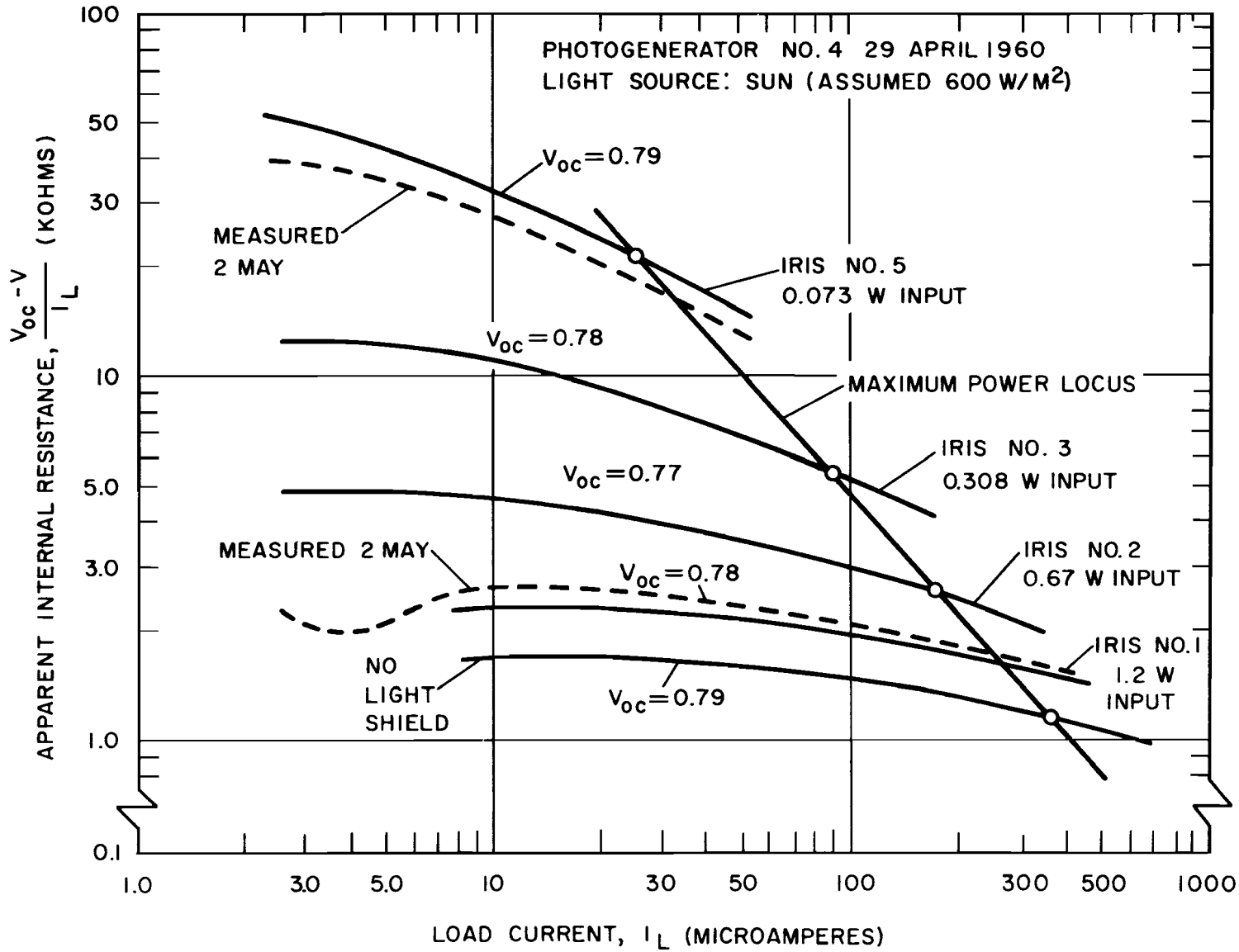

FIGURE V-B-7 PHOTOGENERATOR TESTS

3.0 FUTURE POSSIBILITIES

As shown by the previous discussion, it does not appear that the photoelectric generator will approach the theoretical or practical efficiency of a photovoltaic generator until a technological break-through is achieved. There are several practical problem areas not discussed here which will degrade the photoemissive generator, similar to the degradation suffered in the photovoltaic generator. These include the following:

a. An advantage in weight over other generators will result from the use of light-weight plastic envelopes. For example, the cells could be etched, sealed together to a flat sheet, or fabricated into a balloon shape. However, plastic materials are subject to severe degradation in the UV and X-ray portions of the solar spectrum and from the high-energy corpuscular bombardment in the Van Allen belts and solar plasmas. It is doubtful if plastics could provide adequate structural support for long periods of time in an ambient space environment.

b. The semiconducting properties of the cathode material will be drastically changed when exposed to the Van Allen radiation. The use of thick heavy glass covers would negate any weight advantage of the photoemittive generator.

c. A spectrally selective coating is necessary to reflect the unwanted portion of the solar spectrum. Otherwise, emitter generator temperatures will rise to values such that the reverse current will cancel the useful power output.

In summary, the maximum efficiency expected from presently known materials will be on the order of 2 to 3 percent, equivalent to 2.6 to 3.9 watt/ft^2. To provide the 30 lb/kw which has been predicted (Reference V-B-4) as a possibility, the weight of the entire structure would weigh on the order of .12 lb/ft^2 with a 3 percent efficient cell. This specific weight is quite optimistic in light of known structural techniques.

REFERENCE LIST

V-B-1. Peria, W. T. (Physical Electronics Research Laboratory, Institute of Technology, University of Minnesota.) "Photoemission Studies," Scientific Report No. 1, Contract No. AF 33(616)-6455, Sept. 15, 1959.

V-B-2. Sheridan, R. (Boeing Airplane Company) "Future Performance Possibilities of Photoemissive Conversion," Document No. D2-33556, February 27, 1959.

V-B-3. Sheridan, R. (Boeing Airplane Company) "Analysis of a Photoemissive Converter Using Present Materials," Document No. D2-3555.

V-B-4. Jensen, A. S. and Limansky, I. (Westinghouse Electric Corporation, Electronic Tube Dividion) "Photoelectric Conversion." Presented at Annual Power Sources Conference, April 1960.